PFC/JA-86-6

Lower Hybrid Wave Launching and Antenna Design

S.F. Knowlton
M. Porkolab

February 1986

Plasma Fusion Center
Massachusetts Institute of Technology
Cambridge, MA 02139

Submitted for publication in: Nuclear Fusion

This work was supported by the U.S. Department of Energy Contract No. DE-AC02-78ET51013. Reproduction, translation, publication, use and disposal, in whole or in part by or for the United States government is permitted.

LOWER HYBRID WAVE LAUNCHING AND ANTENNA DESIGN[†]

S. F. Knowlton and M. Porkolab

Plasma Fusion Center
Massachusetts Institute of Technology
Cambridge, MA 02139 USA

ABSTRACT

Slow wave antennas in the lower hybrid range of frequencies have been developed to efficiently launch waves within a desired range of the parallel refractive index for the purpose of plasma heating and current drive. The theory of antenna coupling is reviewed, with particular emphasis placed on the performance of the phased waveguide array used in most present-day experiments. Wave launching experiments on linear machines and tokamaks are reviewed and compared with theory. Considerable progress has been made in reducing rf breakdown at high powers in lower hybrid antenna structures, and the numerous techniques are summarized.

[†] This article is to be part of a Nuclear Fusion invited review paper on rf wave lauchers for coupling to plasmas.

3.1 Introduction

High power lower hybrid wave heating experiments are performed on tokamaks and other toroidal devices for the purpose of ion heating, electron heating, and rf current drive [1]. The lower hybrid wave represents the slow wave branch of the cold plasma dispersion relation in the frequency range $\omega_{ce} >> \omega >> \omega_{ci}$, where $\omega/2\pi$ is the frequency and $\omega_{ce}/2\pi$ and $\omega_{ci}/2\pi$ are the electron and ion cyclotron frequencies, respectively. This branch exhibits a resonance (i.e., $k_\perp \to \infty$) at the lower hybrid frequency,

$$\omega_{LH} = \omega_{pi} \left(1 + \frac{\omega_{pe}^2}{\omega_{ce}^2}\right)^{-1/2} , \qquad (1)$$

where $\omega_{pe}/2\pi$ and $\omega_{pi}/2\pi$ are the electron and ion plasma frequencies. The lower hybrid frequency lies between 0.5 and 5 GHz in present-day tokamaks. Since in this frequency regime the free-space wavelength is comparable to, or smaller than the minor radius of the tokamak chamber, open-ended waveguide antennas located in the scrape-off plasma behind the limiter are a convenient means of launching lower hybrid waves in tokamak plasmas. As theoretically predicted by Brambilla, the phased array of waveguides, or grill [2,3], has been shown experimentally to couple very efficiently to the slow wave in the plasma, and such structures have been used in most major lower hybrid heating experiments to date. Excellent coupling efficiency is achieved with the grill (transmission coefficients of 90% are typical) without tuning devices which are often necessary at lower frequencies to match the antenna impedance to that of the plasma. Consequently, the standing wave ratio within the antenna is quite low. Nonetheless, the major practical problem encountered with high power operation of the phased array antenna has been found to be rf breakdown in the evacuated portions of the waveguides which

are open to the tokamak vacuum chamber. A considerable amount of research effort has focused on the prevention of rf breakdown within the antenna. As a result, a number of diverse techniques developed at different laboratories have succeeded in improving the reliability of the grill antenna at the power levels required for significant plasma heating. Since high power rf sources in the lower hybrid range of frequencies are commercially available, the technology of lower hybrid heating is believed to present few major obstacles to applications on future tokamak experiments, including reactors.

In this paper, we review the design and performance of lower hybrid wave couplers used in tokamaks. Particular attention is paid to the analysis and operation of the grill antenna. We begin in Section 3.2 with a brief description of the physics of lower hybrid wave propagation and absorption. Although the antenna coupling efficiency is determined solely by the plasma density at the antenna plasma interface, the rf heating or current drive efficiency in the core plasma is partially dependent on the parallel wave-number spectrum launched by the antenna. Consequently, constraints imposed by optimization of the wave damping processes in the bulk plasma strongly influence the wave coupling physics and the antenna design. The general requirements of the lower hybrid antenna design are outlined in Section 3.3. The theory of matching the antenna electromagnetic fields to the edge plasma wave fields is discussed next in Section 3.4. The Brambilla theory describing the specific coupling behavior of the grill-type antenna is outlined in Section 3.5. The experimental coupling results from a number of lower hybrid heating experiments have been found to be in reasonable agreement with the theoretical predictions; these comparisons will be presented in Section 3.6. The issues of rf breakdown in the antenna, and its elimination are discussed in Section 3.7. Finally, in Section 3.8 we describe some

trends and changes in grill coupler design which are planned or contemplated for future heating experiments and possible reactor heating or current drive schemes.

3.2 Lower Hybrid Wave Propagation

The particular damping mechanism of lower hybrid waves in the plasma core (ion heating, electron heating, or current drive) is dependent on the plasma density and temperature, the magnetic field, and is also strongly affected by $k_\parallel = n_\parallel \omega/c$, the parallel wave vector of the lower hybrid wave (where $n_\parallel$ is the index of refraction along the magnetic field, $k_\parallel = \vec{k} \cdot \vec{B}/B$, and c is the speed of light). The $n_\parallel$ spectrum of the lower hybrid wave power, which is determined by the antenna geometry, is important in achieving the desired heating result. In this section, the basic properties of the propagation and absorption of lower hybrid waves are summarized in order that (1) the requirements on the $n_\parallel$ spectrum launched by the antenna be understood, and (2) one is provided with an introduction to a more detailed discussion of the coupling physics in the next sections. More complete and informative treatments of lower hybrid wave propagation can be found in a number of references [4-6]; in particular, lower hybrid wave propagation and damping in tokamak plasma geometries are reviewed in Ref. [7].

Wave propagation in a cold plasma is described by the following wave equation for the rf electric field $\vec{E}$:

$$\nabla \times \nabla \times \vec{E} - \frac{\omega^2}{c^2} \vec{\vec{K}} \cdot \vec{E} = 0 \ , \qquad (2)$$

where $\vec{\vec{K}}$ is the dielectric tensor in a Cartesian coordinate system:

$$\vec{\vec{K}} = \begin{pmatrix} S & -iD & 0 \\ iD & S & 0 \\ 0 & 0 & P \end{pmatrix} .$$

The elements of the dielectric tensor are written in the notation of Stix [4]. The magnetic field of the tokamak, B_o, is assumed to point in the z-direction. The plasma density decreases in the x-direction. In the cylindrical geometry model of a tokamak, the x-direction corresponds to the radial direction, the y-direction to the azimuthal (poloidal) direction, and the z-direction to the toroidal direction. For the lower hybrid range of frequencies, the inequality $\omega_{ci} << \omega << \omega_{ce}$ is valid, and the components of the cold plasma dielectric tensor may be approximated as

$$S = 1 + \frac{\omega_{pe}^2}{\omega_{ce}^2} - \frac{\omega_{pi}^2}{\omega^2}$$

$$P = 1 - \frac{\omega_{pe}^2}{\omega^2} \qquad (3)$$

$$D = \frac{\omega_{pe}^2}{\omega\omega_{ce}} .$$

For a homogeneous plasma, the wave Eq. (2) may be written as

$$\vec{n}(\vec{n} \cdot \vec{E}) - n^2\vec{E} + \vec{\vec{K}} \cdot \vec{E} = 0 , \qquad (4)$$

where $\vec{n} = c\vec{k}/\omega$ is the refractive index. In a weakly inhomogeneous plasma the dispersion relation may still be obtained in a WKB sense from Eq. (4). Since the plasma parameters are nearly constant along the z-axis, and the grill determines $n_\parallel$ at the plasma edge, the WKB dispersion relationship may be written in the following form:

$$An_\perp^4 + Bn_\perp^2 + C = 0 \tag{5}$$

where

$$n_\perp^2 = n_x^2 + n_y^2$$

$$A = S$$

$$B = (n_\parallel^2 - S)(S + P) + D^2$$

$$C = P\,[(n_\parallel^2 - S)^2 - D^2]\ .$$

The dispersion relation has two solutions corresponding to the slow and fast waves:

$$n_\perp^2 = \frac{-B \pm (B^2 - 4AC)^{1/2}}{2A}\ . \tag{6}$$

The solutions are distinct from one another if $B^2 >> 4AC$. In this limit, the approximate roots of the dispersion relation are [5]

$$n_{\perp s}^2 \simeq -\frac{P}{S}(n_\parallel^2 - S) - \frac{D^2}{S} \tag{7a}$$

$$n_{\perp f}^2 \simeq \frac{D^2 - (n_\parallel^2 - S)^2}{(n_\parallel^2 - S) + D^2/P}\ , \tag{7b}$$

where "s" and "f" subscripts refer to the slow and fast branches. A resonance for the slow wave ($n_{\perp s}^2 \to \infty$) exists at the location where $S = 0$, or

$$\frac{\omega_{pe}^2}{\omega_{ce}^2} = \left(\frac{\omega_{ce}\omega_{ci}}{\omega^2} - 1\right)^{-1}\ . \tag{8}$$

In the limit $n_\parallel^2 >> 1 + 2\omega_{pe}^2/\omega_{ce}^2 - \omega_{pi}^2/\omega^2 \simeq 0(1)$, the slow wave is essentially an electrostatic wave, characterized by the simple dispersion relation

$$n_\perp^2 \simeq n_\parallel^2 \frac{m_i}{m_e} \frac{\omega_{LH}^2}{(\omega^2 - \omega_{LH}^2)} \quad . \tag{9}$$

In this approximation, the wave energy emanating from the antenna is confined to so-called resonance cones [8,9], which lie at an angle θ with respect to the magnetic field

$$\tan\theta \simeq \frac{m_e}{m_i} \frac{(\omega^2 - \omega_{LH}^2)}{\omega_{LH}^2} \quad , \tag{10}$$

which is much less than unity for $\omega << \omega_{pe}$. Except near the plasma edge, the wave energy propagates away from the antenna primarily along the magnetic field.

If $B^2 > 4AC$ in Eq. (6), the solution of the dispersion relation predicts two distinct branches as shown in Fig. 1: a slow wave, given by Eq. (7a), and a fast wave, given by Eq. (7b). In general, these roots are distinct as long as $B^2 > 4AC$. However, for a sufficiently low value of $n_\parallel$, the condition $B^2 = 4AC$ may be satisfied at two distinct values of the density, n_e^- and n_e^+, which are both lower than the density at the lower hybrid resonance layer. At these critical densities, the slow and fast modes coalesce, as illustrated in Fig. 1a. The critical densities are given by the relationship [10]

$$\frac{\omega_{pi}}{\omega} = n_\parallel y \pm (1 + n_\parallel^2(y^2 - 1))^{1/2} \tag{11}$$

where $y^2 = \omega^2/\omega_{ce}\omega_{ci}$. The plus sign corresponds to n_e^+ in Fig. 1a and the minus sign to n_e^-. At intermediate densities $n_e^- < n_e < n_e^+$, there is no propagating solution to Eq. (6), since $B^2 < 4AC$. As $n_\parallel$ is increased, the two roots of Eq. (11) coalesce when

$$n_{\parallel crit}^2 = \frac{1}{1 - y^2} \quad . \tag{12}$$

For values of $n_\parallel^2 > n_{\parallel crit}^2$, the slow wave can propagate or is "accessible" to the lower hybrid resonance layer (should it exist in the plasma), as shown in Fig. 1b. If the lower hybrid resonance is present in the plasma, the accessibility criterion reduces to [5]

$$n_\parallel^2 > 1 + \frac{\omega_{pe}^2}{\omega_{ce}^2} \Big|_{\omega = \omega_{LH}} \tag{13}$$

or $|n_\parallel| \gtrsim 1.4$ for typical tokamak plasmas.

When the lower hybrid resonance does not exist in the plasma ($\omega > \omega_{LH}$), electron heating and/or current drive may still take place. In this case, the condition for wave penetration to the maximum density is still given by Eq. (12) if $y^2 < 1$ and $\omega_{pi}^2(o)/\omega^2 > y^2/(1 - y^2)$. Otherwise, accessibility is determined by the negative root of Eq. (11), and the critical value of $n_\parallel$ needed for the slow wave to penetrate to a given density without mode conversion to the fast wave is given by

$$n_{\parallel crit} = \frac{\omega_{pe}}{\omega_{ce}} + S^{1/2} \tag{14}$$

For the PLT lower hybrid experiment parameters [11] (B_o = 26 kG, D_2 gas, $\omega/2\pi$ = 800 MHz) a representative value of the parallel wavenumber during current drive experiments is $n_\parallel = 1.3$ and the fast-slow wave convergence would occur at a density of 1.1×10^{13} cm^{-3}. Waves with smaller values of $n_\parallel$ are "inaccessible" to this density, and are constrained to propagate in the low density plasma between the wall and the fast/slow mode conversion layer, and are commonly referred to as surface waves. This should be compared with the lower hybrid resonant density of $n_e = 5.2 \times 10^{13}$ cm^{-3}, for which accessibility is achieved only for $n_\parallel > 1.34$.

The lower hybrid wave may be absorbed in the plasma by several different mechanisms. Collisionless damping processes occurring in the plasma core are of most interest in a heating experiment. Lower hybrid waves are predicted to be absorbed on ions by "unmagnetized perpendicular ion Landau damping [12], or by ion cyclotron damping at the high harmonics ($\omega \simeq 40$ ω_{ci}, typically) [13,14], or by electron Landau damping [15-17]. Ion heating, at least by linear means, can only occur near the lower hybrid resonance; hence only the slow wave is absorbed by ions. At a density somewhat below the resonant density, the inward-propagating slow wave is predicted to undergo a conversion to a short-wavelength hot-plasma electrostatic wave (see Fig. 1b) which travels back toward the plasma edge [18]. Near this mode conversion layer, the perpendicular wavelength becomes small enough such that the perpendicular phase speed of the wave is comparable to the ion thermal speed ($\omega/k_\perp v_{thi} \simeq O(1)$, where v_{thi} is the ion thermal velocity). Absorption by ions can occur for waves with $n_\parallel$ greater than the $n_{\parallel crit}$ given by the accessibility condition Eq. (14), with higher $n_\parallel$ waves being mode-converted and absorbed at lower plasma densities. However, if anywhere along the trajectory of the wave, $n_\parallel$ is sufficiently high such that parallel phase speed of the wave is comparable to the electron thermal velocity, the wave may be absorbed by electron Landau damping before reaching the ion mode conversion layer. Significant electron heating should take place if [7,17,19]

$$n_\parallel \simeq \frac{\alpha}{\sqrt{T_e}} , \qquad (15)$$

where $\alpha = 5-7$ (depending on linear versus quasi-linear damping) and T_e is the electron temperature in keV.

Electron and ion heating by lower hybrid waves are competitive processes in a high density plasma; electron heating will generally predominate if the ratio of the electron temperature to the ion temperature satisfies the following condition, derivable from Eq. (9) and the wave damping criteria [1]:

$$\frac{T_e}{T_i} \gtrsim \frac{\omega^2}{\omega^2 - \omega_{LH}^2} \quad . \tag{16}$$

If the density is low enough such that $\omega \gtrsim 1.5\omega_{LH}$, this condition is easily satisfied.

If the plasma density is too low for ion interaction to occur and if the electron Landau resonance condition is satisfied, significant absorption of rf power on the fast electron population can occur. Subsequently, electrons diffuse in velocity space to create a suprathermal electron tail. If the antenna launches a unidirectional spectrum with respect to the magnetic field, the suprathermal electron tail is preferentially populated in the direction of wave propagation, and an electron current may by generated in the toroidal direction; this is the principle of rf current drive [20]. Current drive experiments are generally carried out at low plasma densities, both to eliminate the possibility of wave absorption by ions and also to reduce the collisionality of the fast electrons, thereby minimizing the rf power required to maintain the current.

Based on the accessibility condition (Eq. 14) and damping criterion (Eq. 15) described above, the requirements placed on the lower hybrid antenna design may be summarized as follows: for rf current drive, the antenna must be capable of launching a wave spectrum in a preferred direction with respect to the magnetic field. The $n_\parallel$ values in the

spectrum must be above the critical value given by the accessibility condition, and below that at which absorption near the plasma surface would dominate. For typical present day tokamak parameters ($T_e \sim 1$ keV), the appropriate range of $n_\parallel$ is $1.3 \lesssim n_\parallel \lesssim 3.5$. For electron heating, the conditions (15) and (16) should be satisfied near the plasma center; waves with higher $n_\parallel$ will be damped closer to the edge with a correspondingly lower heating efficiency. As the density is raised into the regime given by $\omega \lesssim 1.5\omega_{LH}$, ion heating should occur. The $n_\parallel$ values launched by the antenna should be low enough to avoid electron Landau damping and/or ion absorption near the plasma edge. Of the two branches of the dispersion relation, only the slow wave exhibits a resonance; hence ion heating can only be achieved with the use of this branch, at least by linear mechanisms. Furthermore, the slow wave branch is also preferable for electron heating and current drive, at least in present-day plasmas. However, in high temperature plasmas of the future ($T_e \gtrsim 10$ keV), fast wave current drive may be preferable [21,22]. Electron Landau damping requires that a component of the wave electric field lie along the toroidal magnetic field. The polarization of the waves in the lower hybrid range of frequencies will be discussed in the next section; in brief, however, the z-component of the fast wave branch is relatively small compared to the x- and y-components and the fast wave is only weakly Landau damped. Moreover, fast waves with $n_\parallel^2 > 1$ are evanescent over a wide region in the outer plasma layers and are therefore more difficult to couple into the plasma than slow waves. Fast waves of lower $n_\parallel$ ($|n_\parallel| \lesssim 1.3$) are easier to couple [23], but are resonant only with very energetic electrons. However, finite plasma density at the coupler mouth or finite poloidal wavenumber effects [24] may improve on this problem. To date only preliminary fast

wave coupling and current drive experiments have been performed [25,26]. Consequently, only slow wave antennas are reviewed in this paper.

3.3 Lower Hybrid Antenna Design Criteria

Because of the requirements on the $n_\parallel$ spectrum for the proper heating results, the slow wave antenna is typically a structure periodic in the z-direction with adjacent elements in the array excited out of phase with one another. The rf electric field polarization at the antenna-plasma interface must also be in the z-direction [5]. The phase angle between adjacent elements and the separation between elements are chosen to launch a wave with the desired $n_\parallel$ spectrum and directionality relative to the toroidal field. The $n_\parallel$ spectrum of the antenna is generally calculated by Fourier transformation of the antenna fields; the representative or peak value of the spectrum is roughly

$$n_\parallel \text{ (typ.)} \simeq \frac{c}{\omega \Delta z} \Delta\phi \ , \tag{17}$$

where Δz is the separation between radiative elements, and $\Delta\phi$ in the phase difference in radians between elements. Directional waves are launched for $\Delta\phi \simeq \pm \pi/2$, and standing wave spectra are launched for $\Delta\phi = \pi$. In phase operation ($\Delta\phi = 0$) is rarely employed because of the large inaccessible fraction of the $n_\parallel$ spectrum excited. From the viewpoint of maximizing the rf heating efficiency, it is clear that most of the $n_\parallel$ power spectrum coupled into the plasma should be concentrated in the accessible range. Moreover, if a significant fraction of the input rf power is composed of surface waves with $n_\parallel < n_{\parallel crit}$, impurity influx problems may result at high rf power levels because of unwanted edge plasma heating and/or direct

interaction of the microwaves with limiters or probes. The antenna itself should also be designed to present a good match to the plasma; i.e., to exhibit low reflectivity of the rf power from the plasma surface back toward the rf source. Aside from obvious considerations of overall rf heating efficiency, the natural match of the antenna to the plasma is beneficial from the point of view of reducing the standing wave ratio within the antenna structure and the transmission line. High electric fields in the antenna due to reflection of rf power from the plasma can lead to rf breakdown across the rf vacuum windows or in the residual gas within the waveguides. Rf breakdown problems have been encountered in most high power lower hybrid heating experiments performed thus far. Furthermore, the reflection of a substantial fraction of the incident rf power generally requires that the output of the rf source be protected with a circulator. Though variable tuning elements have been used to improve the match between antenna and plasma in a number of relatively low power experiments, their use is generally avoided because of the increased likelihood of rf breakdown due to the high standing wave ratio in the antenna between the plasma and the tuners, and also because of the necessity of retuning the antenna for different edge plasma conditions and different phasing between radiating elements. Consequently, modern lower hybrid antennas are designed to exhibit minimal reflectivity from a plasma load. This criterion has been achieved in practice on most lower hybrid experiments.

In addition to the rf characteristics of the antenna, other design criteria should be considered with regard to the installation of a lower hybrid antenna in a tokamak. The antenna material must not compromise the plasma purity; hence the antenna should be protected from energetic

particle bombardment (e.g., located in the limiter shadow). All-metal construction is also desirable in this regard. The use of ceramics in the antenna system is usually restricted to the fabrication of vacuum windows. In the reactor, such materials should be shielded from direct line of sight of the plasma since the high neutron fluence may degrade any ceramic material. Given that physical access to the tokamak plasma through a port can often be limited, one final practical consideration in lower hybrid antenna design is the ease of installation of the antenna system into the tokamak.

Broadly speaking, lower hybrid antennas used in tokamak experiments are of two types. In one, electromagnetic waves propagate in a slow wave structure aligned parallel to the magnetic field at the plasma edge [5,27,28]. A generalized slow wave structure is illustrated in Fig. 2. The period of the system is d and the antenna is separated from the plasma by a vacuum layer of width a. The structure is assumed to be infinite in the y-direction, and the plasma density increases in the x-direction. A slow wave can propagate in the z-direction between the wall and the plasma; electric fields in the z-direction are excited within the grooves. The rf power is coupled to the slow wave structure at one end. In principle, such a structure is similar to those used in traveling wave tube amplifiers. Waves with $n_{\parallel}$ values determined by the antenna periodicity are weakly coupled into the plasma; the antenna structure must be made sufficiently long in the z-direction for all of the input rf power to be radiated into the plasma. Aside from matching a transmission line to the slow wave structure, the antenna exhibits little reflectivity back to the rf source. A vacuum seal can be made within the transmission line. The physical antenna structure can be constructed by

rings fixed to the vacuum vessel wall, or by the bellows convolutions of the vacuum liner itself. Alternatively, the grooves can be replaced with elements driven by a transmission line lying along the z-direction. An example of such an antenna is shown in Fig. 3. Longitudinal slow wave structures have been used on early experiments on linear machines [29], on the ACT-1 torus [30], and on the FT-1 [31] and Doublet II [32] tokamak experiments.

In the second type, electromagnetic waves propagating perpendicular to the external magnetic field are launched directly into the edge plasma by waveguides, or in some cases, by loops. Lower hybrid waves which satisfy the accessibility condition are evanescent in the outer layer of the edge plasma where the density is below the critical density given by $\omega_{pe}^2 = \omega^2$. However, this region is extremely thin in present day plasmas and waves may efficiently tunnel through the region between the antenna and the critical layer; for a given $n_\parallel$ spectrum, the coupling efficiency is roughly determined by the width of this evanescent region. According to recent improvements in coupling theory, the antenna face should be placed in an overdense plasma ($\omega_{pe}^2 > \omega^2$) and therefore the evanescent layer in front of the antenna is eliminated. As opposed to the tangential slow wave structure, the "grill" type of antenna must couple strongly to the plasma wave fields for efficient launching of lower hybrid waves since the fraction of the rf power that does not couple to plasma waves is reflected directly back into the waveguides. As discussed in the next section, the antenna-plasma match is controlled by adjusting the density and density gradient directly in front of the antenna; this is commonly done by moving the antenna radially with respect to the vacuum vessel wall. The grill antenna consists of an array of phased waveguides with

the short sides oriented along the toroidal field, as illustrated in Fig. 4. The antenna face lies in the y-z plane. The plasma density increases in the x-direction. The waveguide height is h, and the guide width is b. The fundamental TE_{10} mode carries the incident power; therefore, the electric field of the antenna is in the z-direction. The relative phase angle between adjacent waveguides can be varied by phase shifters either in the high power feed lines to each waveguide, or in the low power rf drive if separate klystron amplifiers are used to feed each waveguide. Thus the $n_{\parallel}$ spectrum and directionality of a given waveguide grill can be varied, allowing greater flexibility than the longitudinal slow wave structure. Vacuum window seals are made in the waveguides or in the waveguide feeds to the grill. With the exception of the ceramic windows, both types of antennas can be made entirely of metal, and located near the vacuum vessel wall, posing minimal contamination problems to the plasma. A photograph and diagram of the Alcator C sixteen waveguide array are shown in Fig. 5 as an example of the grill type antenna. Beryllium oxide ceramic windows are brazed into copper collars which are in turn brazed to the stainless steel waveguide approximately 10 cm from the mouth of the grill. The face of the grill is contoured in the poloidal plane to approximately match the shape of the plasma.

The major practical drawback of the grill-type antenna is the problem of rf breakdown in the open-ended, evacuated waveguides. The nature of rf breakdown will be discussed later in this paper; however, we remark at this point that the choice of the location of the ceramic window is an important part of the overall design of the antenna. As rf breakdown can easily be controlled in the pressurized section of the antenna, it is clear that placement of the vacuum windows at the waveguide mouth would

eliminate the problem of breakdown. Such a solution is not desirable for several reasons: the bombardment of the window by the adjacent plasma would contaminate the plasma and might damage the window, and metallic deposits due to plasma disruptions would eventually make the window opaque to rf transmission. Furthermore, the possibility of neutron damage to the ceramic windows in future reactor-type plasmas will necessitate placing the window out of the line-of-sight of the plasma. Consequently, the vacuum windows in all lower hybrid antennas are recessed from the mouth of the waveguides. In the Alcator C [33], FT [34], and PLT [35] lower hybrid experiments, vacuum windows are brazed well inside the waveguides, but the electron cyclotron resonant layer ($\omega = \omega_{ce}$) is located in the pressurized section of the guides. Rf breakdown of a low pressure gas is much more likely to occur if the applied frequency is close to the local electron cyclotron frequency [36]. In Alcator A, two similar double waveguide antennas were tried: one with the vacuum windows located in front of the cyclotron resonant layers, and the other with the windows recessed such that the cyclotron layer lay in the evacuated part of the antenna [37]. In the latter configuration a power density of 4.5 kW/cm^2 could be achieved before rf breakdown occurred, while in the former at least 8 kW/cm^2 was attainable, indicating that the presence of the cyclotron resonance was indeed detrimental to power transmission.

In other lower hybrid experiments, the vacuum windows are located up to several meters from the mouth of the waveguides. On JFT-2 [38], Wega [39], Petula B [40], and Asdex [41], the windows have been placed in expanded waveguide sections with cross-sectional areas larger than that at the grill mouth. In this manner, the average power density at the window, a component which is susceptible to arcing and thermal stress, is reduced

below that at the grill mouth. In JFT-2, Petula, and Asdex, the volume between the window and grill mouth is pumped to maintain a low residual gas pressure within the waveguides during tokamak discharges, thus reducing the magnitude of breakdown by ionization. A diagram and photograph of the Asdex grill are shown in Fig. 6.

Lower hybrid antennas which combine aspects of both the active grill-type antenna and the passive slow-wave structure have also been proposed [42,43] and tested [42]. This type of antenna takes the form of a waveguide grill with dummy waveguides affixed to either side, as shown in Fig. 7. The depth of the shorted dummy waveguides can be chosen such that the power coupled into a dummy waveguide is re-radiated with the proper phase relationship to adjacent active waveguide, e.g. $\Delta\phi = 180°$ for a dummy waveguide one quarter of a wavelength deep. Although this type of antenna lacks the full versatility of the active grill, it affords the possibility of launching a well-defined $n_{\parallel}$ spectrum if the available port width is limited or if it is desirable to reduce the number of brazed-in windows in a multi-waveguide array. More will be said regarding the active-passive array later.

An example of an entire rf system for a lower hybrid heating experiment is shown schematically in Fig. 8. A high power klystron is used as a power amplifier in the lower hybrid frequency range. The output power from the klystron is directed through a ferrite circulator which protects the klystron from reflections from the plasma load. The power is split into separate transmission lines (either coaxial or waveguide) which in the present example include high power phase shifters for setting the relative phase angle between adjacent waveguides. Directional couplers

in each line monitor the forward and reflected power. Each transmission line feeds a waveguide of the antenna. Vacuum windows are affixed into each waveguide, either within the grill itself, or in each transmission line. The windows are commonly made of beryllium oxide (BeO) or alumina (Al_2O_3), and are often constructed to be one-half-wavelength thick to minimize the VSWR in the transmission line. The grill mouth is inserted through a bellows into a port in the vacuum vessel wall such that the position of the antenna face is moveable with respect to the plasma surface. The narrow gap between the grill and port wall may be shorted electrically with springs mounted near the grill mouth in order to prevent arcing due to rf power coupled into this slit. The rf power system is isolated electrically from the torus, usually by mylar DC breaks in the waveguide feeds to the grill.

An example of a more elaborate setup is the Alcator C system which utilizes several 4 × 4 waveguide arrays [44]. A schematic diagram is shown in Fig. 9. Here each of the four 250 kW klystrons operating at 4.6 GHz feeds one column of the 4 × 4 array. One common master oscillator is used to excite the klystrons. The oscillator power is split four ways, amplified, and passed through electronic phase shifters before being fed to the klystron drive input. In this way, the phase of the output power from each klystron, and hence of the power in each waveguide in a given column, can be set to a fixed value relative to that of the other klystrons. Hence, effective control of the relative phase angle between adjacent waveguides in a given row is achieved. With the electronic phase shifters, the phase angle can be altered during the rf pulse if need be, thereby changing the launched $n_\parallel$ spectrum to conform to evolving plasma conditions. Similar systems in use on other tokamaks have also been described [45,46].

A diagram summarizing the types of waveguide grills used in recent and ongoing lower hybrid experiments on tokamaks is shown in Fig. 10. The choices for window placement used in various grill experiments are also shown in this figure. Single waveguide antennas were tried on early experiments on ATC [47,48] and Alcator A [49]. External tuning systems were required to match the antenna to the plasma load in these experiments. Two-waveguide grills were used on ATC [47,48], Petula [50], and Alcator A [37,51], a three-waveguide grill on T-7 [52], and four-waveguide grills have been used on ATC [47], JFT-2 [38, 53-55], Versator II [56], WT-2 [57,58], Petula [40,59,60], and Wega [39]. Six-waveguide grills have been used on Versator II [61] and PLT [11,35,62], while eight-waveguide grills are in use on Asdex [41] and PLT [63]. With the higher frequencies used in high density, high magnetic field experiments, the vacuum port can often accomodate several set of waveguides stacked vertically, as in FT (2 × 2 array) [34,64] and Alcator C (4 × 4 array) [33,65,66]. On the other hand, the lower hybrid frequency in some tokamaks is too low for the waveguides to fit in the available ports; in these cases, other antenna structures have been used, including the electromagnetic slow wave structures described earlier. In JIPP T-II, a pair of C-shaped waveguides have been to couple to lower hybrid waves [67], while a pair of horizontal loops were employed in early experiments on Wega [68,69]. Other types of antennas were used on the Hybtok-1 [70], WT-1 [71], and CSTN-II [72] tokamaks.

3.4 Theory of Lower Hybrid Wave Coupling

In this section, the theory of lower hybrid wave coupling to the edge plasma is reviewed using the cold plasma model of wave propagation

introduced in Section 3.2. The general problem of coupling to lower hybrid waves at the plasma edge has been addressed by several workers [5,73,74]. The coupling problem is one of matching the impedance of the launching structure to that of the lower hybrid wave in the edge plasma. The Cartesian coordinate system of Fig. 4 is used to describe the geometry of the problem. The y and z components of the rf electric and magnetic fields, E and B, must be continuous in the y-z plane which, for the purpose of analysis, separates the antenna from the plasma.

In the low density regime ($\omega \lesssim \omega_{pe} << \omega_{ce}$) appropriate to the coupling problem, the dispersion relation Eq. (6) can be simplified. Specifically, $S \simeq 1$ in this regime, and if

$$n_\parallel^2 - 1 >> \frac{\omega_{pe}}{\omega_{ce}} , \tag{18}$$

which is easily satisfied in the edge plasma unless $|n_\parallel| \simeq 1$, the solutions of the dispersion relation Eq. (6) are well separated [5]:

$$n_{ls}^2 \simeq - P(n_\parallel^2 - 1) \tag{19a}$$

$$n_{lf}^2 \simeq - (n_\parallel^2 - 1) + \frac{D^2}{(n_\parallel^2 - 1)} . \tag{19b}$$

The polarization of the wave electric fields may be found from the full wave equation. For simplicity, we assume that the wave exhibits no spatial variation in the y-direction ($n_y = 0$). We note that this is desirable from an experimental point of view, since $|n_\perp| = n_x$ as a result, and the penetration rate of lower hybrid wave toward the plasma center is maximized for a given density profile. After elimination of the x-component of the electric field, E_x, the coupled equations for the y and z components, E_y and E_z, are

$$n_\perp^2 E_z + (n_\parallel^2 - 1) PE_z = in_\perp n_\parallel D E_y \qquad (20a)$$

$$n_\perp^2 E_y + \frac{(n_\parallel^2 - 1)^2 - D^2}{(n_\parallel^2 - 1)} E_y = \frac{in_\perp n_\parallel D}{n_\parallel^2 - 1} E_z \quad . \qquad (20b)$$

The first equation represents the slow wave branch, and the second the fast wave branch. Using the low density dispersion relationships, we see that

$$E_y/E_z|_s \approx 0, \text{ and } E_z/E_y|_f \approx 0. \qquad (21)$$

Thus if the launcher excites only electric fields in the z-direction, only the slow wave will be generated at the plasma edge and, if the accessibility condition of Eq. (11) is satisfied, the wave will remain a slow wave in its propagation through the plasma. Regarding the antenna-plasma coupling problem then, only the slow wave equation is considered in solving for the plasma fields E_z and B_y. According to Eq. (19a), slow waves with $|n_\parallel| < 1$ are evanescent everywhere for $\omega^2 < \omega_{pe}^2$. On the other hand, waves with $|n_\parallel| > 1$ are cut off only in the relatively thin region where $\omega^2 \gtrsim \omega_{pe}^2$. The width of this evanescent layer in large part determines the coupling efficiency of slow waves to the plasma. However, we note that if the inequality of Eq. (18) is not satisfied, the solutions of Eq. (6) are not distinct from one another, and coupling to the fast wave can occur. If a substantial fraction of the launched power spectrum is represented by $n_\parallel$ values near 1, the coupling to the fast wave may be significant, and the antenna reflectivity will not be predicted accurately by the slow wave coupling model described below [75,76].

In general, the coupling problem must be treated using the differential wave equation for the electric field, Eq. (2). In the coupling

region in front of the antenna, the sharp density gradient in the scrape-off plasma behind the limiter often renders Eq. (20) invalid, and Eq. (2) must be solved to obtain the electric and magnetic fields in the inhomogeneous edge plasma. As illustrated in Fig. 11, the density profile in front of the antenna is modeled as a density step and a linear density gradient:

$$n(x) = n_o + n_c\ (x/L), \tag{22}$$

where n_o is the density at the antenna face, $n_c = m_e\omega^2/4\pi e^2$, is the cutoff density for the slow wave, and L is the density scale length. The location of the antenna face corresponds to x = 0. The criterion for the validity of the WKB approximation is

$$\left|\frac{1}{k_\perp}\frac{dk_\perp}{dx}\right| < |k_\perp| ,$$

which is equivalent to

$$|x/L| > \left(\frac{1}{2k_\parallel L}\right)^{2/3} - (n_o/n_c - 1) \tag{23}$$

for $n_\parallel^2 >> 1$. The thin plasma layer in which the above inequality is not valid is known as the coupling region, as it is in this layer that the matching of the plasma wave fields to the fields in the waveguides must occur. Since typical density scale lengths in the edge plasma are L = 0.1 - 1 cm, and as the grill is found to couple efficiently into overdense plasmas ($n_o/n_c \gtrsim 1$), the thickness of the coupling region is less than a centimeter. This is the justification for the treatment of lower hybrid coupling as a local matching problem, independent of absorption and evanescence in the interior of the plasma. We remark that in the original treatment of the coupling problem, the density at the waveguide mouth, n_o,

was assumed to be low, $n_o = 0$ or $n_o = n_c$ [17]. Coupling experiments performed on tokamaks were initially found to disagree with the calculated coupling efficiencies in which the density gradient was the only free parameter in the plasma model. An important improvement in the model was made in which the density at the waveguide mouth was also allowed to be adjustable [77,78]. The agreement between the experimental coupling data and the calculated reflectivities is quite good with a variable density step included in the plasma model, which is supported by density profile measurements in recent experiments.

The slow wave equation in the coupling region is obtained from Eq. (2) by setting $E_y = 0$ and eliminating E_x:

$$\frac{\partial^2 E_z}{\partial x^2} + \frac{n_\parallel^2}{n_\parallel^2 - 1} \frac{\partial S}{\partial x} \frac{\partial E_z}{\partial x} - \frac{\omega^2}{c^2} P (n_\parallel^2 - 1) E_z = 0 . \qquad (24)$$

Except for $P = 0$, the second term is small compared to the third one, and is neglected.

Incorporating Eq. (22) into Eq. (24) gives

$$\frac{\partial^2 E_z}{\partial x^2} + \frac{\omega^2 (n_\parallel^2 - 1)}{c^2 L} (L(\mu - 1) + x) E_z = 0 , \qquad (25)$$

where we define μ to be n_o/n_c, the ratio of the density at the waveguide mouth to the cutoff density. Making the substitution

$$u(x) = - \left(\frac{\omega^2}{c^2} \frac{(n_\parallel^2 - 1)}{L}\right)^{1/3} (L(\mu - 1) + x) \qquad (26)$$

allows Eq. (25) to be rewritten as

$$\frac{\partial^2 E_z}{\partial u^2} - uE_z = 0 \ . \tag{27}$$

The solutions to Eq. (27) are the Airy functions. The particular linear combination of the two solutions that we choose is dependent on the far-field radiation condition: from Eq. (19a), the oscillatory solution is chosen for $|n_\parallel| > 1$, and the evanescent one is chosen for $|n_\parallel| < 1$. Because the lower hybrid wave is a backward wave in the direction perpendicular to the magnetic field, the outgoing asymptotic solution should be proportional to $e^{-ik_\perp x}$. For this general discussion, we will consider only the propagating solution, as lower hybrid antennas preferentially launch waves with $|n_\parallel| > 1$. However, in the numerical solutions, matching of the fields is performed over the effective range $-\infty < n_\parallel < +\infty$, truncated at an appropriately large value of $n_\parallel$.

The propagating solution to Eq. (27) is

$$E_z(u) = - iAi(u) + Bi(u) \ , \tag{28}$$

where Ai and Bi are the Airy functions of the first and second type. The rf magnetic field in the plasma is obtained from Faraday's law:

$$B_y(u) = i \frac{c}{\omega(n_\parallel^2 - 1)} \left[\frac{\omega^2}{c^2} \frac{(n_\parallel^2 - 1)}{L}\right]^{1/3} \left(- i \frac{\partial Ai(u)}{\partial u} + \frac{\partial Bi(u)}{\partial u}\right) \ . \tag{29}$$

The procedure for solving the coupling problem is the matching of the transverse plasma wave fields of Eqs. (28) and (29) to the transverse antenna fields in the coupling phase of the antenna face at x = 0:

$$\begin{aligned} E_z(u_o) &= E_{zi}(0) + E_{zr}(0) \\ B_y(u_o) &= B_{yi}(0) - B_{yr}(0) \ , \end{aligned} \tag{30}$$

where from Eq. (26),

$$u_o = u(x = 0)$$

and $E_{zi}(x)$ and $B_{yi}(x)$ are the incident electric and magnetic fields imposed by the antenna, and $E_{zr}(x)$ and $B_{yr}(x)$ are the reflected fields of the antenna. The field reflection coefficient $[E_{zr}(0)/E_{zi}(0)]$ is

$$\Gamma = \frac{(Z_p/Z_o) - 1}{(Z_p/Z_o) + 1}, \tag{31}$$

where

$$Z_p = \frac{E_z(u)}{B_y(u)} \tag{32}$$

is defined to be the wave impedance of the plasma and

$$Z_o = \frac{E_{zi}(x = 0)}{B_{yi}(x = 0)} \tag{33}$$

is the wave impedance of the antenna. Defining $Z_p/Z_o = |Z|e^{i\phi}$, we find that the power reflection coefficient, $|\Gamma|^2$, can be minimized for $|Z| = 1$, $-\pi/2 < \phi < \pi/2$.

3.5 Spectrum and Coupling Efficiency of the Grill

We now consider the specific coupling behavior of the waveguide grill illustrated in Fig. 4. The coupling theory for the passive slow wave structure shown in Fig. 2 is given in Refs. [5,27], while that for an active, transmission-line type radiator is given in Ref. [28]. The analysis of the grill antenna in this review follows that of Brambilla [3]. The antenna fields, both incident and reflected, are superpositions of the normal modes of the waveguides. The height of the waveguides, h, ($\lambda_o/2 < h < \lambda_o$, where λ_o is the free space wavelength) is chosen such that only

the fundamental TE_{10} mode can propagate, while the width of each waveguide, b, determines the $n_\parallel$ spectrum of the launched wave, as indicated in Eq. (17). The spectrum excited by the grill can be varied by changing the relative phase between adjacent waveguides.

Although a general theory of coupling from two-dimensional waveguides of arbitrary cross-section has been formulated [79], for the purpose of making a tractable analysis it is reasonable to consider the waveguides to be infinitely high because h/b is typically large (in the range of 6-20). The waveguide fields may then be written as

$$E_z^{wg}(x,z) = \sum_{p=1}^{N} e^{i\phi_p}\, \theta_p(z)\Big[\sum_{n=0}^{\infty}(\alpha_{np}e^{ik_n x} + \beta_{np}e^{-ik_n x})\cos\frac{n\pi(z - z_p)}{b}\Big] \tag{34a}$$

$$B_y^{wg}(x,z) = \sum_{p=1}^{N} e^{i\phi_p}\, \theta_p(z)\Big[\sum_{n=0}^{\infty}\frac{\omega}{ck_n}(\alpha_{np}e^{ik_n x} - \beta_{np}e^{-ik_n x})\cos\frac{n\pi(z - z_p)}{b}\Big] \tag{34b}$$

$$E_z^{wg}(x,z) = -\,i\,\frac{c}{\omega}\,\frac{\partial B_y^{wg}}{\partial x} \tag{34c}$$

where we have followed Brambilla's notation: p is the waveguide number, z_p is the z-coordinate of the edge of the pth waveguide, and ϕ_p is the phase factor associated with the pth waveguide. The function $\theta_p(z)$ is a "window" operator: it is equal to unity for $z_p < z < z_p + b$ and zero elsewhere. The sum over the n modes includes both propagating and evanescent ones. Evanescent TM modes must be included to ensure realistic boundary conditions at the waveguide mouth. Specifically, use of the evanescent TM modes permits the correct matching to the x-component of the electric field of the plasma wave. Since this incident electric field is polarized in the z-direction and coupling to the fast wave is neglected ($E_y = 0$),

excitation of the evanescent TE modes can be ignored. The coefficients α_{np} and β_{np} are the amplitudes of the incident and reflected nth mode fields in the pth waveguide, respectively. The waveguide wave vector of the nth mode is

$$k_n = (\omega^2/c^2 - n^2\pi^2/b^2)^{1/2} \quad . \tag{35}$$

Because of the assumption of infinitely high waveguides, there is no spatial variation of the fields in the y-direction; hence there are no m modes. With this approximation, we also note that in grills consisting of more than one row of waveguides, e.g. in the Alcator C and FT systems, adjacent rows do not couple to one another, and the theoretical analysis of these arrays is identical to that for a single-rowed grill. Because the incident wave is assumed to be in the fundamental TE_{10} mode, α_{np} vanishes for $n \neq 0$.

The assumption of infinitely high waveguides is not expected to introduce a large inaccuracy into the coupling calculation. Though rectangular waveguides launch a spectrum which is finite in n_y, the values of $|n_y|$ are limited to less than unity because of the minimum waveguide height required for fundamental mode propagation. The cutoff density for slow waves, given by

$$\frac{\omega_{pe}^2}{\omega^2} = 1 + \frac{n_y^2}{n_\parallel^2 - 1} \tag{36}$$

is almost unchanged by the inclusion of a small value of n_y except for values of $|n_\parallel|$ near 1, and the antenna reflectivity is essentially unaffected by the assumption of infinitely high waveguides. On the other hand, the antenna wave impedance is somewhat different for rectangular waveguides than for parallel plate guides. The impedance of a TE mode in

an evacuated waveguide is $Z_{TE} = -\omega/ck_{mn}$, while the impedance of a TM mode is $Z_{TM} = -ck_{mn}/\omega$, where k_{mn} is the wave vector of the mnth rectangular waveguide mode:

$$k_{mn} = (\omega^2/c^2 - m^2\pi^2/h^2 - n^2\pi^2/b^2)^{1/2} \quad . \tag{37}$$

Although the coupling physics is unchanged, the higher antenna impedance of the finite height grill reduces the edge density and density gradient required for good coupling, as will be shown later.

The matching of the antenna fields to the plasma fields is performed as follows: the forward and reflected waveguide fields at the grill mouth are matched to generalized vacuum fields in front of the grill (written in terms of Fourier integrals):

$$E_z(x,z) = \int_{-\infty}^{\infty} \frac{\omega}{c} [\sigma(n_\parallel)e^{ik_\perp x} + \rho\,(n_\parallel)e^{-ik_\perp x}]e^{i(\omega/c)n_\parallel z}\, dn_\parallel \tag{38a}$$

$$B_y(x,z) = \int_{-\infty}^{\infty} \frac{i\,(\omega/c)}{(n_\parallel^2 - 1)^{1/2}} [\sigma(n_\parallel)e^{ik_\perp x} - \rho\,(n_\parallel)e^{-ik_\perp x}]e^{i(\omega/c)n_\parallel z}\, dn_\parallel \tag{38b}$$

Here, $\sigma(n_\parallel)$ is the coefficient corresponding to the field incident on the plasma and $\rho\,(n_\parallel)$ the coefficient for the reflected field from the plasma. For a given $n_\parallel$, the field reflectivity of the plasma is

$$Y(n_\parallel) = \frac{\rho\,(n_\parallel)}{\sigma(n_\parallel)} \quad . \tag{39}$$

The vacuum region in front of the grill is employed as a mathematical convenience, and is usually assumed to have zero width. The vacuum wave fields are matched to the plasma fields of Eqs. (28) and (29). With the matching of the wave fields at the plasma-vacuum and vacuum-grill inter-

faces, the solution of the coupling problem is complete and the unknown quantities $\sigma(n_\parallel)$, $\rho(n_\parallel)$, and β_{np} are determined. The reflectivity of the pth waveguide is $|\beta_{op}|^2/|\alpha_{op}|^2$. The $n_\parallel$ spectrum of the rf power launched into the plasma is obtained from the Poynting flux in the x-direction at the plasma-vacuum boundary:

$$S_x(n_\parallel) = -\frac{c}{8\pi}\,\mathrm{Re}(E_z B_y^*) \tag{40}$$

$$= \frac{c}{4\pi}\,\frac{|\sigma(n_\parallel)|^2}{(n_\parallel^2 - 1)^{1/2}}\,\mathrm{Im}Y(n_\parallel)$$

where the Fourier transforms of expressions Eq. (38) for the vacuum fields have been used.

As indicated by Eq. (40), the calculated power spectrum becomes singular at $|n_\parallel| = 1$, and is zero for $|n_\parallel| < 1$ since waves in this spectral range are evanescent for $\omega_{pe}^2 > \omega^2$. By including the fast wave in the coupling analysis, Brambilla has shown that the calculated spectrum near $|n_\parallel| = 1$ predicts resonant eigenmodes resulting from repeated reflection of inaccessible waves between the fast/slow mode conversion layer and the fast and slow wave cutoffs [75]. However, the total power radiated in the inaccessible range is not significantly different from the simpler case in which only the slow wave is considered. Moreover, the narrow spectral features of the eigenmodes are likely to be smeared out by absorption and geometrical effects. Regardless of the details, we note that the singularity at $|n_\parallel| = 1$ can strongly influence the launched $n_\parallel$ spectrum unless the width of the grill in the z-direction is much longer than the typical parallel wavelength, i.e., for low values of the phase angle $\Delta\phi$ or for grills with fewer than four elements. The accessibility of the low $n_\parallel$ portion of the spectrum to the plasma core is poor.

3.5.1 Numerical Analysis

The numerical scheme by which the matching of the antenna and plasma fields is performed may be summarized as follows [3]. The waveguide electric fields are matched to the vacuum fields across the whole face of the grill, i.e., across the waveguide openings and waveguide walls. The grill is assumed to be embedded in a conducting wall which is flush with the mouth of the waveguides. Thus E_z is zero everywhere in the coupling plane except in front of the waveguides. The waveguide magnetic fields can only be matched to the vacuum fields in front of the waveguide openings, as currents can flow in the septi between waveguides and in the conducting plane to either side of the array. Depending on the desired accuracy of the calculation, the number of evanescent modes retained in the numerical calculation is typically limited to 3 or 4. However, for a rough estimate of the reflection coefficient and the power spectrum, it is sufficient to keep only the fundamental mode in the analysis.

To provide physical insight into the computed predictions of the antenna reflectivity, the conditions for optimal coupling can be estimated analytically for a number of limiting cases. For simplicity, the rf power spectrum launched by the grill is replaced by a single representative $n_\parallel$ value ($|n_\parallel| > 1$) which is determined by the antenna dimensions and the relative waveguide phasing. The plasma fields are matched directly to generalized antenna fields of impedance Z_0. For this analytic treatment, only the fundamental TE_{10} waveguide mode is considered; therefore from Eqs. (33) and (37) the antenna impedance is simply

$$Z_0 = - [1 - (c\pi/\omega h)^2]^{-1/2}. \qquad (41)$$

Note that typically $h \simeq 0.8\lambda$ and hence $Z_o \simeq -1.2$. For comparison, $Z_o = -1.0$ for parallel plates of infinite extent. The cases considered below are: $|u_o| \gg 1$ with $u_o < 0$; $|u_o| < 1$; and $|u_o| \gg 1$ with $u_o > 0$, where u is given by Eq. (26).

The case of $|u_o| \gg 1$ and $u_o < 0$, which is valid for $n_\parallel^2 \gg 1$ and $\mu \gg 1$, corresponds to the presence of an overdense plasma at the grill mouth. The appropriate asymptotic expansions for the Airy function solutions are [80]

$$-iAi(u_o) + Bi(u_o) \cong \pi^{-1/2}|u_o|^{-1/4}\exp\left(-i[2/3\ |u_o|^{3/2} + \pi/4]\right) \tag{42a}$$

$$-i\frac{dAi(u_o)}{du} + \frac{dBi(u_o)}{du} \cong i\pi^{-1/2}|u_o|^{1/4}\exp\left(-i[2/3\ |u_o|^{3/2} + \pi/4]\right). \tag{42b}$$

This approximation is equivalent to that of WKB validity at the grill mouth, i.e., the inequality (23) is satisfied. In this limit, the plasma wave impedance is

$$Z_p \simeq -\left[\frac{(n_\parallel^2 - 1)}{(\mu - 1)}\right]^{1/2}. \tag{43}$$

In the high density approximation the quantity Z_p/Z_o is real and positive, and is independent of the density gradient. Optimal coupling for a given value of $n_\parallel$ is predicted for $Z_p/Z_o = 1$, or for [77,78]

$$\mu = 1 + [1 - (c\pi/\omega h)^2](n_\parallel^2 - 1). \tag{44}$$

This relationship determines the density at the grill mouth, $n_o = \mu n_c$ for perfect matching for a given value of $n_\parallel$. Non-zero antenna reflectivity in this idealized model is due to the finite width of the spectrum. Clearly, the dependence of the minimum reflectivity condition on the

launched $n_\parallel$ spectrum is strong. The optimal density increases with $n_\parallel^2$; thus for best coupling at $\Delta\phi = 180°$ we expect the grill position to be at a higher density than for lower phase angles between waveguides. Furthermore, we note that if the grill is moved further into the plasma from the optimal coupling position for the dominant $n_\parallel$ value, the plasma impedance decreases and the reflected signal is, in this ideal approximation, 180° out of phase with the incident power. Conversely, if the grill mouth is retracted to a density lower than the optimal one, the plasma impedance becomes higher, and the reflection coefficient is in phase with the incident signal. Thus the phase of the reflected power in the antenna is expected to undergo a significant shift as the antenna is moved through the optimal coupling position.

The original Brambilla theory [3] was performed in the limit of $|u_o| \ll 1$ corresponding to $\mu \approx 1$. In this limit, we use the series expansions for the Airy functions, keeping only the lowest order terms [80]:

$$-iAi(u_o) + Bi(u_o) \approx 2 \frac{3^{-2/3}}{\Gamma(2/3)} e^{-i\pi/6} \tag{45a}$$

$$-i \frac{dAi(u_o)}{du} + \frac{dBi(u_o)}{du} \approx 2 \frac{3^{-4/3}}{\Gamma(4/3)} e^{i\pi/6}, \tag{45b}$$

where Γ is the Gamma function. The plasma impedance is then [5]

$$Z_p = - \frac{\Gamma(4/3)}{\Gamma(2/3)} (9\omega L/c)^{1/3} (n_\parallel^2 - 1)^{2/3} e^{-i\pi/6}. \tag{46}$$

The impedance is partially reactive, and an ideal match cannot be obtained for any value of $n_\parallel$. As before, however, an optimal coupling condition

can be found. The reflection coefficient is minimized for $|Z_p/Z_o| = 1$, or for

$$\frac{dn}{dx} = \left[\frac{\Gamma(4/3)}{\Gamma(2/3)}\right]^3 \left(\frac{9m_e\omega^3}{4\pi ce^2}\right) [1 - (c\pi/\omega h)^2]^{3/2}(n_\parallel^2 - 1)^2 \qquad (47)$$

The density gradient required for good coupling in this approximation is also strongly dependent on the value of $n_\parallel$.

Finally, for the case of $u_o > 0$, $|u_o| >> 1$ (grill density near zero and shallow density gradients), the appropriate asymptotic expansions of Bi and dBi/du give the following results [80]:

$$- iAi(u_o) + Bi(u_o) \simeq \pi^{-1/2} u_o^{-1/4} \exp(2/3\, u_o^{3/2}) , \qquad (48a)$$

$$- i \frac{dAi(u_o)}{du} + \frac{Bi(u_o)}{du} \simeq \pi^{-1/2} u_o^{1/4} \exp(2/3\, u_o^{3/2}) , \qquad (48b)$$

and the plasma impedance is

$$Z_p \simeq - i(n_\parallel^2 - 1)^{1/2}. \qquad (49)$$

In this limit, the antenna is totally reflective because of the purely reactive impedance. To summarize the three limits, the best coupling should be achieved in the first case for which the grill mouth is situated in an overdense plasma.

3.5.2 Examples

Computed $n_\parallel$ spectra of the power radiated into the plasma are shown in Fig. 12 for the grills used in lower hybrid experiments on the Versator II and Alcator C tokamaks. The spectra illustrated in Fig. 12a are those

excited by the Versator four waveguide grill. The waveguides are 2.45 cm wide, 24 cm high, and separated by 0.6 cm thick walls. The rf frequency is 800 MHz. The incident power is taken to be identical in each guide. The $n_\parallel$ spectra shown are calculated for relative phase angles between adjacent waveguides of $\Delta\phi = 0°$, 90°, and 180°. For this example, we have taken the density gradient to be $\nabla n = 5.3 \times 10^{11} cm^{-4}$ and density at the grill mouth to be $n_o = 8 \times 10^{10} cm^{-3}$ (ten times overdense). The Versator plasma is relatively cold ($T_e \simeq 400$ eV, $T_i \simeq 150$ eV) by major tokamak standards, and the power spectrum was designed to peak near $n_\parallel \simeq 5.5$ for $\Delta\phi = 180°$. In Fig. 12b, the corresponding $n_\parallel$ spectra of the four waveguide Alcator C grill are depicted. The frequency is 4.6 GHz, and the waveguide dimensions are 0.8 cm in width and 5.75 cm in height. The septa between waveguide openings are 0.2 cm thick. The assumed density gradient is $\nabla n = 1.3 \times 10^{13} cm^{-4}$ and the density at the grill-plasma interface is $n_o = 2.6 \times 10^{12}\ cm^{-3}$ (also ten times overdense). The $n_\parallel$ spectra for the Alcator experiment are characterized by lower values of the parallel wavenumber than those for the Versator grill since the Alcator plasma is considerably hotter ($T_e \simeq 1.5$ keV, $T_i \simeq 1.0$ keV) than that of Versator. The spectrum of the Alcator grill for $\Delta\phi = 180°$ exhibits a fundamental peak near $n_\parallel = 3$. As with the Versator grill, this peak corresponds to the peak in the Fourier spectrum of the antenna electric fields that one would expect from the grill geometry (see Eq. 17). For $\Delta\phi = 90°$, the power spectra are asymmetric in $n_\parallel$, with approximately 70% of the power flowing in the positive z-direction and the remainder in the opposite direction. Consequently, this phasing is suitable for current drive experiments. Also note that the power flowing in the positive z-direction is represented by relatively low $n_\parallel$ values characteristic of

the grill geometry, while the power in the negative direction is radiated in satellite bands at higher values of $n_\parallel$. The presence of the sidebands in the spectrum results from the square wave, or gap, excitation of the rf fields at the plasma surface. As the current drive efficiency is predicted to be proportional to $1/n_\parallel^2$, the effect of a significant fraction of the incident rf power radiated with relatively high $n_\parallel$ values in the "wrong" direction may not be serious. In fact, a toroidal wave propagation analysis predicts that the higher $n_\parallel$ values launched in the negative z-direction are absorbed near the plasma surface [7]. For the Alcator C current drive experiment with typical plasma parameters of a central density of $n_{eo} = 1 \times 10^{14} cm^{-3}$ and a toroidal field of $B_o = 8$ T in deuterium, the critical value of $n_\parallel$ for accessibility to the center is 1.43. For the current drive spectrum illustrated in Fig. 12b ($\Delta\phi = 90°$), approximately 38% of the spectrum in the positive z-direction, or 24% of the total radiated power, is inaccessible to the plasma center. The critical value of accessibility can be lowered by increasing the toroidal field: for the same central density as above and a toroidal field of 10 T, the value of $n_{\parallel crit}$ is reduced to 1.32, and only 19% of the total power is inaccessible. The current drive efficiency, referenced to the total power injected into the plasma, may then be expected to be higher for this latter case. Indeed, this has been observed experimentally on the Alcator C tokamak [65].

For $\Delta\phi = 0°$, the $n_\parallel$ spectra shown in Fig. 12 are again symmetric and, as expected, concentrated near $|n_\parallel| = 1$. A large fraction of the launched power is inaccessible, and as we will see shortly, the reflectivity of the grill is high because the electric field spectrum of the grill is concentrated near $n_\parallel = 0$. Consequently, this phasing is rarely used in heating experiments.

The inaccessible part of the spectrum can be reduced by several methods. The number of waveguides in the grill may simply be increased while keeping the periodicity, or individual waveguide width, constant. The power spectra at $\Delta\phi = 90°$ for two, four, eight, and sixteen waveguide grills for Alcator C parameters is shown in Fig. 13. As expected, the power spectrum is narrower for grills with more waveguides. At 10 T, the inaccessible fraction of the total power in each case is 21%, 19%, 15%, and 4% respectively. However, the total grill width is usually limited by the available port size, hence the number of waveguides in the grill is often fixed by port geometry considerations. As mentioned earlier, the number of waveguides could be effectively increased by adding passive waveguides to the sides of the active array. The dummy waveguides could be mounted on the vacuum vessel wall to either side of the port opening such that they would not add to the width of the hardware which must be able to fit through the port. Alternatively, the fraction of power radiated in the low $n_\parallel$ portion of the spectrum can be reduced by increasing the incident power in the central waveguides relative to that in the outer ones [81]. For the Alcator C four waveguide grill phased at $\Delta\phi = 90°$ and plasma parameters such that $n_{\parallel crit} = 1.32$, the inaccessible fraction is reduced from 19 to 16% of the total radiated power if the incident power in each of the outer two waveguides is one-fourth the power in each of the central two. However, for a given maximum power in a waveguide, the total power injected into the tokamak is reduced compared to the usual case of equal powers in each waveguide. Since the maximum power carried in a waveguide is usually limited by rf breakdown, the power which can be coupled to the plasma is always smaller for this technique of unequal powers; consequently, it is rarely used in present

day experiments. We also remark that the calculated directionality of the antenna is not significantly changed by the above techniques to obtain a narrower $n_\parallel$ spectrum. Generally though, we conclude that the predicted $n_\parallel$ spectra launched by the waveguide grill satisfy the general requirements of the lower hybrid antenna described in Section 3.3.

We consider next the predicted coupling efficiency of the waveguide grill. In Fig. 14, the calculated reflectivity of a four waveguide grill with the same dimensions as that in Fig. 12b is plotted versus the density at the waveguide mouth for several different values of the density gradient. The phase is taken to be $\Delta\phi = 180°$. As predicted earlier, the reflectivity is seen to be relatively insensitive to the value of the density gradient when the grill mouth is located in an overdense plasma. More importantly, the reflectivity exhibits a broad minimum, indicating that good coupling should be relatively easy to achieve in practice.

The reflectivity versus density at the grill mouth is plotted in Fig. 15 for $\Delta\phi = 0°$, 90°, and 180°. The antenna reflectivity for $\Delta\phi = 0°$ is predicted to be relatively high for all densities, as the electric field spectrum of the grill is similar to that for a single waveguide, i.e., peaked near $n_\parallel = 0$, and plasma waves with such parallel wave numbers are evanescent in the plasma. The optimal coupling density is higher for $\Delta\phi = 180°$ than for $\Delta\phi = 90°$, which is in accordance with the prediction of Eq. (44).

A scan of the reflectivity versus phase angle between waveguides is illustrated in Fig. 16. The plasma density at the grill mouth is taken to be five times overdense and the density gradient is $6.6 \times 10^{12} cm^{-4}$. The reflectivity exhibits a minimum near $\Delta\phi = 135°$, which agrees well with the analytic estimate of $\Delta\phi = 145°$ given by Eqs. (17) and (44).

In conclusion, the multi-waveguide grill can be expected to launch $n_\parallel$ spectra which largely satisfy the accessibility criterion $n_\parallel^2 > n_{\parallel crit}^2$. The coupling theory predicts that there exists an optimal coupling position for the grill at densities typical of scrape off layer plasmas, and that this coupling position is not overly sensitive to variations in the edge density or its gradient.

3.5.3 Validity of the Model

Before turning to the experimental results and their comparison with the coupling theory, we briefly discuss some of the limitations of the coupling theory presented. Thus far, the effect of plasma curvature, both in the poloidal and toroidal directions, has not been included in the analysis. We can expect that the plasma curvature in the poloidal direction does not significantly change the calculated coupling efficiency as the rf power in a rectangular waveguide is peaked on the midplane. Moreover, in experiments for which the grill height is comparable to the plasma diameter, the grill mouth is usually contoured to conform to the outer surface of the plasma; therefore the plasma density at the grill mouth is nearly uniform along the poloidal extent of the grill.

The effect of toroidal curvature on the coupling should also be small. Because the coupling is not extremely sensitive to variations in the density in front of the waveguide, the small difference in density from one waveguide mouth to the the next ($\Delta n \approx b^2/R_o \; dn/dx$ where R_o is the major radius of the outer wall of the tokamak) should not significantly affect the coupling. Furthermore, the mouth of the grill can easily be contoured in the toroidal direction to conform to a constant density, as illustrated in Fig. 6a.

Though the density gradient in the edge plasma has been taken to be linear in the plasma model, the edge density profile in most tokamaks has been found to be roughly exponential, and can be expressed in the form

$$n = n_o e^{-x/\ell} \tag{50}$$

where n_o is the density at the grill mouth, and ℓ is the density scale length. The value of ℓ is obtained from density profile measurements. The result is usually consistent with the simple analytic estimate

$$\ell \approx (\Delta L D_\perp / c_s)^{1/2} \tag{51}$$

where ΔL is the toroidal separation between limiters, c_s is the local ion sound speed, and $D_\perp$, the particle diffusion coefficient in the edge plasma, is given by Bohm diffusion. Typical values of ℓ range from 0.2-1 cm. Bellan and Porkolab have solved the wave equation for the slow wave in an exponential gradient [82], and the solution of the waveguide coupling problem for such a profile has been obtained by Romanelli and Santini [83]. The reflection coefficient differs by less than 15% from the value calculated using the linear gradient. This finding is not surprising, as we have seen that the coupling is relatively insensitive to the gradient, especially when the grill is located in an overdense plasma for optimal coupling.

Nonlinear processes in the edge plasma, e.g., modification of the density gradient in front of the grill due to the ponderomotive force have been considered by a number of workers [84-90]. In these treatments, the ponderomotive force due to high power rf injection is predicted to depress, or in some cases, spatially modulate the plasma density at the grill mouth. Nonlinear effects are expected to become important if the rf energy density becomes comparable to the local plasma energy density

$$\frac{E_{rf}^2}{8\pi n(T_e+T_i)} \approx O(1) \ . \qquad (52)$$

Numerical results show that the reflectivity increases when the ponderomotive force becomes significant, as the plasma is pushed away from the grill mouth along the field lines. The radiated $n_\parallel$ spectrum is also modified. However, experimental observations during high power grill coupling on tokamak plasmas have not yet provided conclusive evidence for such nonlinear modifications of the coupling. Since typically $n_{wgd} \sim 10\ n_c$, $E_{rf}^2 \ll 8\pi n\ (T_e + T_i)$ and hence the experimental findings are not surprising. Furthermore, ionization of residual gas by the strong rf fields in the scrape-off layer could easily fill up the density cavities in front of the grill mouth. We will discuss the experimental results in more detail in the next section, but it appears that the linear theory of coupling adequately represents the rf coupling physics of present-day lower hybrid heating experiments.

3.6 Experimental Coupling Results

In general, results obtained from experimental studies of lower hybrid wave coupling and propagation are in relatively good agreement with the theory of lower hybrid wave launching discussed in the last sections. Measurements performed on linear plasma machines have shown that slow electrostatic waves are indeed launched by waveguide grills and other such slow wave structures, as measured directly with rf probes in the plasma [29,42,91-94]. Measurements of the parallel wavenumber are more difficult to make in tokamak plasmas because probes cannot be used in the plasma interior; however, laser scattering techniques have been utilized recently for detecting the density fluctuations associated with lower

hybrid waves propagating within the plasma, and the $n_\parallel$ spectrum of the waves may be inferred from these measurements [95-99]. Regarding the coupling efficiency of lower hybrid antennas, the results from many experiments indicate that the waveguide grill exhibits reflection coefficients which are also in reasonable agreement with the theoretical predictions. Maximum coupling efficiencies in the range 85-95% have been relatively easy to achieve in practice.

3.6.1 Coupling Experiments on Small Devices

The basic aspects of lower hybrid wave propagation were first investigated in small plasma machines. Fisher and Gould verified the existence of resonance cones for electron plasma waves [9]; Briggs and Parker showed that lower hybrid waves, which represent the low frequency end of the electron plasma wave branch, also propagate along resonance cones [91]. In both of these experiments, the waves were excited by a point, or dipole, source which launches a very broad spectrum of $n_\parallel$ values. Bellan and Porkolab experimentally verified the lower hybrid wave dispersion relation by launching waves with well-defined values of $n_\parallel$ (and hence $n_\perp$) [29]. The rf antenna in their study was a slow wave structure periodic in the z-direction consisting of a set of rings mounted on the vacuum vessel wall. The rings were actively driven by an rf source; the relative phase between the adjacent rings was $\Delta\phi = 180°$. Probe measurements confirmed that waves with wavelengths defined by the dimensions of the slow wave antenna were indeed launched into the plasma.

Multi-waveguide grill coupling was first investigated by Bernabei et al. [92] on a linear plasma device. The theoretical predictions of the launched $n_\parallel$ spectrum and coupling efficiency of waveguide grills were borne out by this study and subsequent studies. In this experiment, electron plasma waves ($\omega >> \omega_{LH}$) were launched by a two-waveguide grill with the waveguides excited 180° out of phase with one another. The dominant $n_\parallel$ value of the grill was calculated to be about 2.2, while the $n_\parallel$ value measured with probes in the plasma was 2.1. There was little evidence of a surface wave propagation along the plasma periphery in this case; thus a large fraction of the incident rf energy was coupled into electrostatic plasma waves. When the grill was withdrawn a small distance from the chamber wall, the reflectivity was found to increase and evidence of a surface wave was detected, indicating that the evanescent layer in front of the antenna indeed regulates the coupling efficiency and influences the launched $n_\parallel$ spectrum.

Further confirmation of the grill coupling behavior was provided by Bernabei et al. [93] and Motley et al. [94]. The coupling efficiency of single, double, and quadruple waveguide arrays were investigated and found to be in reasonable agreement with the Brambilla calculations for input power densities up to 0.1 kW/cm^2. In Fig. 17 the measured reflectivity of a double waveguide array is plotted versus $\Delta\phi$, and is seen to compare favorably with the theoretical prediction. The directionality of the phased array was verified with the quadruple array. The phase between waveguides was set to $\Delta\phi = 60°$, and rf probe measurements on opposite sides of the antenna along the z-axis showed a 5 dB asymmetry in the received power. For a two-waveguide grill, plasma waves were found to be excited most efficiently for an adjacent waveguide phasing of $\Delta\phi = 180°$;

for $\Delta\phi = 0°$, the resonance cone as detected by probes was absent and the grill reflectivity was high. Interferometric measurements with probes showed the penetrating plasma waves to be of short wavelength ($n_\parallel = 2\text{-}2.5$) and the surface waves to have longer wavelengths ($n_\parallel \simeq 1$). The accessibility condition was verified by lowering the magnetic field; below a threshold value of the field, little of the wave power of the twin waveguide grill ($n_\parallel \lesssim 3$) satisfied the accessibility condition, and the ratio of the detected surface wave signal to the penetrating wave signal was found to increase strongly with decreasing magnetic field. It is interesting to note that in this experiment, the antenna reflectivity did not change significantly as the magnetic field, and hence the accessibility condition, was varied. This result provides confirmation of the conjecture that the lower hybrid wave coupling depends only on the $n_\parallel$ spectrum of the antenna and the evanescent region immediately in front of the waveguide and is insensitive to reflections occurring further in the plasma.

Motley et al. [42] have compared the performance of a two-waveguide array with that of a six-waveguide array with the same waveguide width (i.e., two grills with the same axial periodicity but different numbers of radiating elements). The amplitude of the surface wave component radiated by the six-waveguide grill was found to be about a factor of 3 below that for the two-waveguide grill, indicating that the $n_\parallel$ spectrum was indeed narrower and better defined by the former than the latter. In this experiment, only the central two waveguides of the six-waveguide array were actively fed; the outer two elements on each side were passive waveguides, each one-quarter wavelength long and electrically shorted at the rear, as shown in Fig. 7. In this manner, the rf power coupled into a dummy waveguide is re-emitted 180° out of phase, and the grill is

similar to a six-waveguide array phased at $\Delta\phi = 180°$ with reduced powers in the outer waveguides. Regardless of the details, it is clear from the experimental data that the $n_\parallel$ spectrum launched into the plasma is indeed narrower for grills with more waveguides, as predicted by the coupling theory.

Nonlinear effects due to high power injection have been studied in several experiments on linear machines [100,101]. With the injection of sufficient rf power, $(E_z^2/8\pi nT \approx 1)$, the plasma density in the thin layer (width $\approx$ 5 mm) immediately in front of the grill was depressed below the value several centimeters away from the antenna along the magnetic field [100], in accordance with nonlinear coupling theories. Convective eddies due to local heating in front of the grill have also been observed, and gave rise to asymmetric up-down density profiles facing the antenna [101]. For normal operating gas pressures, however, the reflectivity of the antenna did not increase as the power was raised, as increased ionization and cross-field convection during the rf pulse were found to increase the average plasma density in the vicinity of the grill. Consequently, though nonlinear coupling effects are indeed observed, their relation to tokamak experiments is not straightforward because of other factors affecting the density in front of the antenna.

3.6.2 Lower Hybrid Coupling Experiments on Tokamaks

Similarly to the linear machine studies described above, coupling measurements performed during high power lower hybrid heating experiments on tokamaks have shown that the grill exhibits good impedance matching to the plasma and that the coupling is reasonably well described by the

Brambilla theory. Though this result is not surprising, it was not considered unlikely that lower hybrid wave launching into toroidal plasmas could prove to be somewhat different than that observed on small linear machines. In particular, the edge plasma in a tokamak is known to be turbulent, with density fluctuation levels of $\delta n/n$ = 5-100% being typical [102-104]. It is possible that these density fluctuations could scatter the incident lower hybrid wave and reflect a significant fraction of rf power back into the antenna. Furthermore, the ($n_\perp$, $n_\parallel$)spectrum launched by the antenna may be altered by scattering from density fluctuations with significant n_θ components [105-107]. Subsequent modifications by toroidal effects and magnetic shear could substantially change the initial $n_\parallel$ spectrum [7,108-113]. Thus the wave spectrum reaching the damping region may be significantly different from the calculated Brambilla spectrum. Consequently, optimization of the grill design for devices with strong toroidal features, i.e., low aspect ratio, and with significant edge turbulence may be difficult.

Reflectivity Measurements

Results from grill coupling experiments performed at relatively low powers ($P_{rf} \lesssim 10$ kW) have been found to be in reasonable agreement with the Brambilla theory. Depending on the density gradient in front of the waveguides, the antenna reflectivity exhibits a maximum for $\Delta\phi = 0°$ and a minimum for $\Delta\phi$ = 90°-180°. For comparison of the measured reflectivities with the theoretical predictions, measurement of the density profiles in front of the antenna have been performed in a number of tokamaks. The density gradient in Alcator C has been measured with moveable probes attached above the grill [33], in PLT with a probe placed in an adjacent

port [114], and in Versator II with probes inserted through the waveguides (with no rf applied) [115]. Microwave interferometry has also been used on Wega and Petula to measure line-averaged density of the plasma in front of the grill during rf injection [40,116]. In general, quantitative comparisons of the theoretical and experimental coupling coefficients versus density gradient were not particularly good when the original Brambilla theory (zero density at the waveguide mouth) was used. However, experimental measurements of the density in the vicinity of the waveguide mouth showed the plasma to be overdense ($\omega_{pe}^2 >> \omega^2$). With the inclusion of a finite density step in the plasma model, the calculated and measured reflectivities have been found to be in fair agreement for most experiments in which the edge density profile was measured. In Fig. 18, the experimental reflectivity of the Versator grill for $\Delta\phi = 0°$, 90°, and 180° is plotted versus the position of the antenna. The horizontal axis represents the location of the grill face along the major radius of the tokamak; the plasma density increases to the left in the figure. The calculated reflectivities represented by dashed lines are also shown in the figure. The density and density gradients in front of the grill were measured by probes in the absence of rf power. For $\Delta\phi = 90°$ and 180°, the calculated coupling behavior is similar to the observed coupling. Both experimental and theoretical reflectivities exhibit minima near the same location, and as expected, the minimum for $\Delta\phi = 90°$ occurs at a lower density than for $\Delta\phi = 180°$. For $\Delta\phi = 0°$, the correspondence between the calculated and observed coupling is not as good, although both are seen to be higher than that for the other two phasings. However, we remark that the coupling theory is not expected to be valid for this phasing, as coupling to the fast wave may be significant. Moreover, with the larger surface wave

component expected to be launched for $\Delta\phi = 0°$ the details of the port geometry near the waveguide (gaps between the grill and port walls, nearby limiters, etc.) can be expected to influence the coupling. For the other phasings, however, the observed reflectivity is quite similar to that calculated from the Brambilla model.

A comparison of individual waveguide reflectivities for $\Delta\phi = 180°$ from the Petula B experiment is shown in Fig. 19. Again, there exists a qualitative similarity between the data and the theoretical calculation. Coupling experiments on Wega in which only the central waveguides of the grill were fed (to better simulate the boundary conditions in the theoretical model) also obtained good agreement with the Brambilla calculations [117]. Moreover, the phase of the reflected signal was measured in the Wega coupling experiment, and was observed to undergo a large phase shift as the grill was moved through the optimal coupling position. This indicated that the grill was indeed coupling into an overdense plasma in which the wave impedance was resistive (see Eq. 43). In summary, the modified coupling theory appears to explain the observed grill-plasma coupling behavior on tokamaks. It is possible that the density step modification was not needed in the basic verification of the coupling theory performed on linear machines. In particular, in these low density experiments the frequency used (2.45 GHz) was high so that $\omega >> \omega_{LH}(o)$, and therefore the plasma densities at the waveguide mouth were not overdense. It is worth noting that early versions of the coupling theory predicted that the grill could not couple well to waves of high $n_\parallel$ because of the surface evanescence; however, with the verification of the modified Brambilla theory, the conclusion is that it is possible to efficiently launch waves of any $n_\parallel$ excited by the antenna by merely adjusting the position of the grill within the edge density profile.

In high power rf experiments performed on tokamaks to date, little clear evidence of nonlinear grill coupling efficiency due to ponderomotive effects has been noted. Although nonlinear coupling behavior has been reported in some studies [38,118], rf breakdown may have been responsible for the variation in grill reflectivity with incident rf power [55]. In lower hybrid experiments on Alcator C, the rf power was varied such that the power density ranged from .05 W/cm^2 to 9 kW/cm^2, and no significant difference in the coupling efficiency over this span was observed [33]. Similar results were obtained on Petula B up to a power density of 3.4 kW/cm^2 [59] and on Alcator A up to 4.5 kW/cm^2 [37]. These findings are perhaps not surprising as the edge densities in tokamaks are relatively high; hence the quantity $E^2/8\pi nT$ is substantially less than unity even at the highest power densities achieved. In addition, strong ionization of the background neutral gas in the presence of rf power may maintain relatively high densities at the waveguide mouth, as suggested by the results obtained on a linear device [100].

Measurements of the $n_\parallel$ Spectrum

As mentioned earlier, measurement of the $n_\parallel$ spectrum launched by the grill into a tokamak plasma is more difficult than in a linear, steady-state machine. Moreover, toroidal ray tracing and wave scattering theories predict that the launched $n_\parallel$ spectrum of the antenna may be substantially modified during wave propagation towards the plasma interior. However, there is substantial indirect evidence to suggest that, at least near the plasma edge, the grill indeed launches the $n_\parallel$ spectrum predicted by the Brambilla theory and that the launched spectrum shifts in the proper direction when the waveguide phasing is altered. For example, since the grill reflectivity depends

strongly on the $n_\parallel$ spectrum of the waves excited by the antenna (see Eq. 43), the qualitative agreement between theory and the experimentally observed coupling efficiency suggests that the grill launches the predicted wave number spectrum. Furthermore, the directionality of the grill antenna has been verified in a number of rf current drive experiments: the current drive efficiency was found to be much higher with the grill phased to launch waves in the direction of the electron ohmic drift rather than in the opposite direction [54,61]. The effect of changing the waveguide widths to alter the $n_\parallel$ spectrum for a given phasing has been checked on a number of tokamaks. In particular, experiments on Wega showed that when a grill with relatively wide waveguides ($n_\parallel$(typ.) $\simeq$ 3 for $\Delta\phi = 180°$) was exchanged for one with narrower waveguides ($n_\parallel$(typ.) $\simeq$ 6 for $\Delta\phi = 180°$) the lower hybrid waves were found to interact with lower energy ions in the latter case [39]. A similar effect was observed in the Versator experiment [115]. These findings are consistent with slower waves being launched by the narrower waveguide grill, which is to be expected from the general coupling theory.

The most definitive measurements of the launched wave spectrum were carried out recently by using microwave and laser scattering techniques. In these experiments, the perpendicular wave vector of the lower hybrid wave is measured by the scattering of an incident microwave or laser beam from density fluctuations associated with the lower hybrid wave. The beam passes through the poloidal plane of the tokamak. The parallel wave number is inferred from this measurement and from the use of the lower hybrid dispersion relation, for which the plasma density in the scattering region must be known. Lower hybrid waves have been detected by 2mm microwave scattering on the Versator [119] and Wega [120] tokamaks. On

the Alcator A [95,96] and C [97,98] tokamaks and on the ACT-1 toroidal device [99] the wave spectrum of lower hybrid waves was actually measured by CO_2 laser scattering techniques. A spectrum measured by CO_2 laser scattering in the Alcator C tokamak is shown in Fig. 20. The scattering volume for this measurement was a vertical chord through the plasma located at a radius of 0.7 a_L to the outside of the magnetic axis, where a_L is the limiter radius. The $n_\parallel$ values were obtained from the $n_\perp$ measurements by assuming the scattering volume to be located near the midplane, i.e. at the maximum density along the vertical chord. The calculated Brambilla spectrum exhibits good agreement with the experimental data, confirming that the correct spectrum is indeed launched by the grill into a tokamak plasma.

3.6.3 Conclusion

In summary, the results of low power coupling experiments have demonstrated that lower hybrid waves can be launched efficiently by grill couplers and other types of antennas without resorting to external tuning hardware. The grill antenna has proven to be a versatile and convenient means of coupling to lower hybrid waves: the launched spectrum can be varied by simply changing the phase angle between adjacent waveguides and the coupling efficiency can be maximized by the appropriate placement of the grill mouth within the edge density profile. Although the grill is strongly coupled to the plasma, both the calculated and experimentally observed reflectivities are only weakly dependent on the value of the density at the grill mouth. Consequently, it is generally not difficult to achieve a low antenna reflectivity for a variety of discharge conditions

even if the plasma parameters evolve during the shot. Therefore, "mode-tracking" to maintain good coupling efficiency has not been required in any experiment to date, and is not envisioned to be necessary for future ones.

3.7 High Power Operation of the Grill and Rf Breakdown

Although the grill has been shown experimentally to couple well to the plasma even at high power levels, rf breakdown in the evacuated portion of the grill was observed in most experiments to cause sudden jumps in the reflectivity. Such problems appear to be endemic to waveguide couplers in which all or part of the antenna is open to the vacuum chamber. The elimination of these breakdown problems is a major concern for grill design and construction.

In lower hybrid antenna systems, two types of breakdown are distinguished. The first is characterized by sudden ($\Delta t \lesssim 10$ μsec) increases in individual waveguide reflectivities. This breakdown is associated with arcing in the waveguides which may be due to either a series arc between two sections of a waveguide wall which have a poor electrical contact between them, or more commonly, due to an arc across the waveguide. Examination of the arc tracks show that the arcs travel back toward the vacuum window. The ceramic windows may be damaged as a consequence of metallic deposition due to arcing, and continued high power operation may not be possible. In most lower hybrid systems, the formation and propagation of arcs is inhibited by an arc detector circuit which automatically shuts off the rf power in the event of a sudden increase in reflectivity in any of the waveguides.

The more common occurrences of breakdown are related to plasma formation within the evacuated waveguides, both during operation into vacuum and into the tokamak plasma. The formation of plasma in the waveguides is inferred from the observed variations in the reflected power and phase during the rf pulse. The reflected phase typically shifts in the negative direction over a multi-hundred microsecond time scale when breakdown and plasma formation take place. These gradual shifts in the reflected phases are interpreted as a change in the dielectric constant of the waveguide due to an increasing plasma density within the waveguides. Unlike arcs, the plasma generated during the rf pulse does not appear to damage the antenna; however, power transmission of the grill is reduced by the presence of this waveguide plasma, and phase control is lost.

In the last several years, a great deal of progress has been made in the understanding of rf breakdown in this application. The high power coupling results of early lower hybrid heating experiments and subsequent breakdown investigations performed on rf test stands under controlled conditions have shed light on the processes contributing to rf breakdown [121-130]. The results obtained from these studies have aided in the design of modern grill couplers capable of operating reliably at relatively high power densities.

It has long been known that the plasma formation observed in lower hybrid antennas is related to the surface condition of the walls of the evacuated waveguides. The processes by which the waveguide plasma is created are likely to be electron multiplication by secondary electron emission (SEE), electron-stimulated desorption (ESD) of contaminants on the waveguide walls, and impact ionization of the residual neutral gas in

the waveguides. The power to maintain the discharge is supplied by the oscillatory energy of the electrons in the rf electric field in the evacuated portion of the waveguides between the vacuum windows and the antenna mouth. The maximum kinetic energy of these electrons is

$$\varepsilon_e = \frac{e^2E^2}{2m\omega^2} \tag{53}$$

where E is the peak rf electric field in the waveguide. In several lower hybrid antenna systems on tokamaks, the vacuum windows are located up to several meters from the vacuum vessel. In this case, the electron cyclotron resonance layer due to the magnetic fields of the tokamak must be within the evacuated part of the antenna. At or near the resonance, electrons will gain energy at the expense of the rf electric field. The typical energy with which an electron strikes the wall is [36]

$$\varepsilon_e = \frac{e^2E^2}{2m\omega^2}\left[\frac{\cos^2\alpha}{(1+\nu^2/\omega^2)} + \frac{\sin^2\alpha}{2}\left(\frac{1}{(1-\omega_{ce}/\omega)^2+\nu^2/\omega^2} + \frac{1}{(1+\omega_{ce}/\omega)^2+\nu^2/\omega^2}\right)\right] \tag{54}$$

where α is the angle between the magnetic field and the rf electric field, and ν is the electron-wall collision frequency (this being the largest electron collision frequency to this physical situation). During rf injection into the tokamak plasma, the presence of electron cyclotron resonance in the guides enhances the plasma formation because electrons gain energy above their maximum rf oscillatory energy, increasing the magnitude of both SEE and ESD.

The source of electrons to initiate the breakdown is the waveguide wall. If the secondary electron emission coefficient, δ (defined as the ratio of the number of secondary electrons escaping the surface to the number of incident electrons) of the wall is greater than one, as is usually the case for most metals without extensive surface cleaning, electron multiplication will occur as electrons accelerated in the electric field strike the wall. As the secondary electron emission coefficient is an increasing function of electron impact energy up to 400-500 eV for all impact angles relative to the waveguide surface [131,132], SEE increases with the incident rf power. The threshold level of the rf power at which electron loading effects are noted is probably determined by the multipactor phenomenon [133-135]. Multipactor is a form of resonant vacuum breakdown in which secondary electrons released from one wall drift across the gap and strike the opposite wall. If $\delta > 1$, electron multiplication occurs. In theory, the multipactor breakdown threshold is determined by resonance of the electron trajectories within the waveguides: the onset of multipactor occurs when those electrons which are released with the proper phase relationship to the rf field strike the opposite wall with close to their maximum oscillatory energy for a given rf field and release secondary electrons with the same initial phase with which the primaries were emitted. If a magnetic field with a component perpendicular to the rf electric field is present, the electron trajectories are curved, and multipactor may occur along a single wall of the waveguide [135]. The presence of a magnetic field leads to more complicated electron trajectories [127]; magnetic fields less than or on the order of the electron cyclotron resonant value tend to lower the power threshold for multipactor breakdown. Because δ increases as the angle of incidence

between the primary electron and the metallic surface is reduced, the curved electron trajectories in a magnetic field lead to an overall increase in the secondary electron emission. Moreover, the electron can gain energy from the rf field if the magnetic field is near the cyclotron resonant value [36].

Multipacting modes are often characterized by the number of half-cycles of the rf field that an emitted electron completes before striking the opposite wall. The fundamental 1/2 cycle mode was experimentally identified in early multipactor work [137]. The breakdown field in these experiments was dependent on wall cleanliness, with cleaner walls giving rise to lower values of the secondary electron emission coefficient. Regarding the occurence of breakdown in waveguide grills, it is generally believed that the discharge is initiated by the multipactor effect. The threshold power levels for breakdown in uncleaned or partially-cleaned waveguide grills are in rough agreement with those predicted from multipactor theory [121]. More importantly, the presence of resonant electron trajectories in lower-hybrid waveguides has been confirmed in a number of magnetized test stand experiments in which rf breakdown was observed when the value of the applied magnetic field corresponded to the even cyclotron harmonic: $\omega_{ce} = \omega, \omega/2, \omega/4...$ In these experiments, which have simulated the experimental conditions of a grill on a tokamak, it was conjectured that the breakdown arose from the single surface multipactor effect [128,130].

During rf breakdown in the waveguide, the average plasma density measured by the interferometric technique is found to increase with the incident rf power. Densities on the order of the cutoff density in the

waveguide have been observed [115,121]. Gas is also evolved during rf breakdown, probably resulting from desorption by electron impact on the waveguide walls. In the cases in which the gas has been analyzed, it was found to be hydrogen [125,138]. Although the electron mean free path for impact ionization is considerably longer than the waveguide width, ionization of the neutral gas in the waveguide is believed to be the responsible mechanism for creating the high plasma densities in the waveguide. This is supported by the observation that the threshold power for breakdown during antenna tests typically decreases as the gas pressure in the waveguides is raised from the 10^{-7} Torr level to 10^{-4} Torr [115,121,123]. Although the formation of rf-generated plasmas in cavities, or "plasmoids", is not well understood, they have been observed for many years in a number of experiments. The consequence of plasma formation is strong attenuation of rf transmission by as much as 10-20 dB [135]. Substantial absorption of rf power during breakdown is also believed to take place in waveguide grill antennas. In experiments in which one waveguide in an array was fed and the power coupled into the others (which should be proportional to the transmitted power) was monitored, it was usually found that the transmissivity decreased by a factor of 2-3 during rf breakdown. At the same time, only relatively small changes in the reflected power of the fed waveguide was observed [56,124,125]. The waveguide plasma apparently is responsible for absorbing a large fraction of the incident rf power. In the event of an rf breakdown, the associated uncontrolled phase shifts between adjacent waveguides may be detrimental to the performance of grill and couplers.

3.7.1 Suppression of Rf Breakdown

Most efforts to eliminate breakdown and plasma formation in waveguide antennas have centered on reducing the effective value of the secondary electron emission coefficient below unity so that electron multiplication is eliminated. It is well known that the composition and finish of metallic surfaces have a strong influence on the secondary electron emission coefficient of the metal. In particular, clean surfaces free of hydrocarbons and water vapor generally exhibit lower values of δ than dirty ones [131]. Also, surfaces with microscopic roughness also have lower secondary electron emission coefficients than smooth ones [125,127, 139]. The preparation of waveguide grills for high power are thus oriented towards the waveguide surface cleanliness and finish.

Rf Conditioning

The most common technique used to suppress rf breakdown in waveguide grills, and in high power rf systems in general, is rf conditioning, also known as rf processing or aging. In this method, rf pulses of short duration are repetitively fed into the evacuated grill, and the power is raised until breakdown is observed. With continued pulsing with short rf pulses near or below this level, the breakdown usually ceases, and the rf power may be raised until breakdown recurs. The process is repeated until the desired power level is reached, or until rf conditioning is no longer effective in eliminating the breakdown. The mechanism of rf contioning is not particularly well understood; however, recent surface physics studies [140,141] suggest that the improvement in high power operation due to rf processing results from polymerization of a hydrocarbon

layer on the metallic surfaces of the waveguides, rather than a cleansing of the surface by electron stimulated desorption. The unsaturated carbon polymer surface produced during rf conditioning is believed to absorb a large fraction of the secondary electrons emitted from the metal below. At temperatures above 300°K, the polymer is known to be unstable, and exposure to air or other contaminants can destroy the polymer layer, necessitating reconditioning.

To reach substantial rf power densities (1-10 kW/cm^2) in vacuum, the number of conditioning pulses required for most waveguide antennas is on the order of a thousand. In some cases, rf conditioning has been carried out in a vacuum test stand to reduce the amount of conditioning time on the tokamak. Extensive reconditioning of the grill is often required following prolonged vacuum breaks, and some processing into plasma discharges at the beginning of a day's run is usually necessary to achieve reliable high power injection into the plasma.

Cleanliness

Most grills are vacuum-baked to reduce outgassing once they are installed on the tokamak. Vacuum baking is known to reduce the electron-stimulated desorption coefficient [142]. The bake-out temperature of the assembled grill is typically limited to no more than 400°C to avoid warpage of the antenna. After installation on the tokamak or in an rf test stand, the grill is often baked to 150 - 200° C for at least 24 hours. Standard degreasing procedure is also applied prior to installation. Glow discharge cleaning with electrodes inserted through the top of the waveguides after the grill has been mounted to the tokamak has been found

to be very effective in suppressing breakdown in the Wega and Petula B antennas [124-126]. Auger spectroscopy performed on surface samples in the Petula B test stand has shown that argon glow discharge cleaning greatly reduced the amount of carbon and oxygen on the metallic surface [128]. Moreover, the glow discharge leaves the surface with a microscopically rough finish. As discussed in the next section, such a surface exhibits a low secondary electron emission coefficient for all angles of incidence, and permits a higher rf power transmission without breakdown.

Materials and Surface Finish

As discussed earlier, lower hybrid antennas must be placed in the edge plasma to achieve good coupling. Consequently, they should be made of material similar to the vessel wall or limiters to minimize contamination of the plasma. Most grill antennas to date have been constructed of stainless steel. To reduce secondary electron emission within the waveguides, however, different grill materials and surface coatings have been experimented with. Clean pure titanium is known to have a value of δ below one, and grills constructed of solid titanium have been tried on JFT-2 [143], Versator II [115], Wega [39], and Petula B [40]. Titanium has also been sublimated onto stainless steel grills on Versator II [56] and T-7 [52], and onto a copper coated stainless steel grill on JFT-2 [55]. Tests of a titanium carbide coated stainless steel grill at JAERI have also been planned [123].

After a brief initially successful operation, the titanium launchers become prone to rf breakdown, and it appears that the pure, low-δ titanium surface is difficult to maintain once inside the tokamak. Other procedures,

such as additional pumping of the waveguides and glow discharge cleaning have helped to reduce breakdown in these launchers. On JFT-2, a power density of 1.8 kW/cm^2 at f = 750 MHz into plasma was achieved with a titanium-coated and differentially pumped grill to ensure low gas pressure within the guide [55]. After poor power handling was initially encountered with the Wega solid titanium grill, titanium was evaporated onto the waveguide surfaces at a rapid rate in a low pressure gas atmosphere to produce a rough, or "pulverized" surface [124]. With glow discharge cleaning, the grill was capable of transmitting power densities as much as 2 kW/cm^2 into plasma. Similar beneficial results with glow discharge cleaning have been obtained with an all-titanium grill on the Petula B tokamak [60]. The glow discharge cleaning procedure is carried out at a pressure of about 10^{-2} Torr in argon. The bombardment of the surface by the argon ions impacts to the surface a microscopic graininess with a several micron scale length. The measured reduction of the secondary electron emission coefficient from this type of surface [127,139] is believed to result from geometrical effects, namely the rough surface acts as a trap for escaping secondary electrons. The rough surface is especially effective in reducing the normally high secondary yield of grazing incidence electrons which are the primary cause of breakdown when a magnetic field is present in the evacuated portion of the grill. Following glow discharge cleaning of the Petula B grill, few instances of breakdown occurred during tokamak operation, even though the cyclotron layer is located in the evacuated portion of the grill. In Petula B an incident power density of 3.4 kW/cm^2 has been achieved at f = 1.3 GHz in both a titanium grill with differential pumping, and a stainless steel grill with no additional pumping [60]. In the event of a breakdown in one of the waveguides,

several minutes of glow discharge cleaning in that waveguide was usually sufficient to prevent recurrence of the breakdown [129].

The stainless steel PLT grill was coated with a thin carbon layer after investigations showed that such a surface exhibited a secondary electron emission coefficient below one [122]. The layer was applied by soaking the grill in a carbon-rich varnish and pyrolizing it in a vacuum furnace. The several hundred Angstrom thick carbon layer so obtained was strongly adherent to the stainless steel surface which was previously prepared by sanding and electropolishing. With this coating, the PLT grill has been operated at a power level of 1.6 kW/cm^2 into plasma without breakdown. An antenna system on Versator II was also treated in this manner and achieved similar results [115]. However, the carbon layer was also found to be easily contaminated, and extensive reconditioning was generally required after vacuum breaks and discharge cleaning.

The waveguides of the Asdex lower hybrid coupler have been coated with gold using a special procedure [127]. Gold is deposited on the surface by an electrochemical process, creating a rough-textured, polycrystalline surface which exhibits a low secondary electron emission coefficients ($\delta < 1$) for all angles of incidence. The effect of the gold coating is similar to that of surfaces treated by glow discharge cleaning. Gold was chosen for the Asdex experiment because of its resistance to chemisorption of residual gases in the tokamak. The coating has been shown to be stable, and is also effective in suppressing multipactor breakdown in the presense of a magnetic field. Power densities of 5.4 kW/cm^2 have been achieved during rf injection into the Asdex plasma [41].

Magnetic Fields

The use of an auxiliary magnetic field to eliminate the cyclotron resonance layer in the evacuated portion of the grill has been tried on the Versator II antenna in which the vacuum windows are located two meters from the end of the waveguides. The application of the additional field was found to suppress breakdown in the untreated stainless steel grill when the magnetic field was at least 25% above the cyclotron resonant value everywhere in the evacuated portion of the waveguides. A power density of at least 1 kW/cm^2 into plasma was attainable with this method [144].

High Frequencies

At present, the highest power density at the grill mouth obtained during plasma operation in any lower hybrid experiment is 9 kW/cm^2, achieved in the Alcator C 4.6 GHz experiment [145]. The Alcator C grill is constructed of electropolished stainless steel with the cyclotron resonant region located on the high-pressure side of the windows. The rf frequency of this experiment is also the highest of any lower hybrid facility presently in operation. The improvement in the power threshold for breakdown with higher frequencies is expected because the oscillating electron energy is a decreasing function of frequency (see Eq. 53). The dimensions, specifications, and power-handling capabilities of lower hybrid waveguide grills from a number of experiments are summarized in Table 1. Note that there is indeed a trend toward higher achievable rf power densities with increasing frequency.

Conclusion

As evidenced by the above discussion, the methods employed to increase the power handling capability of the grill antenna have been quite varied, and many have proved to be fruitful. Though rf breakdown has been a major concern in every lower hybrid heating experiment, the improvements made on the grill antenna have enabled the rf power levels in most experiments to be raised to the level of the ohmic power input and above; on Asdex, an injected power level of 800 kW has been achieved for 1 second through a single eight-waveguide array, while on Alcator C, 1.5 MW has been coupled to the plasma with three arrays. The use of novel surface preparation techniques and extensive pumping of the waveguides has suppressed the occurrence of multipactor and cyclotron resonance breakdown in the evacuated grill even in antennas in which the vacuum windows are located several meters from the grill mouth. The use of "in situ" glow discharge cleaning in the Wega and Petula B grills has shown that the antenna cleanliness can be maintained even in the tokamak environment. Therefore, the implementation of grill couplers on future multimegawatt experiments is believed to be technically feasible.

3.8 Future Trends in Lower Hybrid Couplers

Large scale lower hybrid heating and current drive experiments are presently planned for several large scale tokamaks. A 24 MW, 2 GHz system is under construction for use on JT-60 [138,146,147], and major lower hybrid systems have also been proposed for current drive experiments on Tore-Supra ($f = 3.7$ GHz, $P = 8$ MW [148] and electron heating experiments on FTU ($f = 8$ GHz, $P = 8$ MW) [149,150]. The important issues of lower

hybrid coupling especially relevant to these future experiments are the power handling capability of the launchers and the $n_{\parallel}$ spectra required for highly efficient performance in these high temperature plasmas.

3.8.1 Power Requirements of Future Couplers

With the increasing size of tokamaks of the next generation, the available port area for lower hybrid couplers is also expected to be larger. Therefore, although the total rf power inputs in future experiments will be roughly an order of magnitude higher than in present ones, the power density at the antennas is expected to remain the same as in present experiments. The maximum power density in the JT-60 lower hybrid grill is expected to be 4.5 kW/cm^2, which is comparable to power densities already achieved in current experiments. Of greater importance is the need to design couplers with the ability to operate into long pulse or steady state discharges. Active cooling of the waveguide grill will probably be required to solve this problem. The waveguide array designed for JT-60 incorporates a nitrogen gas cooling manifold within the grill structure for this purpose. Hot gas may also be passed through this network to bake the grill to a temperature of 400°C in situ. The inner surfaces of the stainless steel waveguides will be copper coated to reduce resistive heating of the grill during rf pulsing. The rf windows will be located in individual waveguide sections 7 meters back from the antenna mouth, allowing for relatively easy window maintenance. As in JFT-2, the antenna section between the plasma and the windows will be differentially pumped.

The rf frequencies selected for upcoming experiments are generally higher than those used in earlier studies, both because of the higher magnetic fields of new tokamaks, and because of the emphasis placed on electron heating and current drive studies. Such experiments are performed at frequencies typically a factor of two above the central lower hybrid frequency. Since waveguide dimensions are reduced with increasing frequencies, the number of waveguides in a grill will be quite large if the power density is to be kept at levels close to those in present day experiments. The JT-60 grill consists of four rows of waveguides with eight waveguides in each row, while a proposed 8 GHz electron heating experiment on FTU incorporates a design in which 128 waveguides (16 rows of 8 waveguides) are installed through a single port. The grill structure for arrays with so many waveguides can become complicated, however, especially for those with internal windows, as is envisioned for the FTU grill. One simplification of the present grill structure is an array in which the power is split by passive elements into waveguides in the evacuated section of the grill, i.e., after the rf has passed through the vaccum window [151-154]. An example of such an antenna is the "multi-junction" grill [153] which is shown in Fig. 21. Two rf sources feed an eight-waveguide array launching a travelling wave spectrum ($\Delta\phi = \pi/2$). The advantage of such a scheme is that only one vacuum window per grill is required, thereby greatly reducing the fabrication difficulty of the multi-waveguide array. On the other hand, the relative phase control between waveguides is less flexible than in present experiments. Such a grill has been constructed and tested on Petula B [153]. The phase shift between adjacent waveguides is set by reducing the heights of the individual waveguides. The reflectivity of the multi-junction grill is found to be only slightly higher than that of a similar conventional grill. The

maximum power attained in the new grill is about 70% of that in the conventional grill due to higher rf electric fields in the reduced height sections of the multi-junction grill.

3.8.2 Wave Spectrum Considerations

Lower hybrid experiments performed on the higher temperature plasmas in the next generation of experiments will require the launching of a well-defined $n_\parallel$ spectrum. In order to prevent electron Landau damping or mode conversion to the hot ion plasma wave branch from occurring in the outer layers of the plasma, the wave spectrum must be concentrated at relatively low values of the parallel wave number, e.g., $|n_\parallel| \lesssim 2.2$ for a 10 keV plasma. The accessibility condition Eq. (11) must still be satisfied; therefore the launched $n_\parallel$ spectrum should be constrained to a narrow range above $|n_\parallel| \approx 1.5$ for efficient heating and current drive. This may be accomplished by increasing the number of waveguides in the grill along the z-axis, which will be relatively easy to do as the available port size in the new machines will be larger. Another method of narrowing the spectrum around an optimum value is with the use of dummy waveguides or a corrugated vacuum vessel wall on either side of the actively fed grill. An experimental test of the dummy waveguide concept was described earlier in Section 3.6, and the findings were encouraging in that the spectrum indeed exhibited a smaller surface wave component than that of the grill without the dummy waveguides.

As the plasma is heated toward ignition temperatures, the optimal value of $n_\parallel$ for central heating will decrease, and it will be necessary to actively change the launched $n_\parallel$ spectrum or rf frequency over the course

of the discharge. This is relatively easy to perform in actively fed grills with electronic phase shifters in the rf drive units for the klystrons. In the PLT lower hybrid current startup experiments, the phase between waveguides was shifted during the plasma initiation and rf startup to obtain adequate coupling while the edge density was rapidly changing [61]. In the JT-60 lower hybrid rf system, both the phase and the frequency ($f = 2.0 \pm 0.3$ GHz) can be altered during the long rf pulse.

3.8.3 Lower Hybrid Couplers in the Fusion Reactor

In a reactor, the lower hybrid wave may be used for bulk electron heating and current drive. The high electron temperature (T_e = 15-20 keV) of a thermonuclear plasma strongly favors electron Landau damping over direct ion heating for the range of accessible values of $n_\parallel$ in the lower hybrid frequency range. Only for low frequencies ($\omega < \omega_{LH}$) and low values of $n_\parallel$ is ion damping expected to be significant, and this only near the plasma periphery [155]. Because the electrons and ions are closely coupled in a reactor, efficient electron heating will be sufficient to heat the ions to ignition temperatures. In addition, the engineering advantages of a steady state tokamak reactor are significant, making rf current drive on a reactor an option worth investigating [156,157]. However, a number of physics issues need to be resolved in order to determine the suitability of lower hybrid heating of a reactor plasma and what the appropriate coupling structure should be. In particular, the penetration problems of lower hybrid waves are expected to be more severe in high density, high temperature thermonuclear plasmas than in present day discharges. To avoid ion heating near the edge and the possibility of parametric decay of the incident power, the slow wave frequency should be

chosen to be several times the lower hybrid frequency ($\omega \gtrsim 2\omega_{LH}$), or $f > 4$ GHz, typically. Lower hybrid waves which are accessible ($n_\parallel \gtrsim 2$) in a reactor plasma in which $\omega_{pe}^2/\omega_{ce}^2 \sim O(1)$ will be Landau damped at temperatures $T_e \sim 10$ keV, i.e., outside the central core. Because of its weaker damping, the fast wave branch may prove to be more suitable for reactor applications than the slow wave. However, both branches are predicted to be strongly absorbed by a small population of fusion-produced alpha particles [155]; therefore, no heating or current drive can be expected to take place in the core of a burning plasma, e.g., $r/a \lesssim 1/2$, where the alpha concentration will be significant. Nonetheless, central power deposition in a reactor may not be necessary for efficient heating if the plasma current and temperature profiles are "consistent" [158] and independent of heating profiles. In recent neutral beam [159] and ECRH [160] heating studies the global confinement time and increase in plasma energy with auxiliary heating power was found to be constant over a wide range of deposition profiles. In current drive, the plasma hard x-ray emission from the superthermal current-carrying electron is always found to be peaked on-axis [65] while the calculated rf absorption profiles are hollow [161]. Finally, recent results from JET indicate that central heating may lead to unacceptably high sawtooth activity [162]. Therefore, off-axis electron Landau damping may be suitable, and perhaps desirable, for heating of reactor plasmas.

A number of different scenarios have been proposed for current drive in a reactor: fully-driven steady state operation [20,156], low duty-cycle maintenance of the plasma current in a low temperature plasma phase between fusion burns while the ohmic transformer is reverse-biased and "recharged" [156,163,164], and stabilization of sawteeth or $m = 2$ instabilities by

localized current drive [165]. The achievement of the first may require upwards of 100 MW of rf power if theoretical current drive efficiencies for the optimal $n_\parallel$ spectrum can be attained. The second method is comparable to current drive experiments on present generation machines, though again, considerably more power would be required. The suppression of MHD instabilities in a fusion plasma will also require a great deal of rf power which must be deposited in the vicinity of the appropriate rational surface; thus the launched $n_\parallel$ spectrum must be well defined. The successful application of any of these heating or current drive schemes in a large, high density plasma will require a large fraction of circulating power, hence it will be critical that the antenna couple efficiently and selectively to the optimal power spectrum.

From a practical point of view, the phased array of waveguides is particularly well suited for use in a reactor environment for the same reasons that recommend its application in present day experiments; all-metal construction, location well behind the limiter radius at the chamber wall, ease of installation and removal, and the possibility of placing the vacuum windows in regions shielded from the neutron flux. A number of technical developments must be pursued. High power long pulse or CW operation will require active cooling of the arrays by gas or liquid manifolds. Moreover, the installation of ceramic windows outside the blanket adds additional complexity because of the problems of preventing breakdown in the long evacuated sections of the waveguide. However, the problems of heat loading and many-waveguide arrays with exterior windows are being addressed in present studies, e.g., JT-60, and are not considered to be major impediments to the development of a phased array for a reactor.

Based on present perceptions of the parameters of a reactor plasma discussed above, the grill should launch a narrow $n_\parallel$ spectrum concentrated at low values of $n_\parallel$ just above the accessibility limit in order to take advantage of the high current drive efficiency of high phase velocity waves. If the m = 2 instability is to be suppressed, the spectrum must be shaped to provide maximum absorption near the q = 2 surface. For current drive, the spectrum should also be uni-directional. As discussed earlier, the $n_\parallel$ spectrum can be made well defined by employing a grill with many waveguides along the axial direction, although the overall grill reflectivity is predicted to increase with more waveguides. A multi-junction grill with a single window could be used to simplify the feedthrough problem for a 10-20 waveguide array. Dummy waveguides may also be of use in sharpening the spectrum without increasing the reflected power. The directivity of the antenna depends in part on the details of the electric field at the grill mouth, and may be improved with further studies. Some of the power traveling in the wrong direction may be reflected by a grid or plate in the edge region adjacent to one side of the grill [166], although the heat loading and impurity generation problems associated with such a structure needs to be investigated.

In conclusion, the lower hybrid antenna in a reactor will probably look similar to those in contemporary experiments, except that it will include many more radiating elements to sharpen the spectrum. For ease of maintenance, the ceramic vacuum windows may have to be placed a considerable distance from the plasma, and rf breakdown must be prevented using one (or more) of the techniques discussed. To prevent tritium leakage, it may be necessary to use more than one window in a given waveguide line. Finally, due to the large temperature ranges encountered during a

pulse, the $n_{\parallel}$ spectrum may have to be adjusted by changing the relative waveguide phases, so as to track the temperature during the heating or current drive pulse.

3.8.4 Conclusion

The efficiency and versatility of the multi-waveguide grill has been demonstrated in numerous lower hybrid heating experiments performed in the last decade. The question of the reliability of the grill under high power operation has been successfully addressed by a number of groups, and it appears that the power densities required in the next generation of experiments will be possible to achieve. Consequently, while further improvements are expected, the multi-waveguide array, or grill, is expected to remain the leading concept for slow lower hybrid wave launching. Development of fast wave launchers, consisting either of dielectric-loaded phased array of waveguides, or arrays of ridged waveguides, may be required for current drive in reactor grade plasmas.

Acknowledgement

This research was supported by the US Department of Energy under Contract No. DE-AC02-78ET51013.

References

1. For a recent review of lower hybrid heating and current drive experiments, see PORKOLAB, M., IEEE Transactions on Plasma Science, Vol. PS-12 (1984) 107; also, PORKOLAB, M. in Wave Heating and Current Drive in Plasmas, ed. by GRANATSTEIN, V. L., COLESTOCK, P. C., Gordon and Breach, New York (1985) 219.

2. LALLIA, P., Proc. 2nd Topical Conf. on Rf Plasma Heating, Lubbock, Texas (1974) Paper C3.

3. BRAMBILLA, M., Nucl. Fusion 16 (1976) 47.

4. STIX, T. H., The Theory of Plasma Waves, McGraw-Hill, New York (1962).

5. GOLANT, V. E., Zh. Tekh. Fiz. 41 (1971) 2492; Sov. Phys.-Tech. Phys. 16 (1972) 1980.

6. PORKOLAB, M., "Radio Frequency Heating of Magnetically Confined Plasma", in Fusion, Vol. I; ed. by TELLER, E., Academic Press, New York (1981).

7. BONOLI, P., IEEE Transactions on Plasma Science, Vol. PS-12 (1984) 95; also, BONOLI, P., in Wave Heating and Current Drive in Plasmas, ed. by GRANATSTEIN, V. L., COLESTOCK, P. C. Gordon and Breach, New York (1985) 175.

8. KUEHL, H. H., Phys. Fluids 5 (1962) 1095.

9. FISHER, R. K., GOULD, R. W., Phys. Fluids 14 (1971) 857.

10. TROYON, F., PERKINS, F. W., Proc. 2nd Topical Conf. on Rf Heating, Lubbock, Texas (1974) Paper B4.

11. BERNABEI, S., DAUGHNEY, C., EFTHIMION, P., HOOKE, W., HOSEA, J., et al., Phys. Rev. Lett. 49 (1982) 1255.

12. GLAGOLEV, V. M., Plasma Phys. 14 (1972) 315.

13. SIMONUTTI, M. D., Phys. Fluids 18 (1975) 1524.

14. BRAMBILLA, M., Plasma Phys. 18 (1976) 669.

15. SCHUSS, J. J., Phys. Fluids 18 (1974) 1178.

16. BERS, A., Proc. 3rd Symp. on Plasma Heating in Toroidal Devices, Como, Italy, 1976, Editrice Compositori, Bologna (1976) 99.

17. BRAMBILLA, M., Nucl. Fusion 18 (1978) 493.

18. STIX, T. H., Phys. Rev. Lett. 15 (1965) 878.

19. BRAMBILLA, M., CHEN, Y., in Heating in Toroidal Plasmas (Proc. 3rd Joint Varenna-Grenoble Int. Symp., Grenoble, 1982), Vol. II, CEC Brussels (1982) 565.

20. FISCH, N. J., Phys. Rev. Lett. 41 (1978) 873.

21. BERS, A., Proc. 3rd Topical Conf. on Rf Plasma Heating, Pasadena, California (1978) paper A1.

22. WONG, K. L., ONO, M., Nucl. Fusion 23 (1983) 805.

23. THEILHABER, K., BERS, A., Nucl. Fusion 20 (1980) 547.

24. MC WILLIAMS, R., MOK, Y., Fusion Tech. 1 (1985) 283.

25. OLSON, L., MC WILLIAMS, R., GLANZ, J., MOTLEY, R. W., Nucl. Fusion 24 (1984) 1085.

26. GOREE, J., ONO, M., COLESTOCK, P., HORTON, R., MC NEILL, D., PARK, H. Phys. Rev. Lett. 55 (1985) 1669; MC WILLIAMS, R., PLATT, R. C., Fast Wave Current Drive in the Irvine Torus, UCI, Tech. Report 85-45 (1985).

27. D'YACHENKO, V. V., SHCHERBININ, O. N., Zh. Tekh. Fiz. 46 (1976) 2043; also, Sov. Phys.-Tech. Phys. 21 (1976) 1196.

28. MOELLER, C. P., CHAN, V. S., A Slow Wave Structure for Launching Lower Hybrid Waves of Short Parallel Wavelength, General Atomic Company, GA-A14836 (1978).

29. BELLAN, P., PORKOLAB, M., Phys. Rev. Lett. 34 (1975); BELLAN, P., PORKOLAB, M., Phys. Fluids 19 (1976) 955.

30. WONG, K. L., HORTON, M., ONO, M., Phys. Rev. Lett. 45 (1980) 117.

31. GOLANT, V. E., GUSEV, V. K., D'YACHENKO, V. V., IVANOV, V. I., LARINOV, M. M., et al., in Plasma Physics and Controlled Nuclear Fusion Research (Proc. 7th Int. Conf., Innsbruck, Austria 1978) Vol. I, IAEA, Vienna (1979) 113.

32. FREEMAN, R. L., LUXON, J. L., CHAN, V. S., CHIU, S. C., DE BOO, J. C., et al., in Heating in Toroidal Plasmas (Proc. 2nd Joint Varenna-Grenoble Int. Symp., Como, Italy, 1980) Vol. I, CEC Brussels (1980) 317.

33. PORKOLAB, M., SCHUSS, J. J., TAKASE, Y., TEXTER, S., FIORE, C., et al., in Heating in Toroidal Plasmas, (Proc. 3rd Joint Varenna-Grenoble Int. Symp. Grenoble, 1982) Vol. II, CEC Brussels (1982) 469.

34. ALLADIO, F., APICELLA, M. L., BARBATO, G., BARTIROMO, R., et al., in Plasma Physics and Controlled Nuclear Fusion Research (Proc. 7th Int. Conf., Baltimore, Maryland, 1982) Vol. II, IAEA, Vienna (1983) 41.

35. HOOKE, W., BERNABEI, S., BOYD, D., CAVALLO, A., CHU, T. K., et al., in Plasma Physics and Controlled Nuclear Fusion Research, (Proc. 9th Int. Conf., Baltimore, Maryland, 1982) Vol. I, IAEA, Vienna (1983) 239.

36. LAX, B., ALLIS, W. P., BROWN, S. C., J. Appl. Phys. 21 (1950) 1297.

37. SCHUSS, J. J., PORKOLAB, J. TAKASE, Y., COPE, D. FAIRFAX, S., et al., Nucl. Fusion 21 (1981) 427.

38. NAGASHIMA, T., FUJISAWA, N., in Heating in Toroidal Plasmas, (Proc. Joint Varenna-Grenoble Int. Symp. Grenoble, 1978) Vol. II, CEC, Brussels (1979) 281.

39. GORMEZANO, C., BLANC, P., EL SHAER, M., HESS, W., ICHTCHENKO, G., et al., in Heating in Toroidal Plasmas, (Proc. 3rd Joint Varenna-Grenoble Int. Symp. Grenoble, 1982) Vol. II, CEC Brussels (1982) 439.

40. MELIN, G., BERNARD, M., BLANC, P., BRIAND, P., BRIFFORD, G., et al., in Plasma Physics and Controlled Nuclear Fusion Research, (Proc. 9th Int. Conf., Baltimore, Maryland, 1982) Vol. I (1982) 209.

41. ECKHARTT, D., LEUTERER, F., MUNICH, M. IZVOZTCHIKOV, A., RYTER, F., et al., in Heating in Toroidal Plasmas, (Proc. 4th Int. Symp., Rome, 1984) Vol. I, Int. School of Plasma Physics, Varenna (1984) 501.

42. MOTLEY, R. W., BERNABEI, S., HOOKE, W. M., PAOLONI, F. J., Nucl. Fusion 20 (1980) 1207.

43. SCHUSS, J. J., PORKOLAB, M., Proc. 5th Topical Conf. on Rf Plasma Heating, Madison, Wisconsin (1983) Paper A-I.5.

44. SCHUSS, J. J., PORKOLAB, M., GRIFFIN, D., BARILOVITS, S., BESEN, M., et al., Nucl. Tech./Fusion 4 (1983) 1413.

45. ANDREANI, R., PAPITTO, P., SASSI, M., Proc. 10th Symp. on Fus. Tech., Padova, 1978, Vol. I, CEC, Luxembourg (1979) 269.

46. MUNICH, M. J., the LH Group, in Heating in Toroidal Plasmas, (Proc. 4th Int. Symp., Rome, 1984) Vol. II, Int. School of Plasma Physics, Varenna (1984) 1183.

47. BERNABEI, S., DAUGHNEY, C. HOOKE, W., MOTLEY, R., NAGASHIMA, T., et al., Proc. 3rd Int. Symp. on Heating in Toroidal Devices, Como, Italy, 1976, Editrice Compositori, Bologna (1976) 68.

48. PORKOLAB, M., BERNABEI, S., HOOKE, W., MOTLEY, R., NAGASHIMA, T., Phys. Rev. Lett. 38 (1977) 230.

49. RICHARDS, B., PARKER, R. R., Bull. Am. Phys. Soc. 20 (1975) 1313.

50. BRIAND, P., DUPAS, L., GOLAVATO, S. N., SINGH, C. M. MELIN, G., GRELOT, P., LE GARDEAR, R., ZYMANSKI, S., in Plasma Physics and Controlled Nuclear Fusion Research, (Proc 7th Int. Conf., Innsbruck, 1978) Vol. I, IAEA, Vienna (1979) 65.

51. SCHUSS, J. J, FAIRFAX, S., KUSSE, B., PARKER, R. R., PORKOLAB, M., et al., Phys. Rev. Lett. 43 (1979) 274.

52. ALIKAEV, V. V., VDOVIN, V. L. IVANOV, D. P., IVANOV, N. V., IL'IN, V. I., et al., in Plasma Physics and Controlled Nuclear Fusion Research (Proc. 9th Int. Conf., Baltimore, Maryland, 1982), Vol. II, IAEA, Vienna (1983) 153.

53. IMAI, T., NAGASHIMA, T., YAMAMOTO, T., UEHARA, K., KONOSHIMA, S., TAKEUCHI, H., YOSHIDA, H., FUJISAWA, N., Phys. Rev. Lett. 43 (1979) 586.

54. YAMAMOTO, T., IMAI, T., SHIMADA, M., SUZUKI, N., MAENO, M., et al., Phys. Rev. Lett. 45 (1980) 716.

55. UEHARA, K., NAGASHIMA, T., in Heating in Toroidal Plasmas, (Proc. 3rd Joint Varenna-Grenoble Int. Symp., Grenoble, 1982), Vol. II, CEC, Brussels (1982) 485.

56. KNOWLTON, S., CHEN, K. I., LUCKHARDT, S. C., MC DERMOTT, F. S., PORKOLAB, M., Proc. 4th Topical Conf., Austin, Texas (1981) Paper C11.

57. NAKAMURA, N., CHO, T., KUBO, S., SHIMOZUMA, T., KAWAI, H., et al., Phys. Rev. Lett. 47 (1981) 1902.

58. KUBO, S., NAKAMURA, N., CHO, T., NAKAO, S., SHIMOZUMA, T., et al., Phys. Rev. Lett. 50 (1983) 1994.

59. Petula Group, in Heating in Toroidal Plasmas, (Proc. 2nd Joint Varenna-Grenoble Int. Symp., Como, Italy 1980) Vol. I. CEC, Brussels (1980) 343.

60. VAN HOUTTE, D., AGARICI, G., BLANC, P., BRIAND, P., BRIFFORD, G. et al., in Heating in Toroidal Plasmas, (Proc. 4th Int. Symp., Rome, 1984) Vol. I., Int. School of Plasma Phys. Varenna (1984) 554.

61. LUCKHARDT., S., C., PORKOLAB, M., KNOWLTON, S. F., CHEN, K. I., FISHER, A. S., MC DERMOTT, F. S., Phys. Rev. Lett. 48 (1982) 152.

62. JOBES, F. STEVENS, J., BELL, R., BERNABEI, S., CAVALLO, A., et al., Phys. Rev. Lett. 52 (1984) 1005.

63. BERNABEI, S., CAVALLO, A., CHU, T. K., HOOKE, W., JOBES, F., et al., in Rf Plasma Heating (Proc. 6th Top. Conf., Pine Mountain, GA, 1985) AIP, New York (1985) 135.

64. ALLADIO, F., BARBATO, E., BARDOTTI, G., BARTIROMO, R., BRACCO, G., et al., Nucl. Fusion 24 (1984) 725.

65. PORKOLAB, M., SCHUSS, J. J., LLOYD, B., TAKASE, Y., TEXTER, S., et al., Phys. Rev. Lett. 53 (1984) 450.

66. PORKOLAB, M., LLOYD, B., TAKASE, Y., BONOLI, P., FIORE, C., et al., Phys. Rev. Lett. 53 (1984) 1229.

67. OHKUBO, K., TAKAMURA, S., KAWAHATA, K., TETSUKA, T., MATSUURA, K., NODA, N., SAKURAI, K., TANAHASHI, S., FUJITA, J., Nucl. Fusion 22 (1982) 203.

68. PACHER, H. D., BLANC, P., DURVAUX, M., GORMEZANO, C., HESS, W., et al., in Plasma Physics and Controlled Nuclear Fusion Research, (Proc. 7th Int. Conf., Innsbruck, 1978) Vol. I, IAEA, Vienna (1979) 97.

69. GORMEZANO, C., HESS, W., ICHTCHENKO, G., MAGNE, R., NGUYEN, T. K., et al., Nucl. Fusion 21 (1981) 1047.

70. TAKAMURA, S., MATSUSHITA, H., SUZUKI, U., OSHIMA, S., VESUGI, Y., OKUDA, T., Nucl. Fusion 20 (1980) 429.

71. NAKAMURA, M., SAITO, T., IKEDA, M., KUBO, S., TERUMICHI, Y., HAMADA, Y., TANAKA, S., in Heating in Toroidal Plasmas, (Proc. 2nd Joint Grenoble-Varenna Int. Symp., Como, Italy, 1980) Vol. I, CEC, Brussels (1980) 385.

72. USHIGUSA, K., TAKAMURA, S., OKUDA, T., Nucl. Fusion 24 (1984) 751.

73. PARKER, R. R., RLE Progress Report No. 102, MIT, July 1971.

74. PURI, S., TUTTER, M., Nucl. Fusion 14 (1974) 93.

75. BRAMBILLA, M., Nucl. Fusion 19 (1979) 1343.

76. FICHET, M., FIDONE, I., Plasma Phys. 21 (1979) 901.

77. FUKUYAMA, A., PhD Thesis, Theoretical Investigations of Nonlinear Effects in Lower Hybrid Wave Heating, Kyoto University (1980).

78. STEVENS, J., ONO, M., HORTON, R., WILSON, J. R., Nucl. Fusion 21 (1981) 1259.

79. BERS, A. THEILHABER, K., Nucl. Fusion 23 (1983) 41.

80. ABRAMOWITZ, M., STEGUN, I., Eds., Handbook of Mathematical Functions, Dover Publications, New York, (1972).

81. KRAPCHEV, V. BERS, A., Nucl. Fusion 18 (1978) 519.

82. BELLAN, P., PORKOLAB, M., Phys. Fluids 17 (1974) 1592.

83. ROMANELLI, F., SANTINI, F., Nucl. Fusion 24 (1984) 219.

84. PORKOLAB, M., GOLDMAN, M. V., Phys. Fluids 19 (1976) 872.

85. MORALES, G. J., Phys. Fluids 20 (1977) 1164.

86. CHAN, V. S., CHIU, S. C., Phys. Fluids 22 (1979) 1724.

87. KRAPCHEV, V. B. THEILHABER, K. S.,. KO, K. C., BERS, A., Phys. Rev. Lett. 46 (1980) 1398.

88. DECYK, V. K., DAWSON, J. M., MORALES, G. J., Phys. Fluids 22 (1979) 507.

89. FUKUYAMA, A., MORISHITA, T., FURUTANI, Y. Plasma Phys. 22 (1980) 565.

90. THEILHABER, K., Nucl. Fusion 22 (1982) 363.

91. BRIGGS R. J., PARKER, R. R., Phys. Rev. Lett. 29 (1972) 852.

92. BERNABEI, S., HEALD, M. A., HOOKE, W. M., PAOLONI, F. J., Phys. Rev. Lett. 34 (1975) 866.

93. BERNABEI, S., HEALD, M. A., HOOKE, W. M., MOTLEY, R. W., PAOLONI, F. J., BRAMBILLA, M., GETTY, W. D., Nucl. Fusion 17 (1977) 929.

94. MOTLEY, R. W., BERNABEI, S., HOOKE, W. M., MC WILLIAMS, R. OLSON, L., Plasma Phys. 21 (1979) 567.

95. SURKO, C. M., SLUSHER, R. E., SCHUSS, J. J., PARKER, R. R., HUTCHINSON, I. H., OVERSKEI, D., SCATTURO, L. S., Phys. Rev. Lett. 43 (1979) 1016.

96. SLUSHER, R. E., SURKO, C. M., SCHUSS, J. J., PARKER, R. R., HUTCHINSON, I. H., OVERSKEI, D., SCATTURO, L. S., Phys. Fluids 25 (1982) 457.

97. WATTERSON, R. L., TAKASE, Y., BONOLI, P. T., PORKOLAB, M., SLUSHER, R. E., SURKO, C. M., Phys. Fluids 28 (1985) 2622.

98. TAKASE, Y., WATTERSON, R. L., PORKOLAB, M. FIORE, C. L., SLUSHER, R. E., SURKO, C. M., Phys. Rev. Lett. 53 (1984) 274.

99. WURDEN, G. A., WONG, K. L., ONO, M., Phys. Fluids 28 (1985) 716.

100. MOTLEY, R. W., HOOKE, W. M., GWINN, C. R., Phys. Lett. 77A (1980) 451.

101. MOTLEY, R. W., HOOKE, W. M., ANANIA, G., Phys. Rev. Lett. 43 (1979) 1799; MOTLEY, R. W., Phys. Fluids 23 (1980) 2050.

102. MAZZUCATO, E., Phys. Rev. Lett. 36 (1976) 792.

103. SURKO, C. M., SLUSHER, R. E., Phys. Rev. Lett. 37 (1976) 1747.

104. SURKO, C. M., SLUSHER, R. E., Phys. Rev. Lett. 40 (1978) 400.

105. OTT, E., Phys. Fluids 22 (1979) 1732.

106. BONOLI, P. T., OTT, E., Phys. Rev. Lett. 46 (1981) 424.

107. ANDREWS, P. F., PERKINS, F. W., Phys. Fluids 26 (1983) 2537.

108. BARANOV, YU. F., FEDEROV, V. I., Pis'ma Zh. Tekh. Fiz. 4 (1978) 800; Sov. Phys.-Tech. Phys. Lett. 4 (1978) 322.

109. BARANOV, YU. F., FEDEROV, V. I., Nucl. Fusion 20 (1980) 1111.

110. BONOLI, P. T., OTT, E., Phys. Fluids 25 (1982) 359.

111. IGNAT, D. W., Phys. Fluids 24 (1981) 1110.

112. BERNABEI, S., IGNAT, D. W., Nucl. Fusion 22 (1982) 735.

113. BRAMBILLA, M., CARDINALI, A., Plasma Phys. 24 (1982) 1187.

114. BUDNY, R., Results from Langmuir Probe Measurements in PDX and PLT, Princeton Plasma Physics Laboratory, PPPL-1876 (1982).

115. KNOWLTON, S., PhD Thesis, Lower Hybrid Heating Experiments on the Versator II Tokamak, Massachusetts Institute of Technology (1983).

116. EL SHAER, M., BLANC, P., GORMEZANO, C., HESS, W., ICHTCHENKO, G. et al., in Heating in Toroidal Plasmas, (Proc. 3rd Joint Varenna-Grenoble Int. Symp., Grenoble, 1982) Vol. II, CEC, Brussels (1982) 571.

117. GORMEZANO, C., MOREAU, D., Lower Hybrid Wave Coupling in the Wega Tokamak, EUR-CEA-FC-1175 (1983).

118. Petula Group, Proc. 9th Eur. Conf. on Cont. Fusion and Plasma Phys., Oxford (1979) 21.

119. RICHARDS, B., PhD Thesis, Collective Scattering from Enhanced Fluctuations in a Tokamak, Massachusetts Institute of Technology (1981); ROHATGI, R., PhD Thesis, A Study of Lower Hybrid Wave Propagation on the Versator II Tokamak Using Microwave Scattering, Massachusetts Institute of Technology (1986).

120. ICHTCHENKO, G., O'CONNOR, W., MORESCO, M., ZILLI, E., VENDRAMIN, A., et al., in Heating in Toroidal Plasmas, (Proc. 3rd Joint Varenna-Grenoble Int. Symp., Grenoble, 1982) Vol. II (1982) 577.

121. PACHER, G. W., GORMEZANO, C., HESS, W., ICHTCHENKO, G., MAGNE, R., et al., Proc. 4th Topical Conf. on Rf Plasma Heating, Austin, Texas (1981) Paper E2.

122. TIMBERLAKE, J., COHEN, S. A., CRIDER, C., ESTEPP, G., HOOKE, W., MANOS, D., STEVENS, J., ULRICKSON, M., J. Vac. Sci. Tech. 20 (1982) 1309.

123. FUJII, T., SAKAMOTO, K., UEHARA, K., IMAI, T., HONDA, M., NAGASHIMA, T., in Heating in Toroidal Plasmas, (Proc. 3rd Joint Varenna-Grenoble Int. Symp., Grenoble, 1982), Vol. III, CEC, Brussels (1982) 1133.

124. GORMEZANO, C., CAPITAIN, J. J., FUTSCH, R., MAGNE, R., PACHER, G. W., PACHER, H. D., SOELDNER, F., in Heating in Toroidal Plasmas, (Proc. 3rd Joint Varenna-Grenoble Int. Symp., Grenoble, 1982) Vol. III (1982) 1141.

125. MELIN, G., BRIAND, P., REY, G., TONON, G., in Heating in Toroidal Plasmas, (Proc. 3rd Joint Varenna-Grenoble Int. Symp., Grenoble, 1982) Vol. III (1982) 1157.

126. REY, G., BRIAND, P., MELIN, G., TONON, G., in Heating in Toroidal Plasmas, (Proc. 3rd Joint Varenna-Grenoble Int. Symp., Grenoble, 1982), Vol. III (1982) 1165.

127. DERFLER, H., BRINKSCHULTE, H., LEUTERER, F., PERCHERMEIER, J., SPITZER, H., in Heating in Toroidal Plasmas, (Proc. 4th Int. Symp., Rome, 1984) Vol. II, Int. School of Plasma Physics, Varenna (1984) 1261.

128. TONON, B., BIBET, P., DAVID, C., MOULIN, D., REY, G. in Heating in Toroidal Plasmas, (Proc. 4th Int. Symp., Rome 1984) Vol. II, Int. School of Plasma Physics, Varenna (1984) 1277.

129. BRIAND, P., BIBET, P., GORMEZANO, C., MELIN, G., REY, G., Petula Group, in Heating in Toroidal Plasmas, (Proc. 4th Joint Varenna-Grenoble Int. Symp., Rome, 1984) Vol. II, Int. School of Plasma Physics, Varenna (1984) 1286.

130. LEUTERER, G., LH Group, in Heating in Toroidal Plasmas, in Heating in Toroidal Plasmas, (Proc. 4th Int. Symp., Rome, 1984) Vol. II, Int. School of Plasma Physics, Varenna (1984) 1293.

131. MASSEY, H. S. W., BURHOP, E. H. S., Electronic and Ionic Impact Phenomena, Oxford University Press, London (1952), and references therein.

132. RUZIC, D., MOORE, R., MANOS, D., COHEN, S., J. Vac. Sci. Tech. 20 (1982) 1312.

133. FARNSWORTH, P. T., J. Franklin Inst. 218 (1934) 411.

134. See WACHOWSKI, H. M., Aerospace Corporation Report No. TDR-269 (9990)-5 (1964); and Hughes Aircraft Company Report No. P65-29 (1965) and references therein.

135. HATCH, A. J., Nucl. Instr. and Methods 41 (1966) 261.

136. PRIEST, D. H., Microwave J. 6 (1963) 55.

137. HATCH, A. J., WILLIAMS, H. B., Phys. Rev. 112 (1958) 681.

138. FUJII, T., IMAI, T., SAKAMOTO, K., SAIGUSA, M., IKEDA, Y., Proc. 10th Symp. Fus. Eng., Philadelphia, Pennsylvania, 1983, Vol. II., IEEE, New York (1983) 1476.

139. THOMAS, S., PATTINSON, E. B., J. Phys. D: Appl. Phys. 3 (1970) 1469.

140. GRUNDER, M., HALBRITTER, J., J. Appl. Phys. 51 (1980) 5396.

141. HALBRITTER, J., J. Appl. Phys. 59 (1982) 6475.

142. MATHEWSON, A., ACHARD, M. H., Proc. 7th Int. Vac. Congr. and 3rd Joint Conf. on Solid Surf., Vienna, Vol. II (1977) 1217.

143. SUZUKI, N., OHTSUKA, H., SUGIE, T., OGIWARA, N., KASAI, S., et al., J. Nucl. Materials 93 and 94 (1980) 282.

144. KNOWLTON, S. F., PORKOLAB, M., LUCKHARDT, S. C., in Heating in Toroidal Plasmas, (Proc. 3rd Joint Varenna-Grenoble Int. Symp., Grenoble, 1982) Vol. III, CEC, Brussels (1982) 1149.

145. PORKOLAB, M., SCHUSS, J. J., LLOYD, B., TAKASE, Y., TEXTER, S., et al., Proc. 5th Top. Conf. on Rf Plasma Heating, Madison (1983), Paper B1.

146. SHIMOMURA, Y., MATSUDA, S., NAGASHIMA, T., in Heating in Toroidal Plasmas, (Proc. 3rd Joint Varenna-Grenoble Int. Symp., Grenoble, 1982) Vol. III, CEC, Brussels (1982) 1007.

147. MATSUDA, S., NAGASHIMA, T., SHIMOMURA, Y., in Heating in Toroidal Plasmas, (Proc. 4th Int. Symp. Rome, 1984) Vol. II, Int. School of Plasma Physics, Varenna (1984) 1385.

148. AYMAR, R., in Heating in Toroidal Plasma, (Proc. 3rd Joint Varenna-Grenoble Int. Symp., Grenoble, 1982) Vol. III, CEC, Brussels (1982) 953.

149. SANTINI, F., BARBATO, C., ROMANELLI, F., in Heating in Toroidal Plasma, (Proc. 3rd Joint Varenna-Grenoble Int. Symp., Grenoble, 1982) Vol. III, CEC, Brussels (1982) 999.

150. SEGRE, S. E., in Heating in Toroidal Plasmas, (Proc. 4th Int. Symp., Rome, 1984) Vol. II, Int. School of Plasma Physics, Varenna (1984) 1400.

151. MOTLEY, R. W., HOOKE, W. M., Nucl. Fusion 20 (1980) 222.

152. NGUYEN, T. K., MOREAU, D., in Heating in Toroidal Plasmas, (Proc. 3rd Joint Varenna-Grenoble Int. Symp., Grenoble, 1982) Vol. II, CEC, Brussels (1982) 591.

153. GORMEZANO, C., BRIAND, P., BRIFFORD, G., HOANG, F. T., NGUYEN, T. K., MOREAU, D., REY, G., Nucl. Fusion 25 (1985) 419.

154. NGUYEN, T. K., MOREAU, D., Slow-Wave Lower Hybrid Couplers for Heating and Current Drive in Large Scale Tokamak Plasmas, Int. School of Plasma Phys. Course and Workshop of Rf Waves to Tokamak Plasmas, Varenna (1985) [to be published].

155. WONG, K. L., ONO, M., Nucl. Fusion 24 (1984) 615.

156. EHST, D. A., Nucl. Fusion 19 (1979) 1369.

157. EHST, D. A., CHA, Y., HASSENEIN, A. M., MAJUNDAR, S., MISRA, B., STEVENS, H. C., Nucl. Eng. and Design/Fusion 2 (1985) 305.

158. COPPI, B., Comments Plasma Phys. and Cont. Fusion 5 (1980) 261.

159. SPETH, O., EBERHAGEN, A., GEHRE, O., GERNHARDT, I., JANESHITZ, G., et al., in Conttrolled Fusion and Plasma Physics, (Proc. 12th Eur. Conf., Budapest, 1985) Vol. II, EPS (1985) 284.

160. PRATER, R., BURRELL, K. H., EJIMA, S. JAHNS, G. L., LIN, S. H., MOELLER, C. P. Doublet III Plysics Group, Summary of Electron Cyclotron Heating Physics Results from the Doublet III Tokamak, GA Technologies Report GA-A17939 (1985).

161. BONOLI, P., ENGLADE, R., submitted to Phys. Fluids.

162. JACQUINOT, J., ANDERSON, R., ARBEZ, J., BARTLETT, D., BEAUMONT, B., et al., in Plasma Phys. and Cont. Nucl. Fus. 27 (1985) 1379.

163. FISCH, N., in Heating in Toroidal Plasmas, (Proc. 3rd Int. Symp. Grenoble, 1982) Vol. III, CEC, Brussels (1982) 841.

164. LEUTERER, F., ECKHARTT, D., SOLDNER, F., BECKER, G., BERNHARDI, K., et al., Phys. Rev. Lett. 55 (1985) 75.

165. IGNAT, D. W., RUTHERFORD, P. H., HSUAN, H., Feedback Stabilization of Magnetic Islands by Rf Heating and Current Drive, Int. School of Plasma Physics Course and Workshop of Rf Waves to Tokamak Plasmas, Varenna (1985) [to be published].

166. MC WILLIAMS, R., OKUBO, M., PLATT, R. C., SHEEHAN, D. P., Phys. Fluids 28 (1985) 11.

TABLE 1
Summary of Lower Hybrid Grill Couplers on Tokamaks

Machine	Freq.(GHz)	No. of wgds per grill	Wgd dim. (cm)	Wgd Material	Coating	$\omega_{ce} > \omega$?	Additional Pumping?	Max. power density(kW/cm^2)
JFT-2	.65,.75	4	3.3 x 29	SS	Cu,Ti	No	Yes	1.8
ATC	.8	4	2.5 x 20	SS	-	Yes	No	0.6
PLT	.8	6	3.5 x 22	SS	C	Yes	No	1.6
Versator II	.8	4	2.5 x 24	SS	-	No	No	1.0
Versator II	.8	4	1 x 21	SS	C	No	No	1.6
JIPP-T II	.8	2	14 x 68(c-shaped)	SS		Yes	No	1
Wega	.8	4	2 x 24.4	Ti SS	Ti	No No	-	2
T-7	.9	3	2 x 22.0	SS	Ti	No	No	1.9
WT-II	.915	4	1.3 x 18.5		-		No	0.5
Petula B	1.25	4	1.8 x 16.5	Ti	Ti	No	Yes	3.4
Petula B	1.25	4	1.9 x 16.5	SS	-	No	No	3.4
Asdex	1.3	8	3.0 x 16.5	SS	Cu,Au	No	Yes	5.4
JT-60	1.7-2.3	32(8 x 4)	3 x 11.5, 1.8 x 11.5	SS	Cu	No	Yes	4.5(planned)
Alcator A	2.45	2	1.3 x 8.1	SS	-	Yes	No	4.5
Alcator A	2.45	2	1.3 x 8.1	SS	-	No	No	8
FT	2.45	4(2 x 2)	1.5 x 7.1	SS	-	Yes	No	6
PLT	2.45	8	1.0 x 10.0	SS	-	Yes	No	5(planned)
Versator II	2.45	4	1.0 x 8.6	SS	-	No	No	2.5
Alcator C	4.6	16(4 x 4)	0.8 x 5.8	SS	-	Yes	No	9

Figure Captions

Fig. 1 (a) $n_\perp^2$ versus density, n_e for $n_\parallel < n_{\parallel crit}$. The densities n_e^- and n_e^+ represent the fast/slow mode conversions.

(b) $n_\perp^2$ versus n_e for $n_\parallel > n_{\parallel crit}$.

Fig. 2 Sketch of a passive slow wave structure. The wave propagates in the z-direction between the ribbed structure on the right and the plasma surface represented by the sheet on the left. Longitudinal electric fields are excited in the slots between the ribs.

Fig. 3 The Doublet II slow wave antenna, fed by stripline. Top: view of the antenna from the plasma. The toroidal field lies in the vertical direction. Bottom: cross section of the antenna looking along the magnetic field. Each radiating element is one-half wavelength long. After Ref. [28].

Fig. 4 Diagram of a grill launcher inserted through a port in the vacuum vessel wall. The electric field strength at the face of the grill is shown for relative phase difference of $\Delta\phi = 180°$ between adjacent waveguides.

Fig. 5 (a) Diagram of the Alcator C array. After Ref. [1].

(b) Photograph of the Alcator C sixteen-waveguide grill.

Fig. 6 (a) Diagram of the Asdex eight-waveguide array. The standard window sections at the bottom left are attached to the waveguide vacuum flanges. The grill tip at the right is demountable to allow for installation of grills of different dimensions.

(b) Photograph of the Asdex grill and pumping manifold. After Ref. [46].

Fig. 7 (a) Schematic of twin waveguide launcher on H-1.

(b) Twin waveguide with dummy waveguides attached to improve the spectrum. After Ref. [42].

Fig. 8 Schematic diagram of a lower hybrid heating system. After Ref. [115].

Fig. 9 Schematic diagram of the Alcator C lower hybrid rf heating system. After Ref. [1].

Fig. 10 Summary sketch of the grill couplers and window arrangements used in lower-hybrid heating systems on tokamaks.

Fig. 11 Idealized density behavior near the grill mouth.

Fig. 12 (a) Calculated $n_\parallel$ spectrum of the Versator II 800 MHz four-waveguide grill (waveguide width of 2.45 cm, septum thickness of 0.6 cm) for $\Delta\phi = 0°$, 90°, and 180°. The density at the waveguide mouth is 7.9×10^{10} cm^{-3} and the density gradient is 5.3×10^{11} cm^{-4}. After Ref. [115].

(b) Calculated $n_\parallel$ spectrum of the Alcator C 4.6 GHz grill (waveguide width of 0.8 cm, septum thickness of 0.2 cm). The density at the waveguide mouth is 2.6×10^{12} cm^{-3} and the density gradient is 1.3×10^{13} cm^{-4}.

Fig. 13 Calculated $n_\parallel$ spectrum for a two-waveguide grill (dotted line), four-waveguide grill (dot-dash line), eight-waveguide grill (solid line), and sixteen-waveguide grill (dashed line): at $\Delta\phi = 90°$. The waveguide dimensions and edge plasma conditions are identical to those in Fig. 12b.

Fig. 14 Calculated reflectivity of the Alcator C grill versus the density at the grill mouth for density gradients of $\nabla n = 1.3 \times 10^{12}$ cm^{-4} (solid line), $\nabla n = 1.3 \times 10^{13}$ cm^{-4} (dashed line), and $\nabla n = 6.6 \times 10^{13}$ cm^{-4} (dot-dash line); $\Delta\phi = 180°$. The density axis is labelled in terms of $\mu = n_o/n_c$.

Fig. 15 Calculated reflectivity of the Alcator C grill versus the density at the grill mouth, for $\Delta\phi = 0°$ (solid line), $\Delta\phi = 90°$ (dashed line), and $\Delta\phi = 180°$ (dot-dash line). The density gradient is taken to be $\nabla n = n_o/L$ where $L = 0.2$ cm.

Fig. 16 Calculated reflectivity of the Alcator C grill versus $\Delta\phi$ for $\mu = 5$, $\nabla n = 6.6 \times 10^{12}$ cm^{-4}.

Fig. 17 Reflection coefficient versus phase difference between waveguides of a teflon-loaded double waveguide array on the H-1 linear device. The points represent experimental data and the solid line is the theoretical result derived using the measured density gradient. After Ref. [93].

Fig. 18 Comparison of the theoretical and measured grill reflectivities in the Versator II lower hybrid experiment. The solid lines represent the fits to the experimental data (open symbols) and the dashed lines are the calculated reflectivities (solid symbols). The plasma density increases to the left of the figure. After Ref. [115].

Fig. 19 (a) Calculated reflectivities for individual waveguides in the Petula B grill for $\Delta\phi = 180°$ using the measured density profile in front of the grill mouth. The plasma density increases to the right in the figure.

(b) Experimentally measured reflectivities of the individual waveguides of the Petula B grill. After Ref. [40].

Fig. 20 The measured lower hybrid power spectrum $S(n_\parallel^*)$ in the Alcator C tokamak for $\Delta\phi = 180°$. The solid circles represent the measured spectrum $S(n_\parallel^*)$ where $n_\parallel^*$ is deduced from the measured $k_\perp$. The midplane density) is used for the calculations. The laser beam is at $x/a = 0.7$, and the plasma parameters are $B_o = 8T$ and $\bar{n}_e = 1.5 \times 10^{14}$ cm^{-3} in deuterium. The solid curve is the calculated Brambilla spectrum. After Ref. [97].

Fig. 21 (a) Top view of an eight-waveguide multi-junction grill designed to launch a travelling wave spectrum ($\Delta\phi = \pi/2$). The grill is fed by two standard waveguides excited out of phase with one another. Vacuum seals would be made in each of the large waveguides. The labeled blocks in the small waveguides represent passive phase shifters.

(b) Sections of reduced height waveguides act as phase shifters to set the relative phase difference between adjacent waveguides at the grill mouth. The gradual reduction of waveguide height reduces the mismatch of the phase shifter to the rest of the line. After Ref. [154].

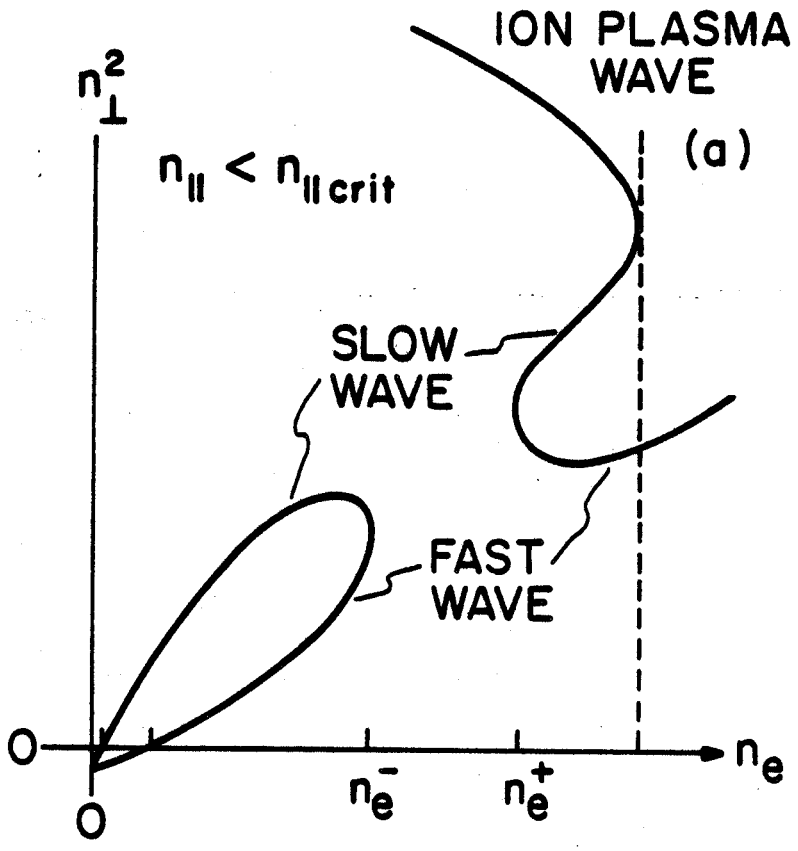
ION PLASMA
WAVE
$n_\perp^2$
$n_{\parallel} < n_{\parallel crit}$
(a)
SLOW
WAVE
FAST
WAVE
O
O
n_e^-
n_e^+
n_e

Figure 1a

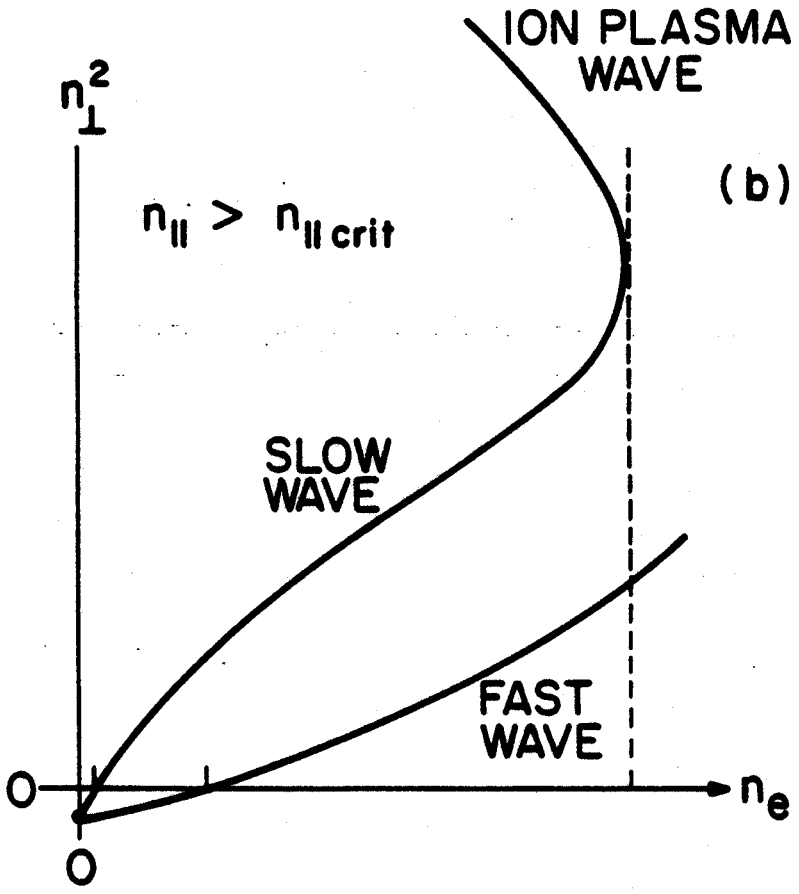
ION PLASMA
WAVE
$n_\perp^2$
(b)
$n_{\parallel} > n_{\parallel crit}$
SLOW
WAVE
FAST
WAVE
0
n_e
0

Figure 1b

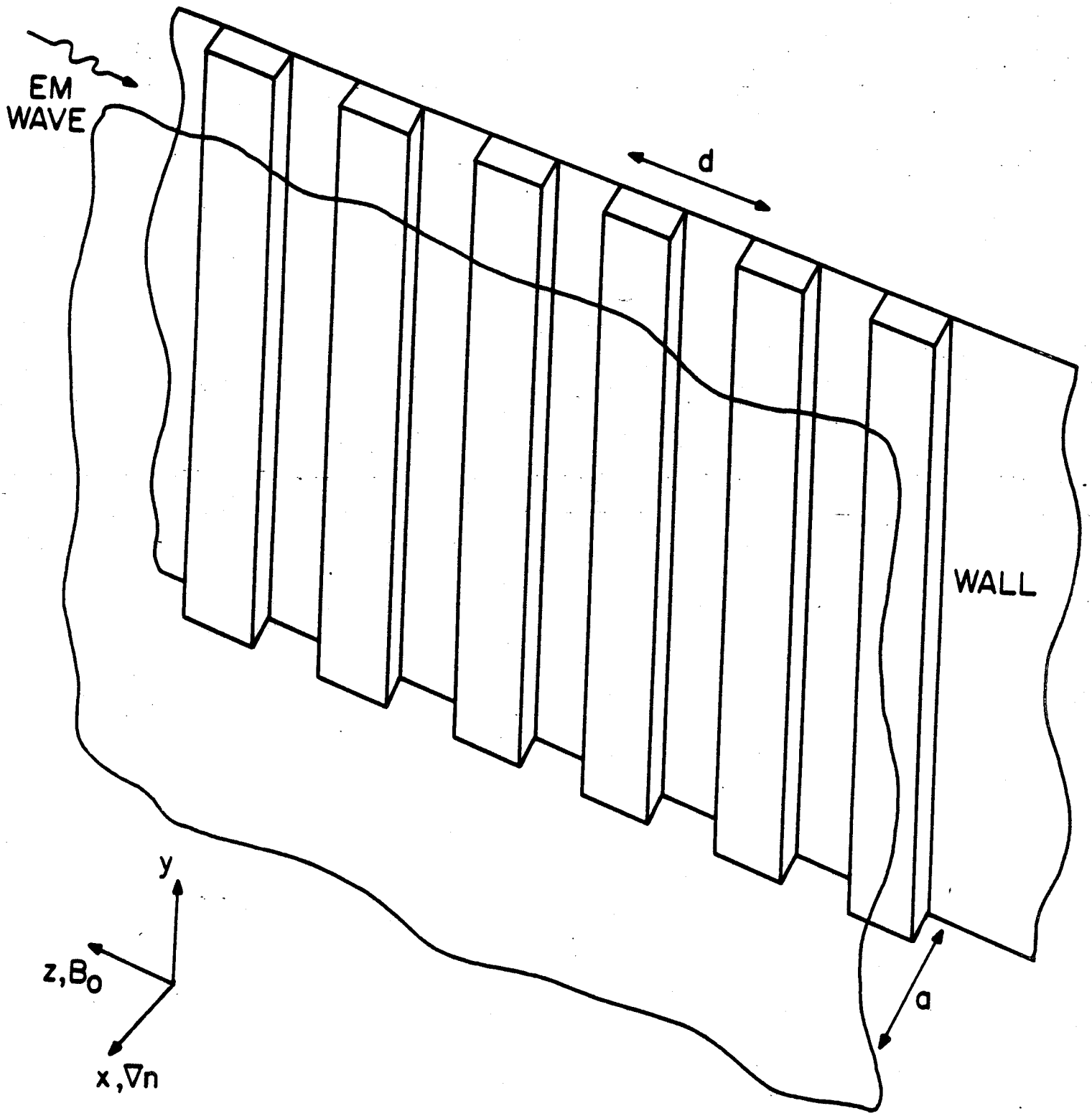

Figure 2

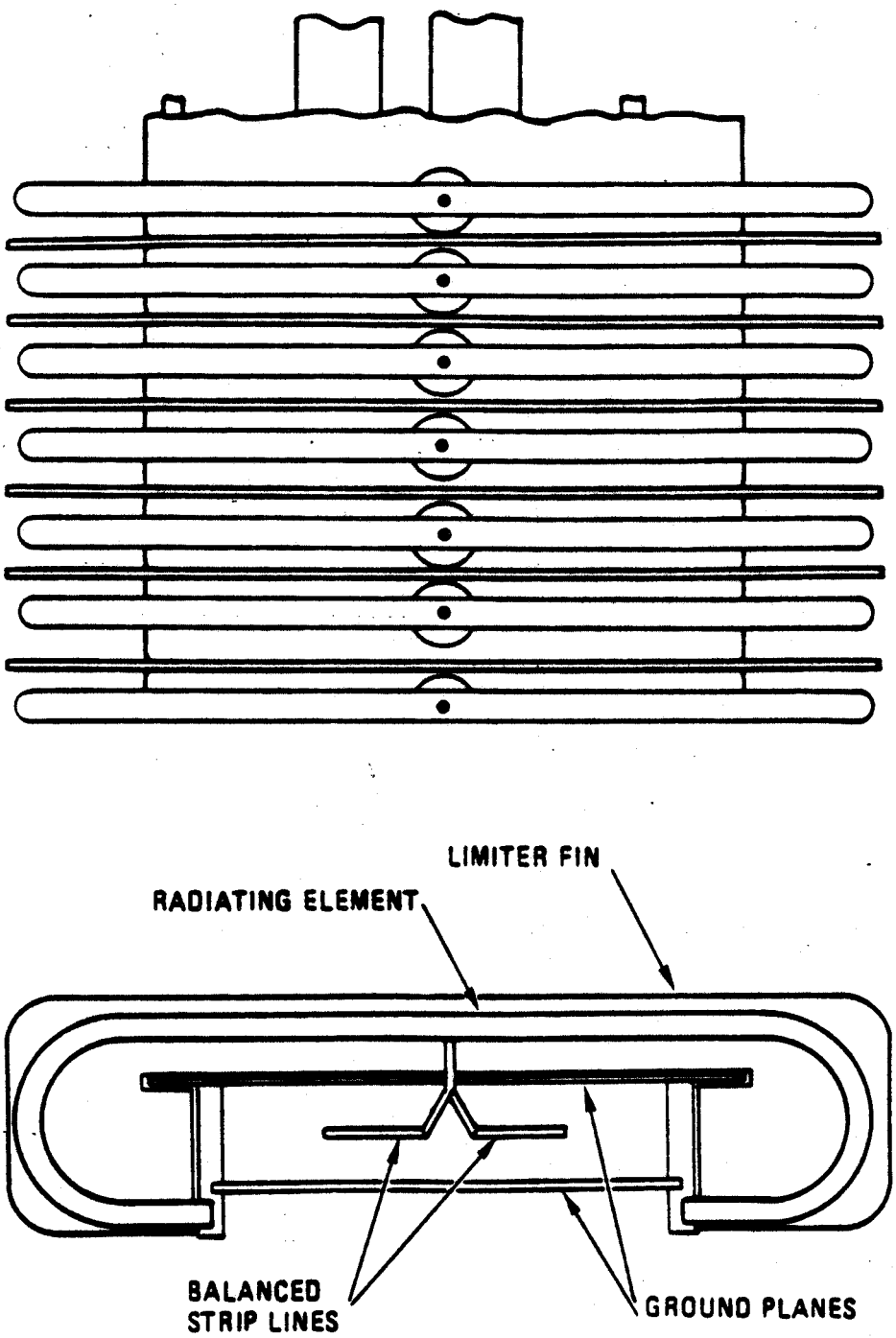
LIMITER FIN
RADIATING ELEMENT
BALANCED
STRIP LINES
GROUND PLANES

Figure 3

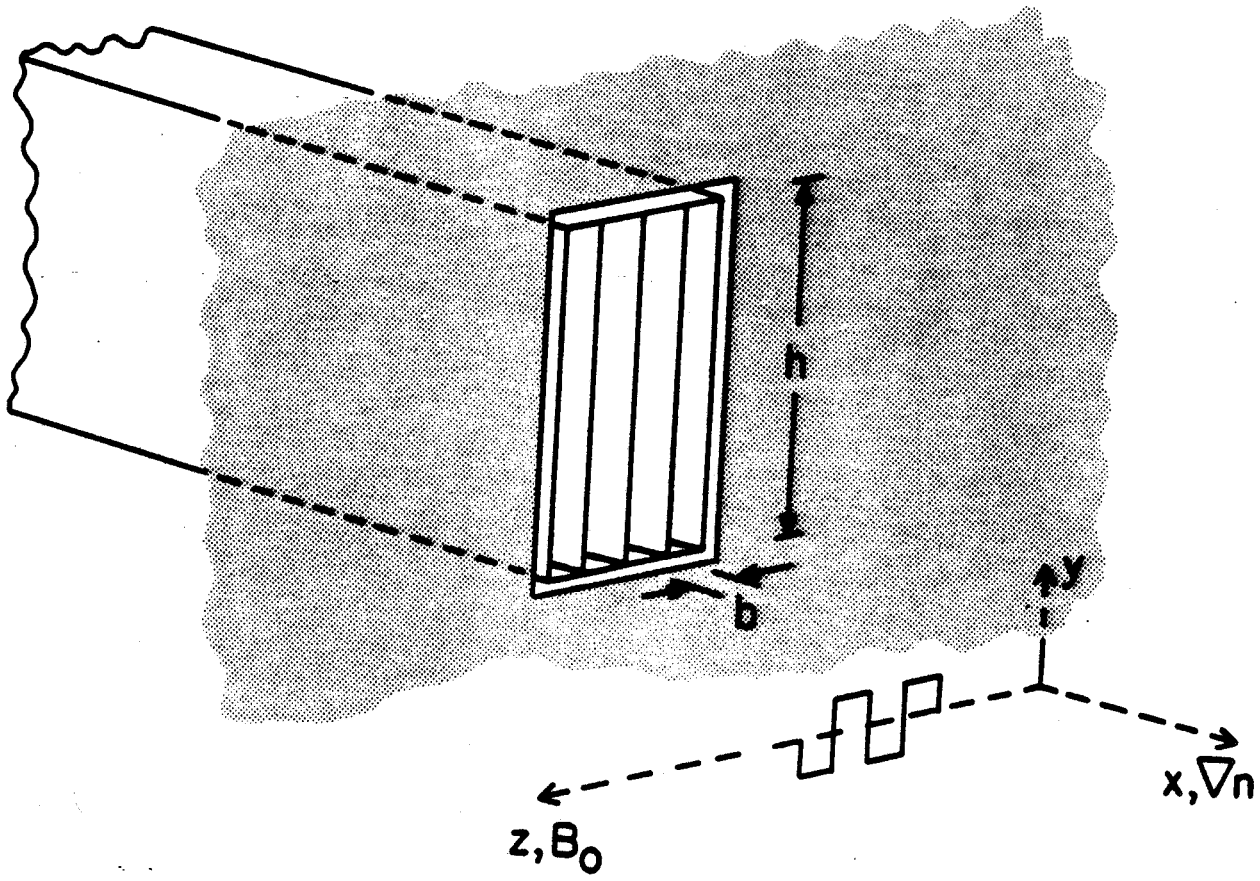

Figure 4

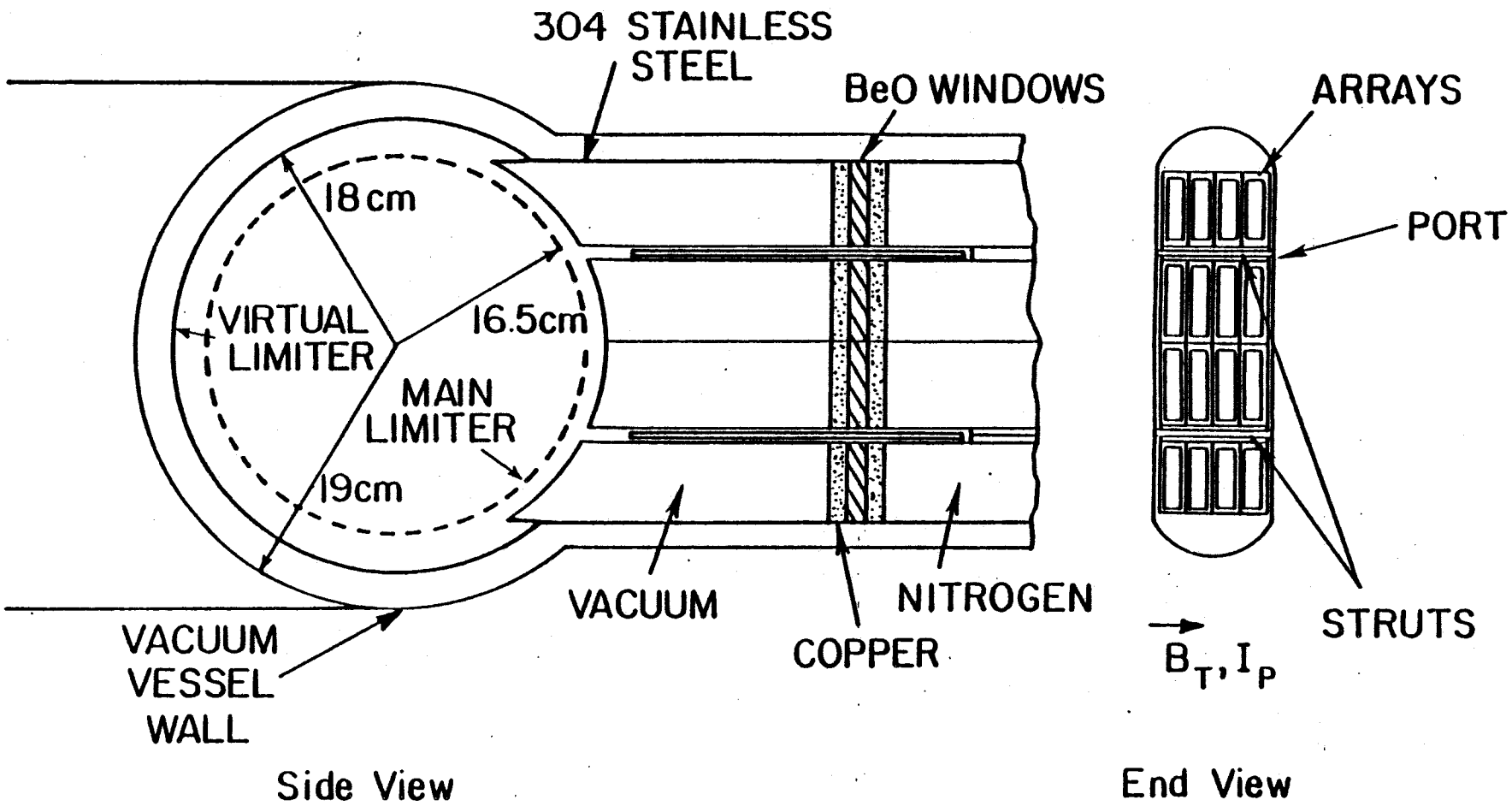
304 STAINLESS STEEL
BeO WINDOWS
ARRAYS
PORT
18cm
16.5cm
VIRTUAL LIMITER
MAIN LIMITER
19cm
VACUUM
NITROGEN
COPPER
STRUTS
VACUUM VESSEL WALL
B_T, I_P
Side View
End View

Figure 5a

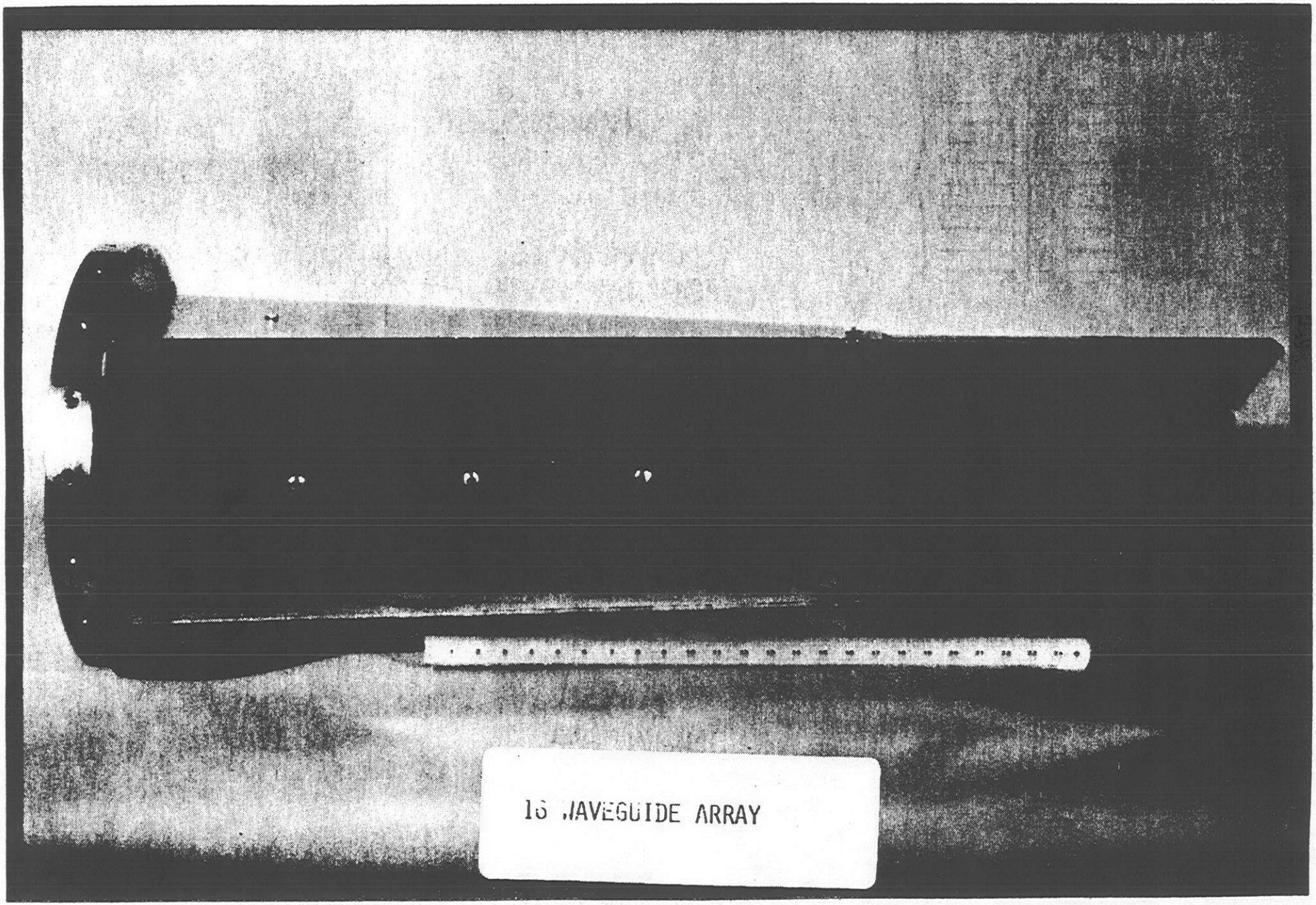

Figure 5b

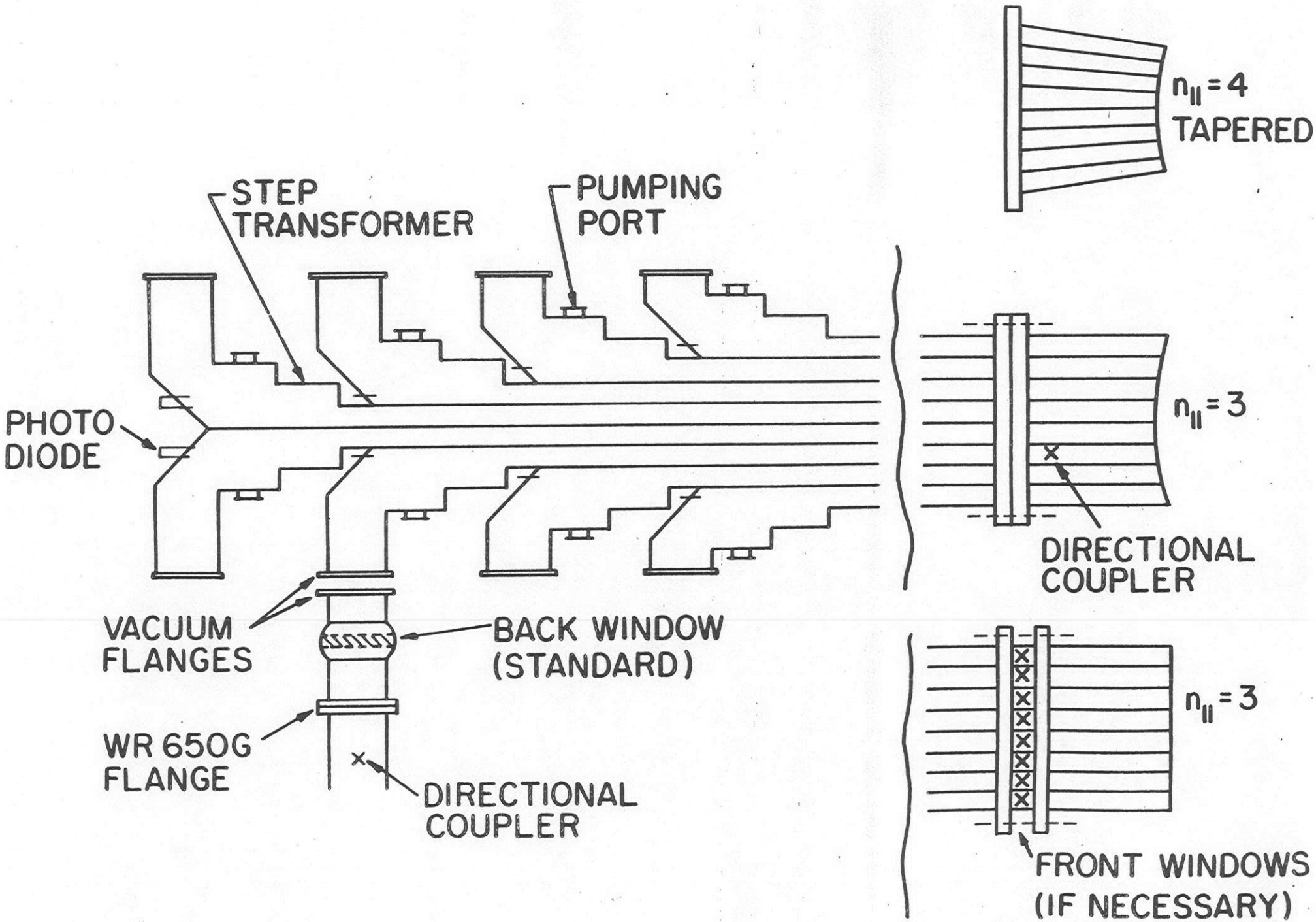
$n_{\parallel} = 4$
TAPERED
STEP
TRANSFORMER
PUMPING
PORT
PHOTO
DIODE
$n_{\parallel} = 3$
DIRECTIONAL
COUPLER
VACUUM
FLANGES
BACK WINDOW
(STANDARD)
WR 650G
FLANGE
DIRECTIONAL
COUPLER
$n_{\parallel} = 3$
FRONT WINDOWS
(IF NECESSARY)

Figure 6a

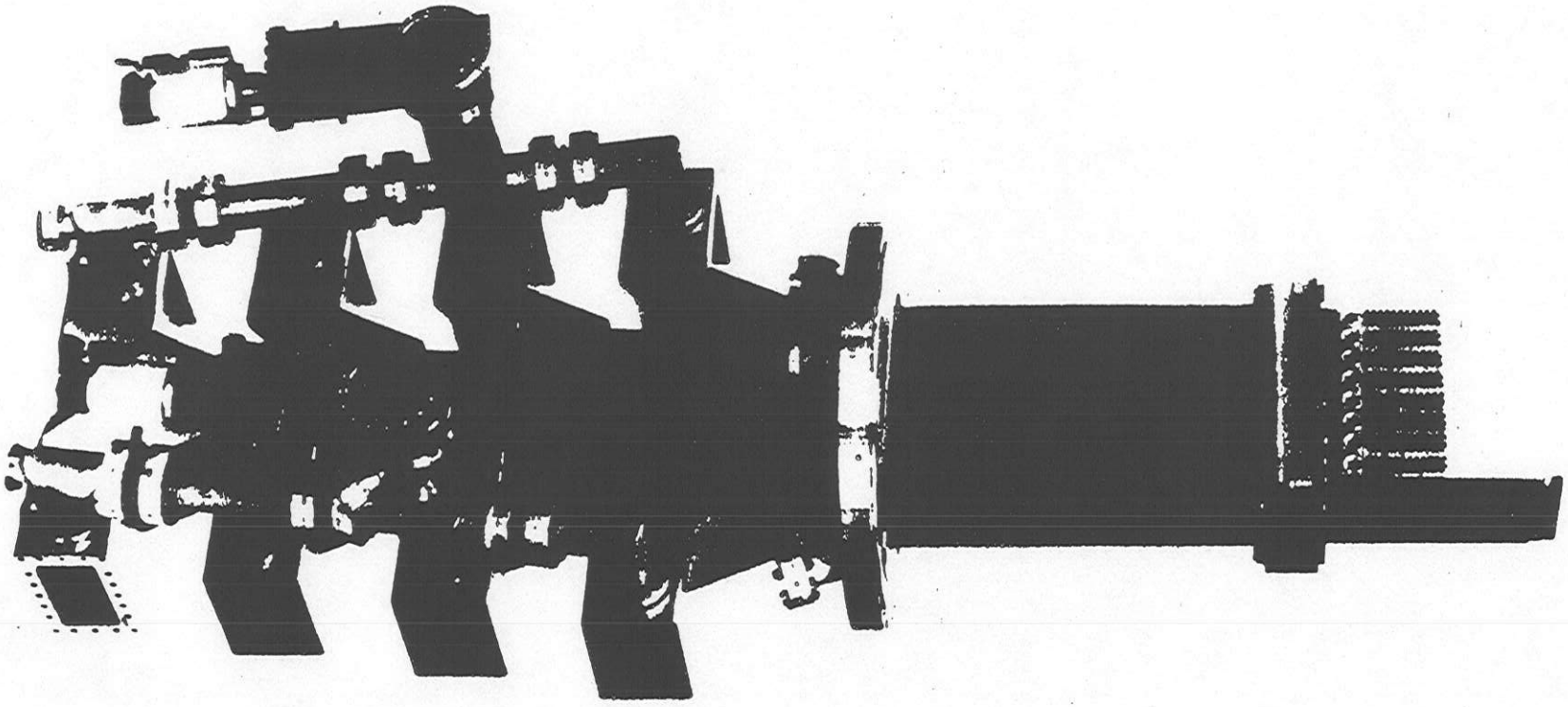

Figure 6b

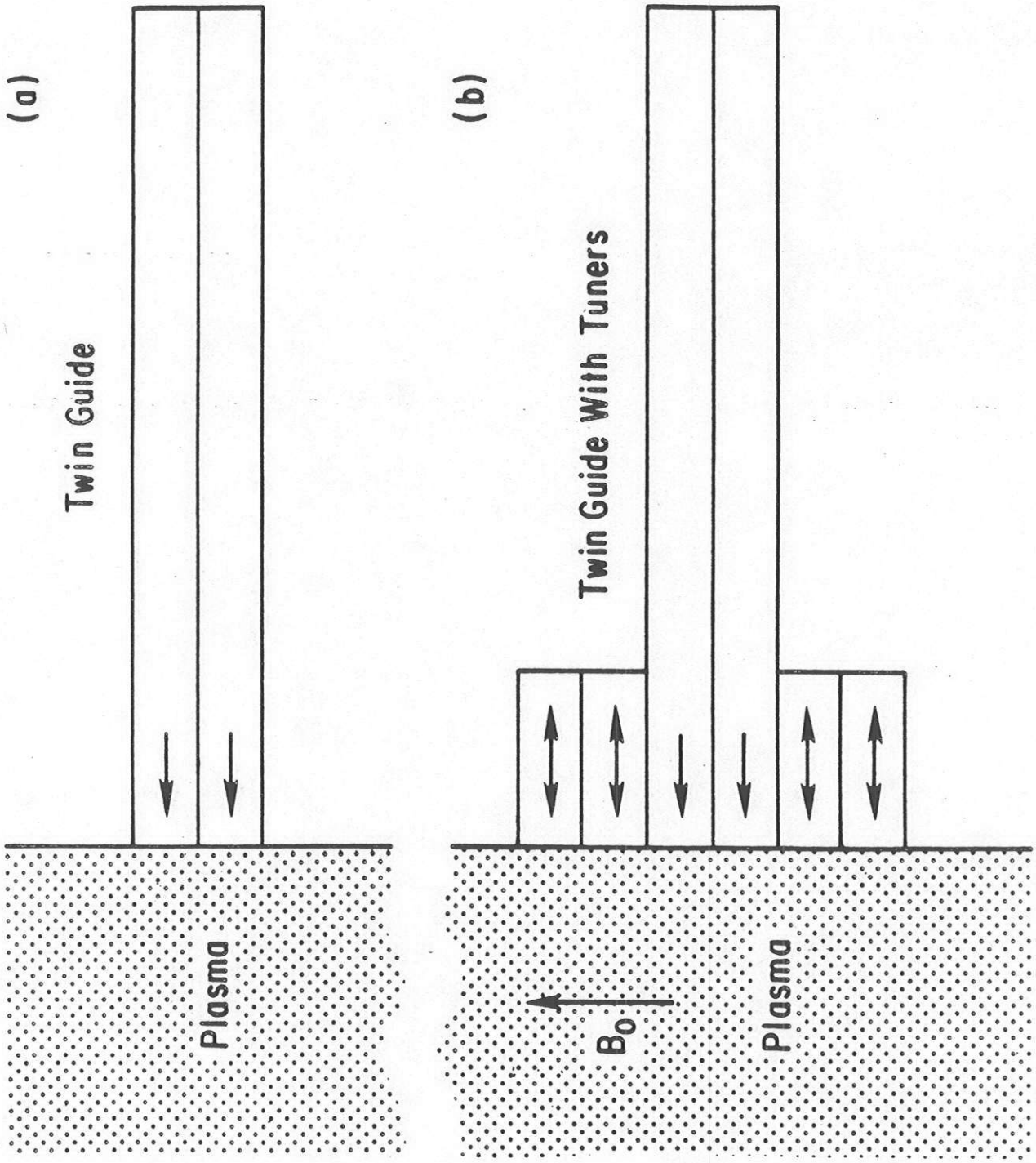

Figure 7

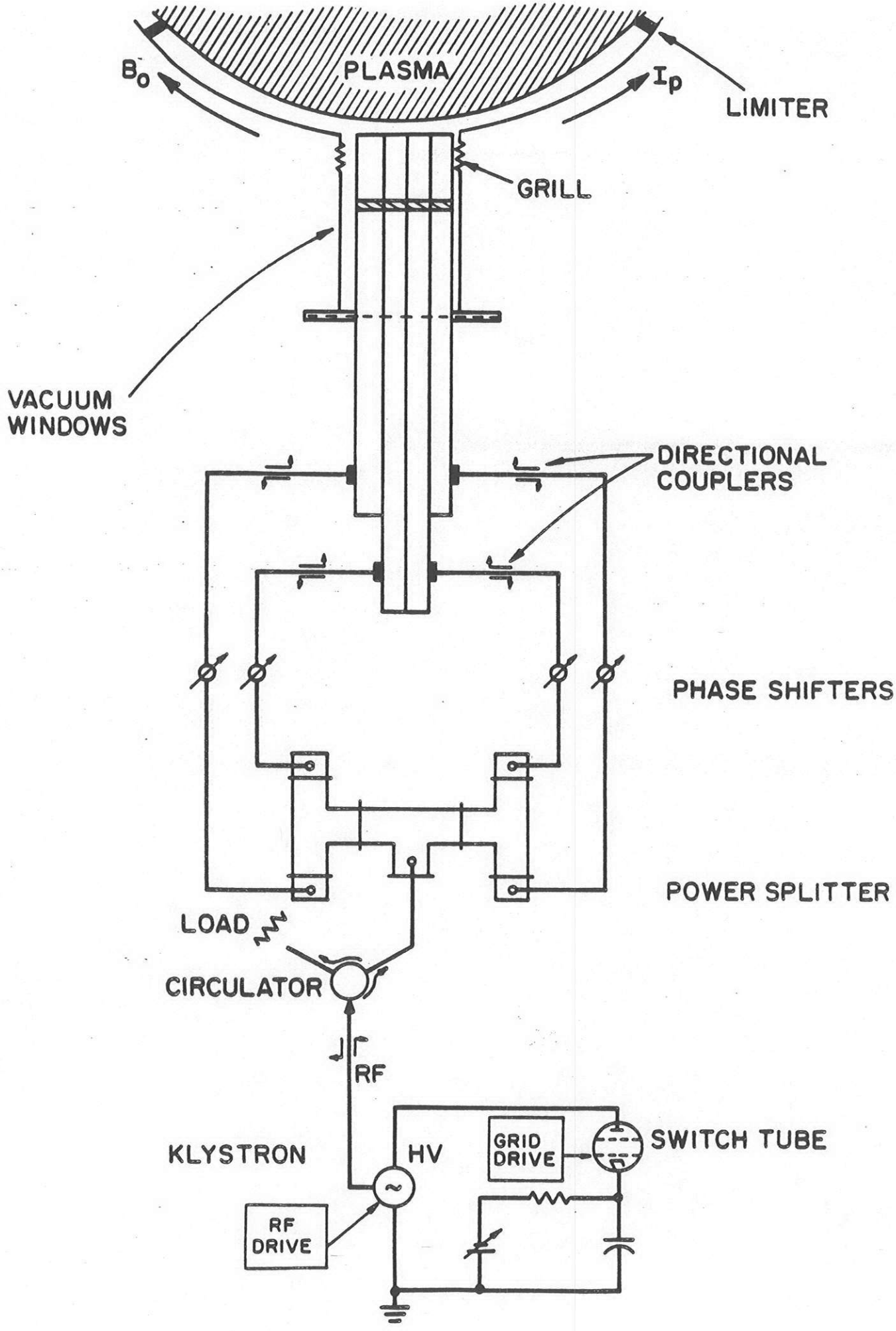
PLASMA
B_o
I_p
LIMITER
GRILL
VACUUM WINDOWS
DIRECTIONAL COUPLERS
PHASE SHIFTERS
POWER SPLITTER
LOAD
CIRCULATOR
RF
KLYSTRON
HV
GRID DRIVE
SWITCH TUBE
RF DRIVE

Figure 8

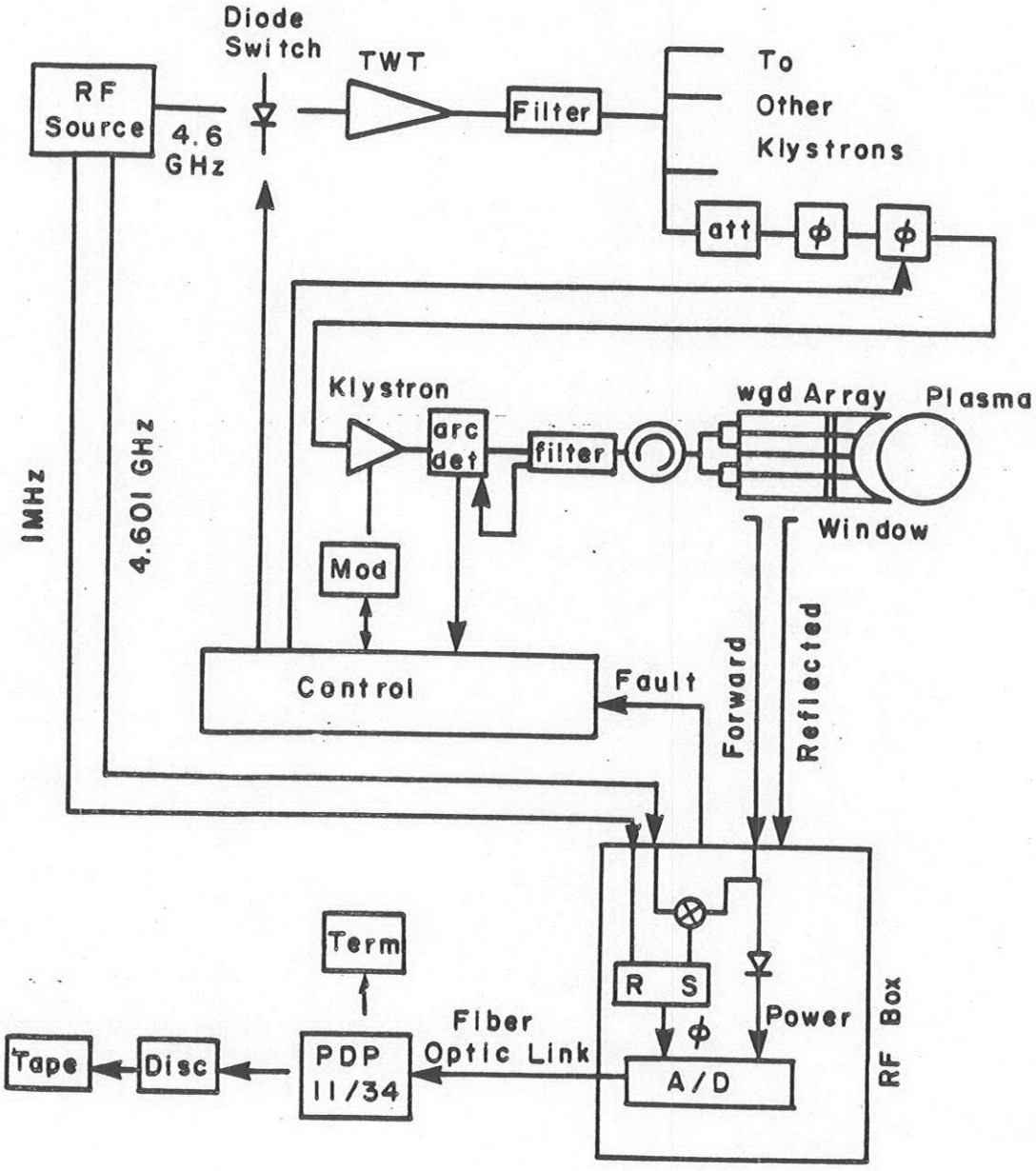
Diode
Switch
TWT
RF
Source
4.6
GHz
Filter
To
Other
Klystrons
att
ϕ
ϕ
Klystron
arc
det
filter
wgd Array
Plasma
Window
1MHz
4.601 GHz
Mod
Control
Fault
Forward
Reflected
Term
R S
ϕ
Power
Fiber
Optic Link
Tape
Disc
PDP
11/34
A/D
RF Box

Figure 9

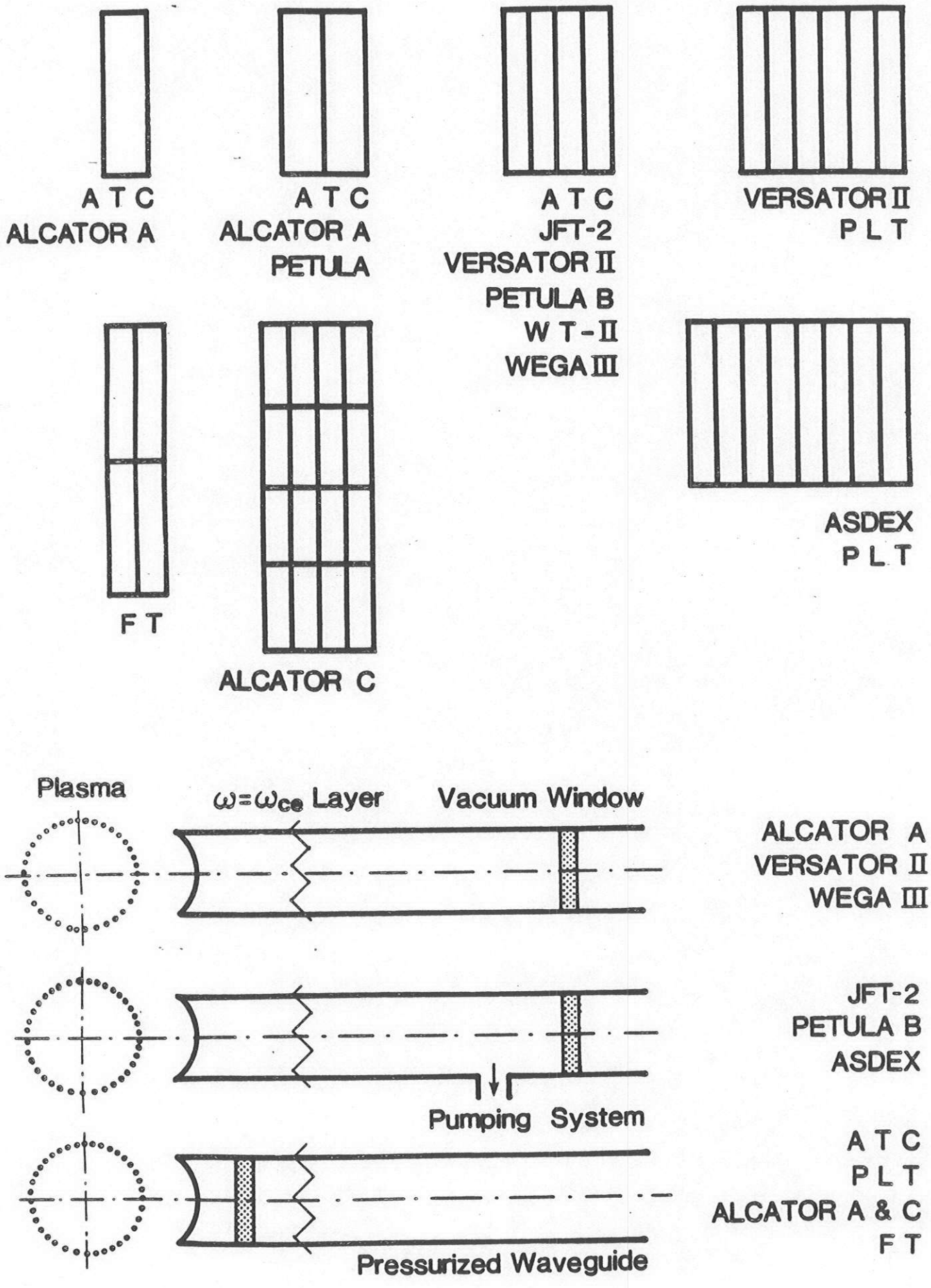
A T C
ALCATOR A
A T C
ALCATOR A
PETULA
A T C
JFT-2
VERSATOR II
PETULA B
W T-II
WEGA III
VERSATOR II
P L T
F T
ALCATOR C
ASDEX
P L T
Plasma
ω=ωce Layer
Vacuum Window
ALCATOR A
VERSATOR II
WEGA III
JFT-2
PETULA B
ASDEX
Pumping System
A T C
P L T
ALCATOR A & C
F T
Pressurized Waveguide

Figure 10

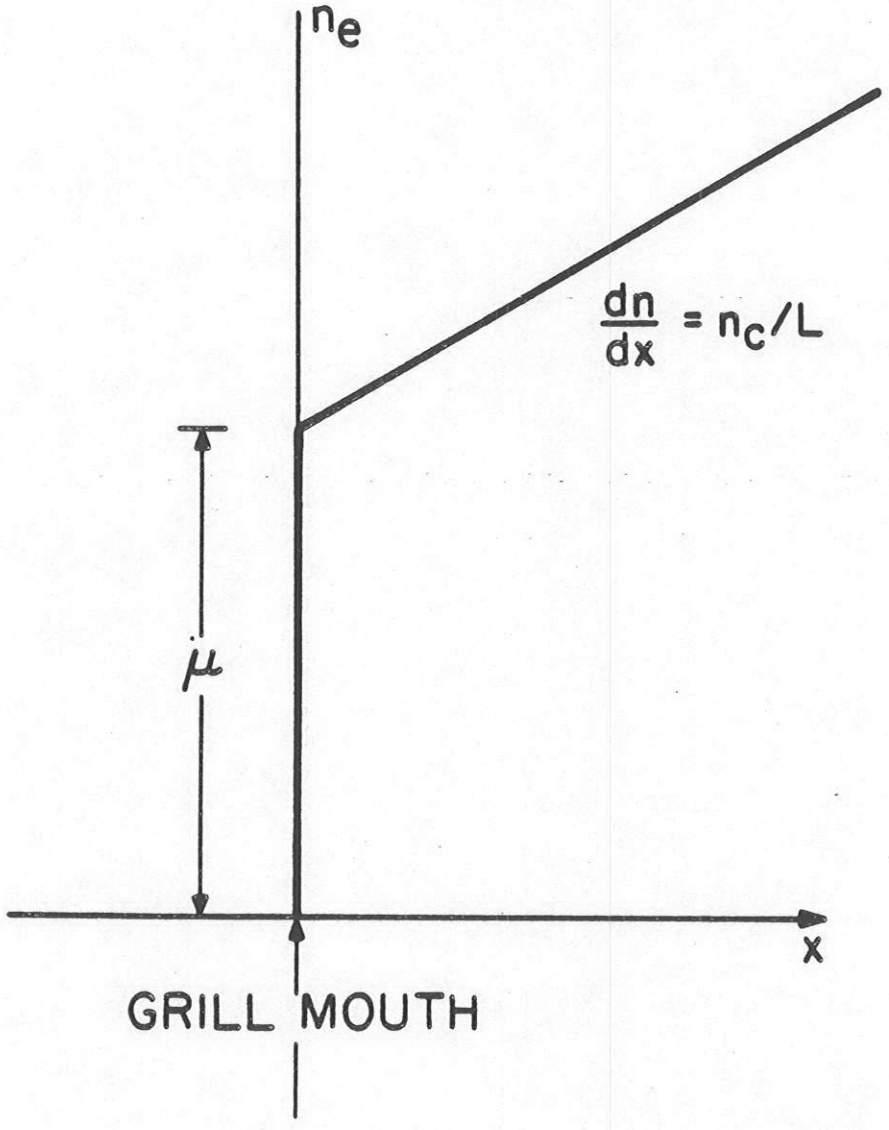

Figure 11

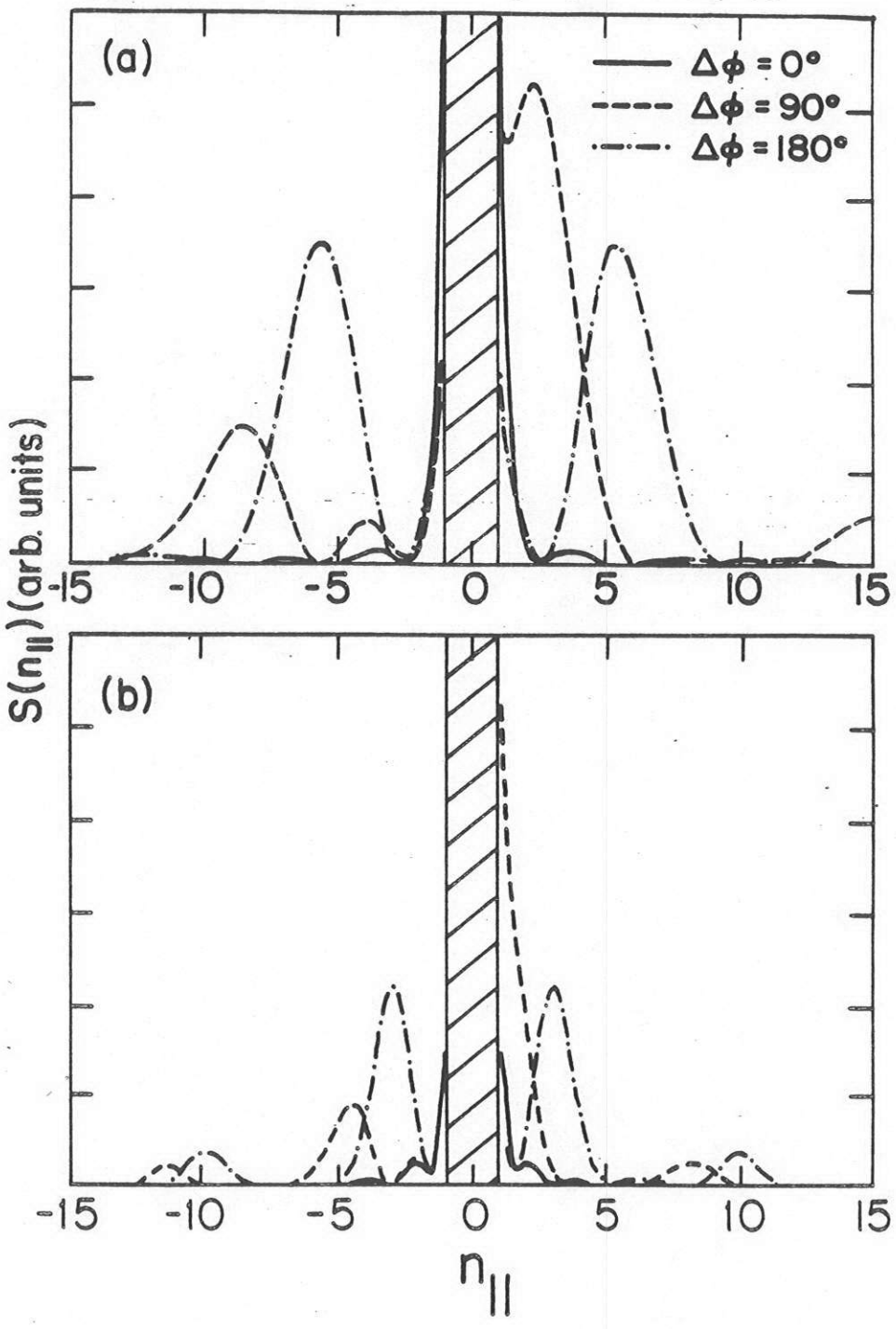

Figure 12

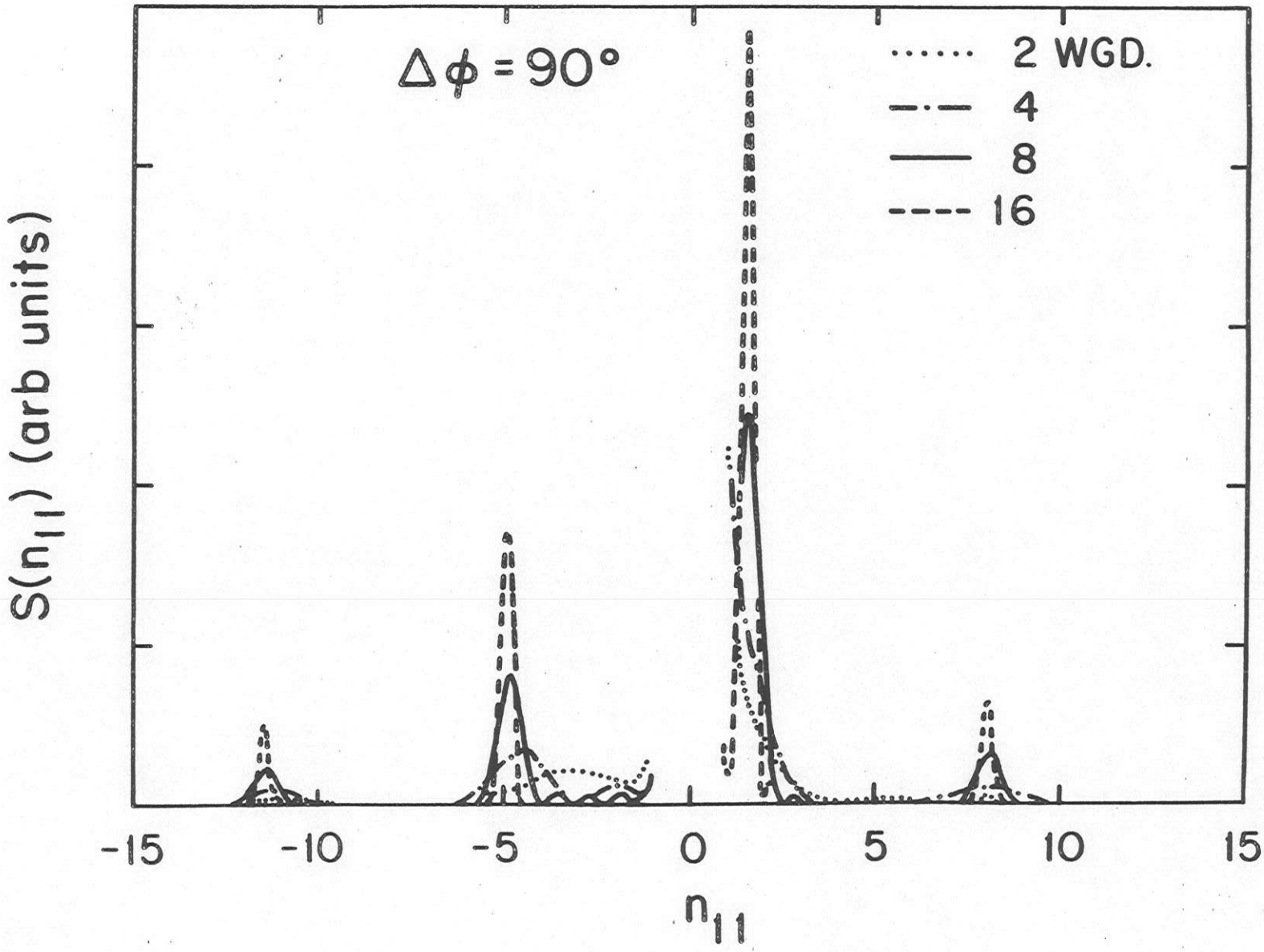

Figure 13

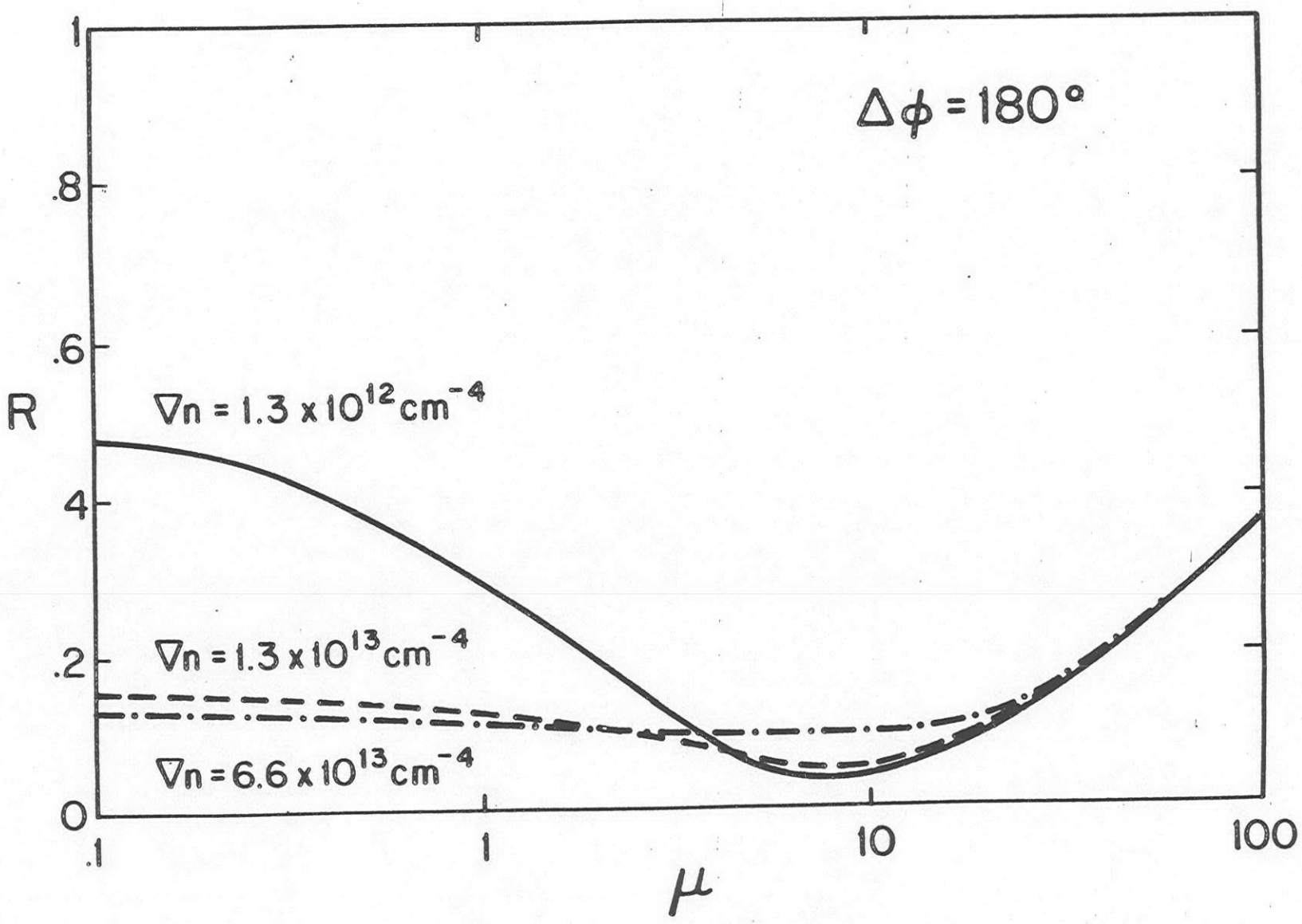
Δφ = 180°
∇n = 1.3 x 10^12 cm^-4
∇n = 1.3 x 10^13 cm^-4
∇n = 6.6 x 10^13 cm^-4
R
μ
1
.8
.6
4
.2
0
.1
1
10
100

Figure 14

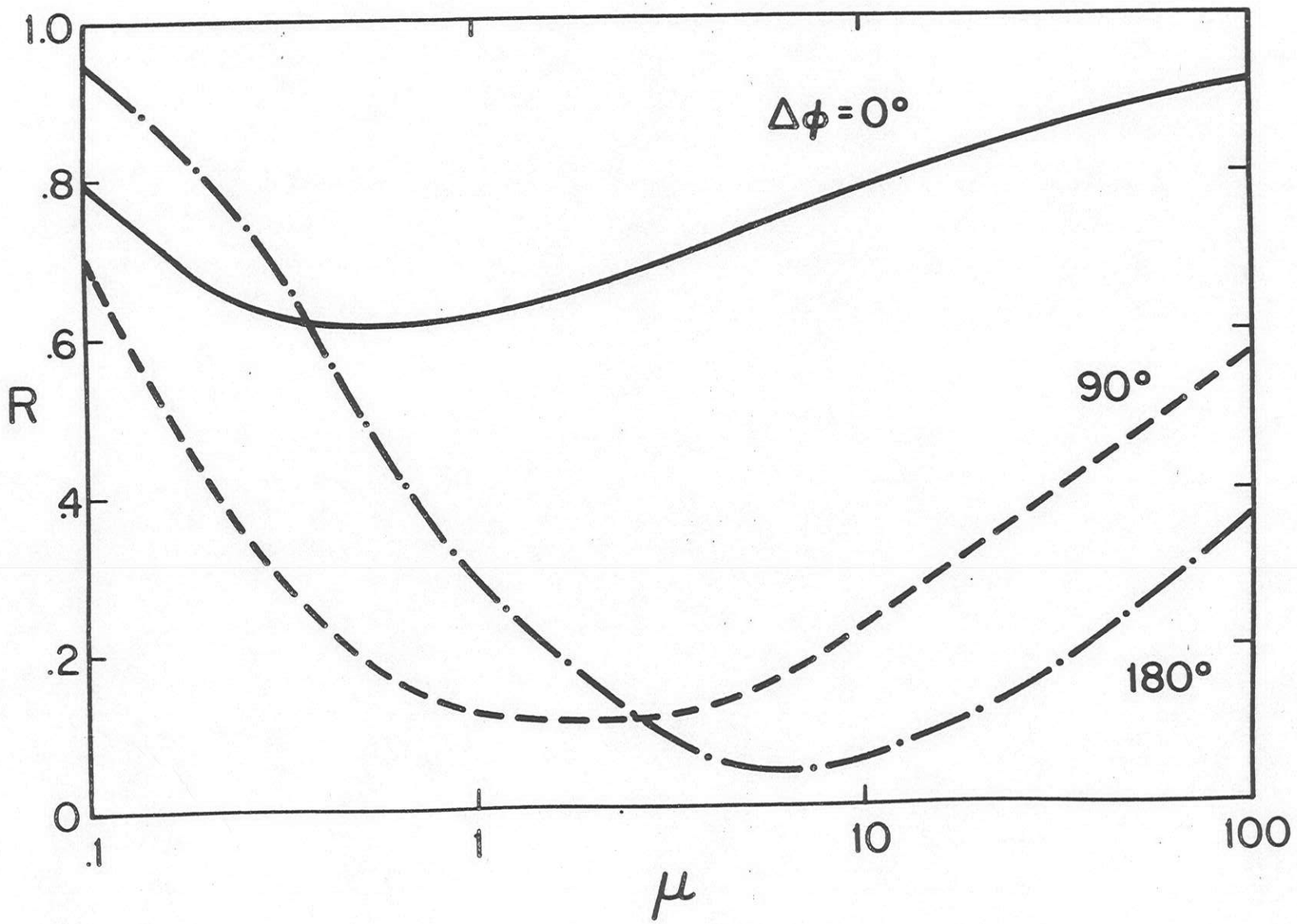

Figure 15

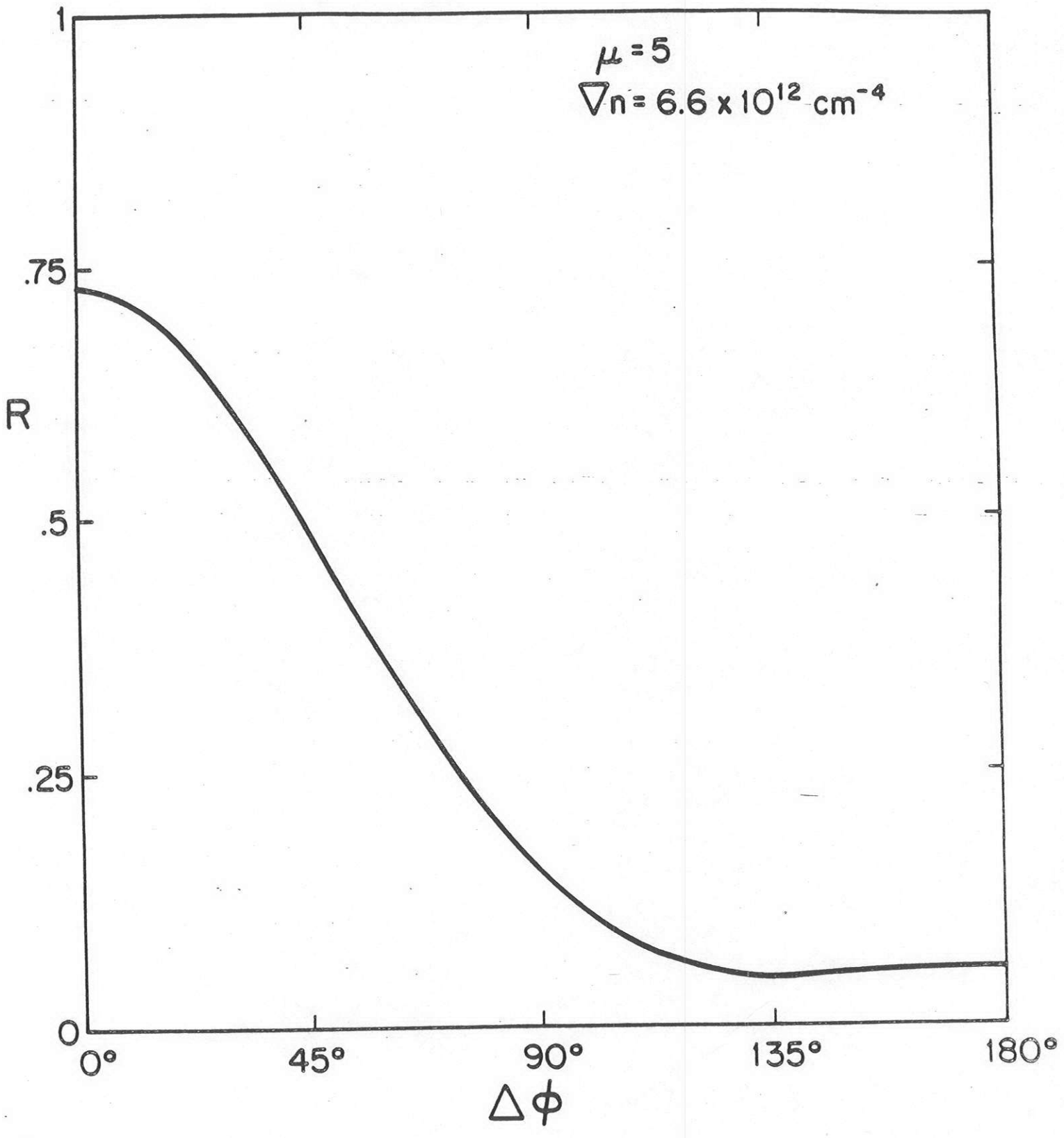

Figure 16

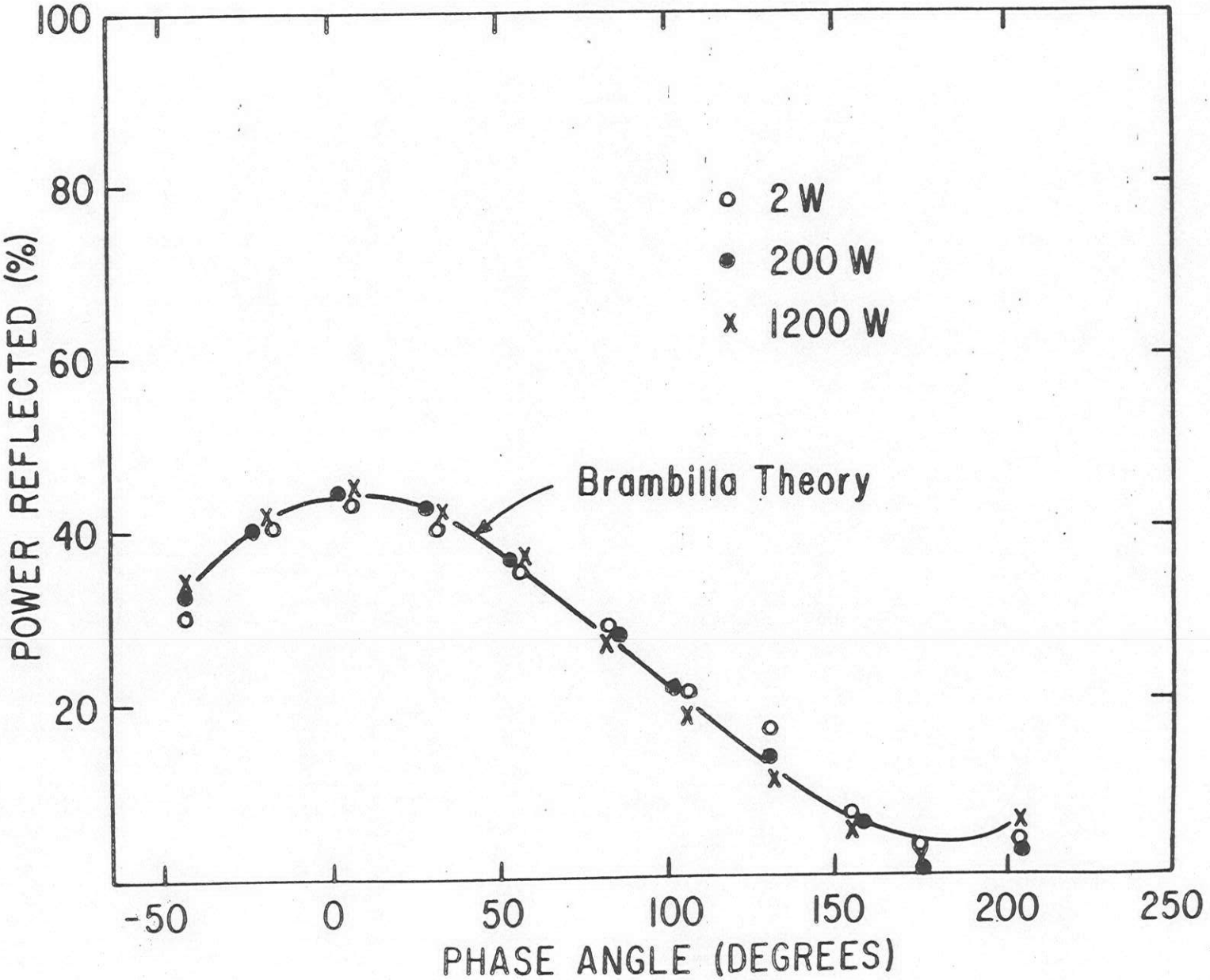
100
80
60
40
20
POWER REFLECTED (%)
2 W
200 W
1200 W
Brambilla Theory
-50
0
50
100
150
200
250
PHASE ANGLE (DEGREES)

Figure 17

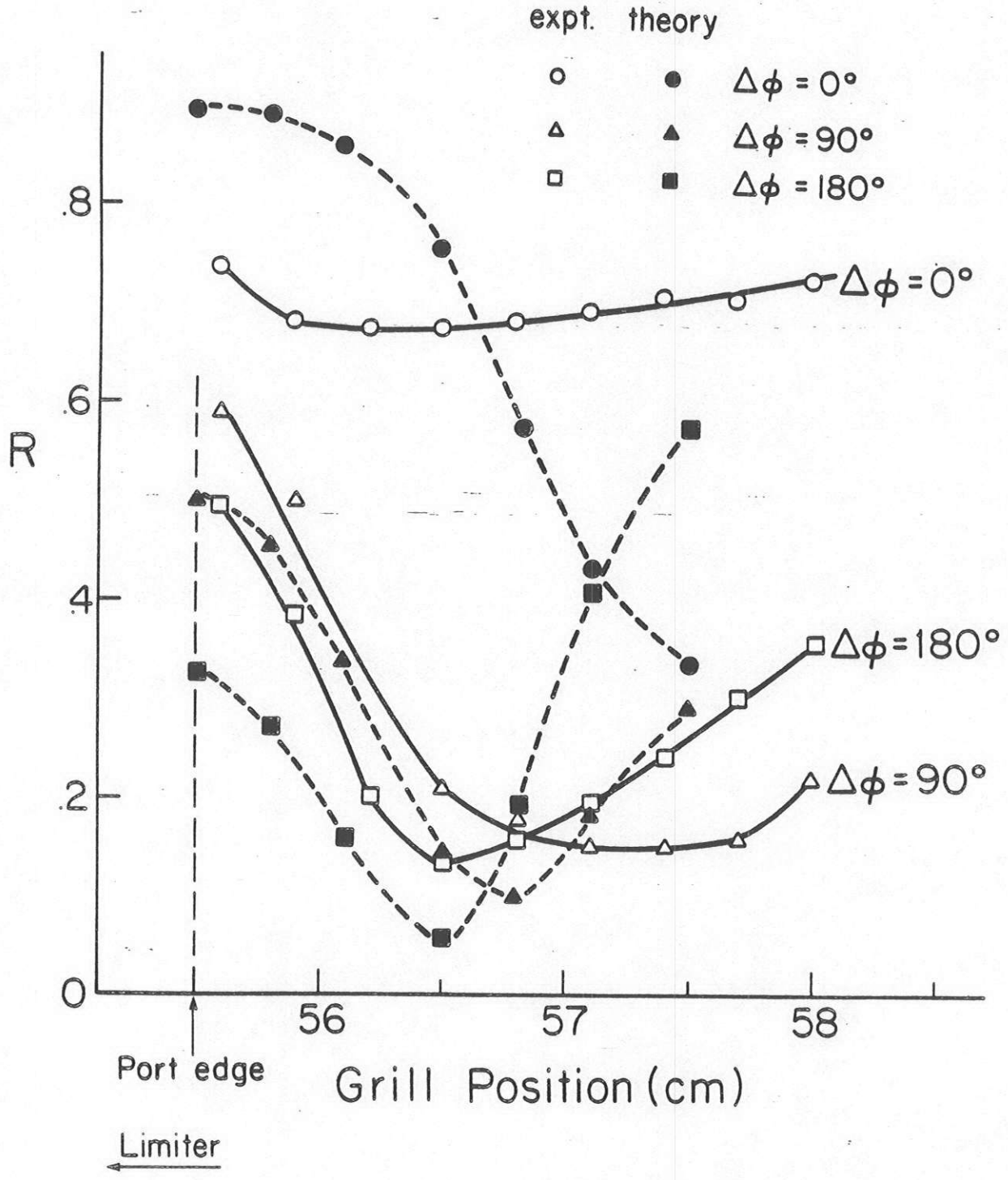
expt. theory
Δφ = 0°
Δφ = 90°
Δφ = 180°
Δφ = 0°
Δφ = 180°
Δφ = 90°
R
.8
.6
.4
.2
0
56
57
58
Port edge
Grill Position (cm)
Limiter

Figure 18

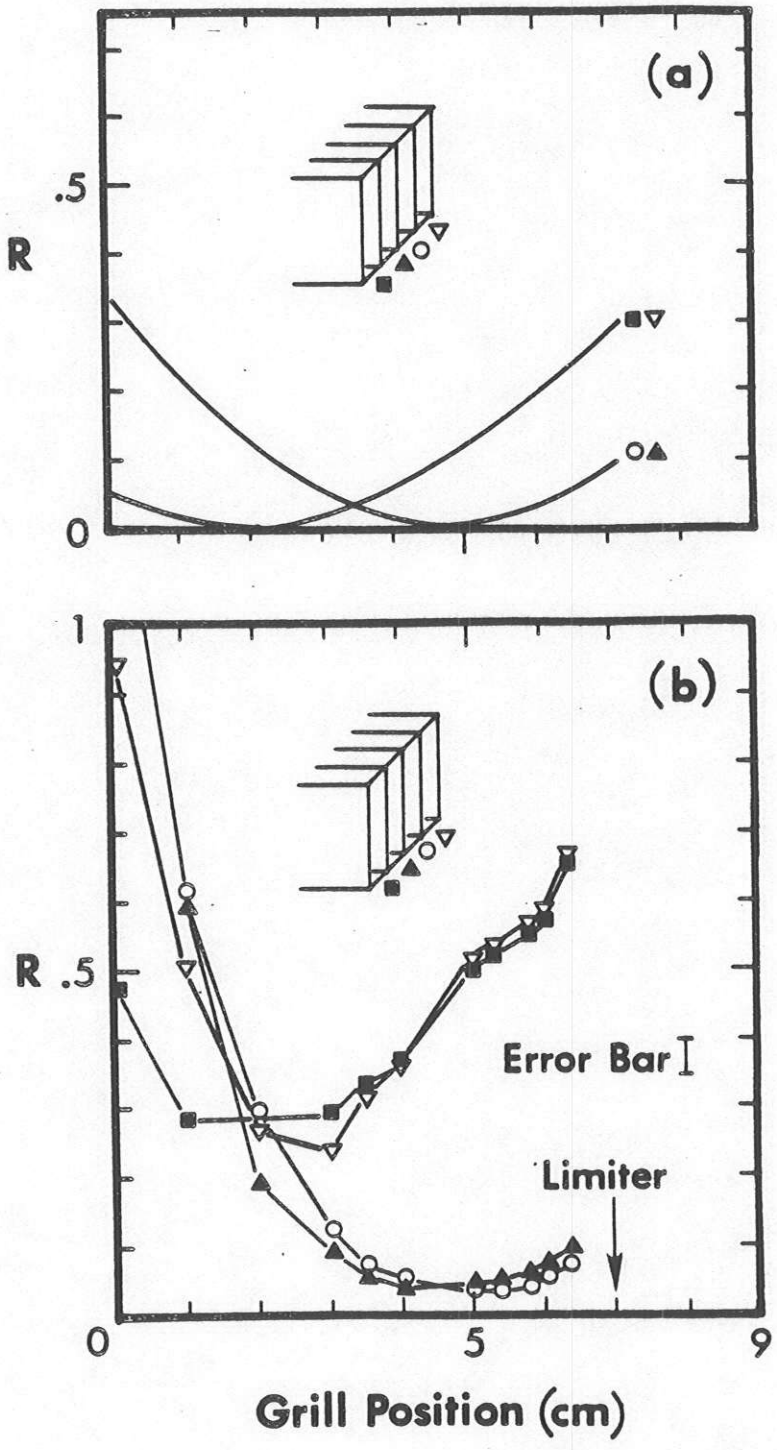

Figure 19

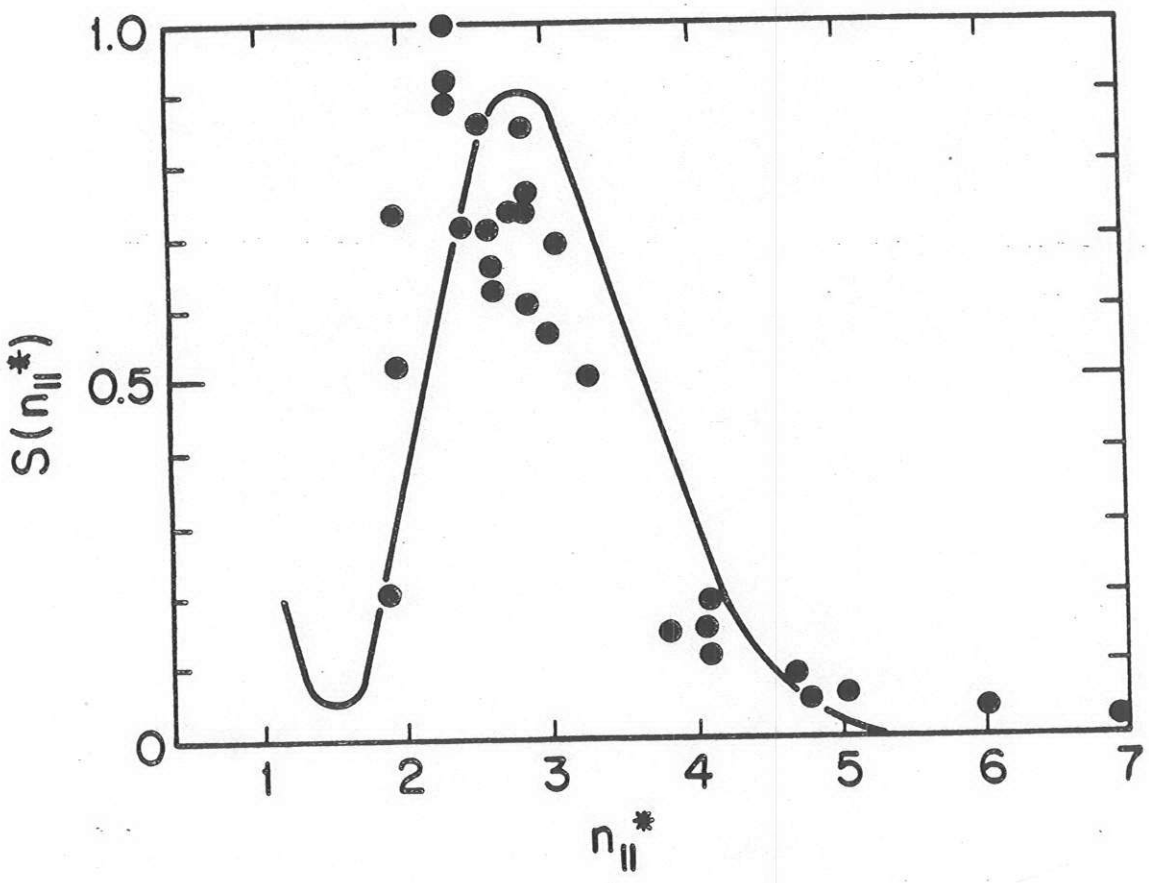

Figure 20

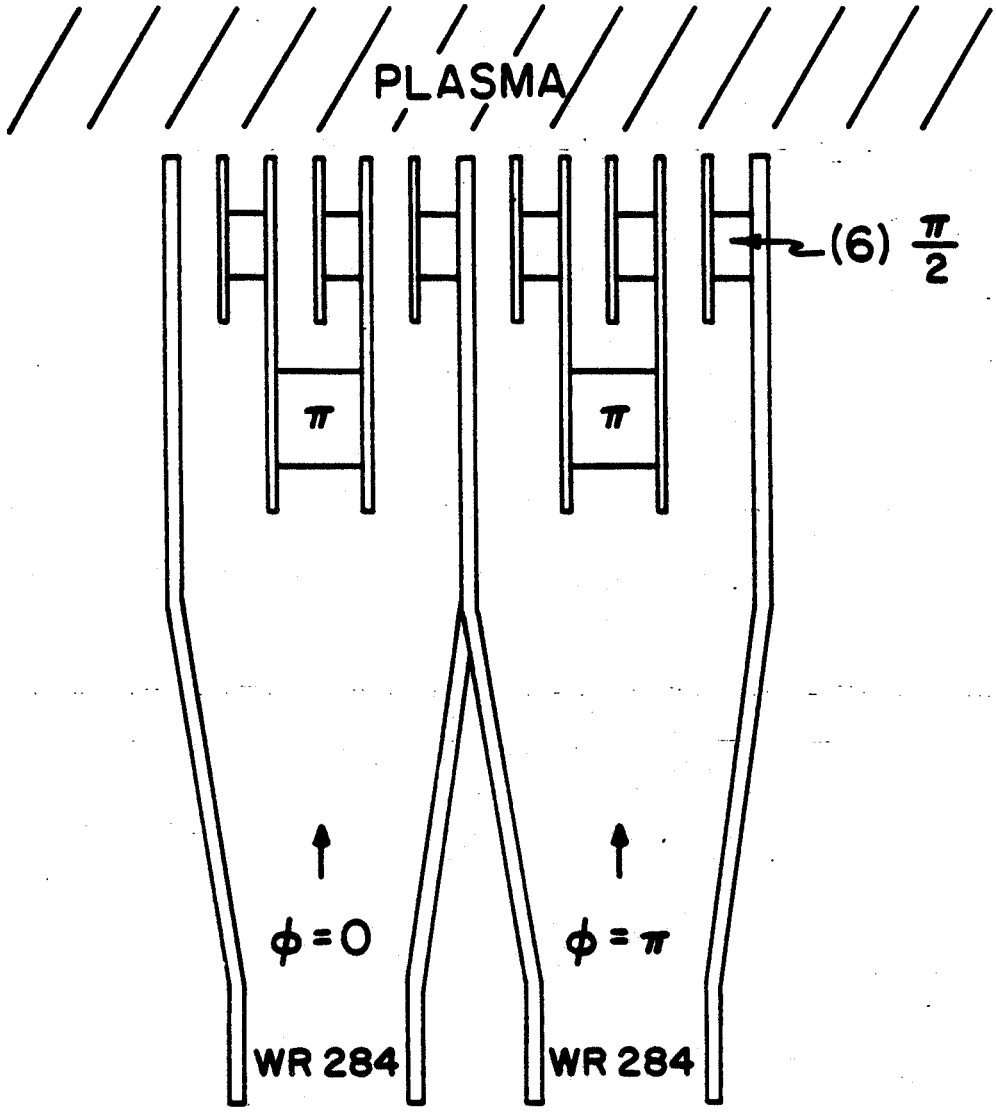

(a)

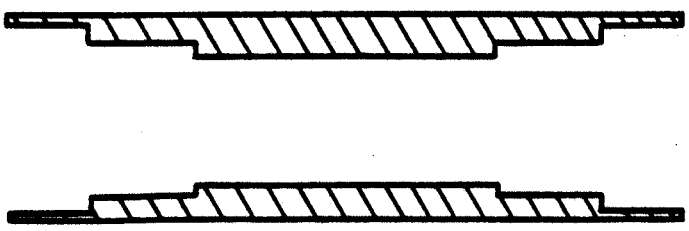

H plane transformer

(b)

Figure 21